NASA CR-121207
SKF AL73P010

FINAL REPORT

ON

DYNAMIC AND THERMAL ANALYSIS OF HIGH SPEED TAPERED ROLLER BEARINGS UNDER COMBINED LOADING

By

ANALYTICAL SERVICES DEPARTMENT
SKF INDUSTRIES, INC.

W. J. CRECELIUS AND D. R. MILKE

PREPARED FOR

NATIONAL AERONAUTICS AND SPACE ADMINISTRATION

NASA LEWIS RESEARCH CENTER
CONTRACT NAS3-15700
R. J. PARKER, PROJECT MANAGER

RESEARCH LABORATORY
SKF INDUSTRIES, INC.
ENGINEERING AND RESEARCH CENTER
KING OF PRUSSIA, PA.

1. Report No.	2. Government Accession No.	3. Recipient's Catalog No.
NASA CR-121207		

4. Title and Subtitle	5. Report Date
DYNAMIC AND THERMAL ANALYSIS OF HIGH SPEED TAPERED ROLLER BEARINGS UNDER COMBINED LOADING	March, 1973
	6. Performing Organization Code
7. Author(s)	8. Performing Organization Report No.
W. J. Crecelius and D. R. Milke	SKF AL73P010
	10. Work Unit No.
9. Performing Organization Name and Address	11. Contract or Grant No.
Analytical Services Department SKF Industries, Inc., 1100 First Avenue, King of Prussia, Pa. 19406	NAS3-15700
	13. Type of Report and Period Covered
12. Sponsoring Agency Name and Address	Contractor Report
National Aeronautics and Space Administration Washington, D.C. 20546	14. Sponsoring Agency Code

15. Supplementary Notes

Project Manager, Richard J. Parker, Fluid System Components Division, NASA Lewis Research Center, Cleveland, Ohio

16. Abstract

THIS REPORT DETAILS THE DEVELOPMENT OF A COMPUTER PROGRAM CAPABLE OF PREDICTING THE THERMAL AND KINETIC PERFORMANCE OF HIGH-SPEED TAPERED ROLLER BEARINGS OPERATING WITH FLUID LUBRICATION UNDER APPLIED AXIAL, RADIAL AND MOMENT LOADING (FIVE DEGREES OF FREEDOM). VARIOUS METHODS OF APPLYING LUBRICATION CAN BE CONSIDERED AS WELL AS CHANGES IN BEARING INTERNAL GEOMETRY WHICH OCCUR AS THE BEARING IS BROUGHT TO OPERATING SPEEDS, LOADS AND TEMPERATURES.

THE PROGRAM WAS USED TO OPTIMIZE THE INTERNAL GEOMETRY AND LUBRICATION SCHEME OF THE TAPERED ROLLER BEARING HAVING THE FOLLOWING BOUNDARY DIMENSIONS AND OPERATING CONDITIONS.

INNER RING I.D.	120.65MM (4.750 INCHES)
OUTER RING O.D.	206.375MM (8.125 INCHES)
TOTAL WIDTH	47.625MM (1.875 INCHES)
RADIAL LOAD	8896 TO 26689 N (2000 TO 6000 LBS.)
AXIAL LOAD	8896 TO 53378 N (2000 TO 12000 LBS.)
SHAFT SPEED	12500 RPM
LUBRICANT INPUT	
TEMPERATURE	346°K (195°F)

THE PROPOSED OPTIMUM BEARING HAS AN OUTER RACEWAY CONTACT ANGLE OF APPROXIMATELY 24°, TWENTY ROLLERS EACH HAVING A LARGE END DIAMETER OF 23.609 MM (0.9295 INCHES), A LENGTH OF 27.742MM (1.0922 INCHES), AN INCLUDED ANGLE OF 5°40' AND A ROLLER END SPHERE RADIUS OF 196.850MM (7.750 INCHES).

THE LUBRICATION SCHEME CONSISTS OF JETS TO THE ROLLER SMALL END SIDE OF THE BEARING AND THROUGH RACE LUBRICATION TO THE FLANGE AT THE ROLLER LARGE END SIDE OF THE BEARING, BOTH AT A RATE OF 227 KG/HR. (500 LB./HR.).

THE WORK WAS PERFORMED BETWEEN MARCH 1972 AND MARCH 1973 UNDER CONTRACT NO. NAS3-15700.

17. Key Words (Suggested by Author(s))	18. Distribution Statement
Tapered Roller Bearings High Speed Dynamic and Thermal Analyses	"At the discretion of the NASA Project Manager"

19. Security Classif. (of this report)	20. Security Classif. (of this page)	21. No. of Pages	22. Price*
Unclassified	Unclassified	125	$3.00

FOREWORD

The work described herein, was conducted by the Analytical Services Department of SKF Industries, Incorporated, under the management of NASA Project Manager, Mr. R. J. Parker, Fluid System Components Division, NASA-Lewis Research Center.

TABLE OF CONTENTS

		Page
1.0	SUMMARY	1
2.0	INTRODUCTION	4
3.0	ANALYSIS	6
3.1	MATHEMATICAL MODEL	6
3.1.1	Bearing Dynamic Model	6
3.1.2	Temperature Mapping Heat Dissipation Model	20
3.1.3	Bearing Geometry Change Analysis from Cold Unmounted to Mounted Operating Conditions	42
3.1.4	Bearing Fatigue Life	55
3.2	ANALYTICAL PROCEDURE-BEARING OPTIMIZATION STUDY	57
3.2.1	Bearing Optimization Study Objectives	57
3.2.2	Roller-End Flange Contact Performance Limitations	58
3.2.3	Preliminary Design Considerations	59
3.2.4	Outer Ring Contact Angle Determination	60
3.2.5	Cage Design	61
3.2.6	Bearing Manufacturing Considerations	61
3.2.7	Roller-End-Flange Contact Lubrication and Geometry	63
3.2.8	Optimum Tapered Roller Bearing Thermal Performance	64
3.2.9	Geometry Change at Operating Conditions	66
3.3	ANALYTICAL RESULTS	67
3.3.1	Bearing Material, Lubricant Film Thickness and Bearing Fatigue Life	67
3.3.2	Contact Load and Cage Slip	67

TABLE OF CONTENTS (CONTINUED)

	Page
4.0 DISCUSSION OF RESULTS	70
5.0 CONCLUDING REMARKS AND PROPOSED FUTURE EFFORTS	72
5.1 ANALYTICAL AND EXPERIMENTAL DATA CORRELATION	72
5.2 STUDY OF CONCENTRATED CONTACTS	72
6.0 REFERENCES	74
TABLES	77
FIGURES	79
ENCLOSURES	
APPENDIX - ROLLER DIMENSIONS FOR SPECIFIED BEARING SECTION AND VARIABLE CONTACT ANGLE	115

LIST OF TABLES

Table No.	Title
1	Preliminary Bearing Designs
2	Performance Parameters at Maximum Load Conditions for the Proposed Optimum Tapered Roller Bearing see Enclosure 2 for Design Details

LIST OF FIGURES

Figure Number	Title
1	Bearing Operating in YZ-Plane
2	Roller Forces and Geometry
3	Roller Raceway Stress Concentrations
4	Tapered Roller Geometry
5	Components of Roller Deflection Due to Radial Load, Misalignment and Crowning
6	MIL-L-23699 Lubricant Viscosity vs. Pressure and Temperature
7	XZ Plane Inner Ring Displacements
8	Cage Types
9	Heat Dissipation and Temperature Map
10.1	Lubricant Distribution Model
10.2	Lubricant Flow Scheme from the Jet (Node 21) Which Feeds the Scoop (Node 20) to the Lubricant Nodes Within the Bearing Cavity
10.3	Lubricant Flow Scheme From the Jets at Side 1 (Node 11) to the Lubricant Nodes Within the Bearing Cavity
11.1	Bearing Assembly Equivalent Sections
11.2	Bearing Assembly Widths, and Roller Path Radii
12	Ring Radial Expansion vs. Rotational Speed Squared
13	Life Adjustment Factor for Lubrication a_3 Film Thickness/ Surface Finish Ratio
14	L-10 Fatigue Life vs. Contact Angle $\mathcal{A}$.
15	Roller-Ring Normal Loads, Roller Centrifugal Force and Cage Slip Percent vs. Outer Ring Contact Angle

LIST OF FIGURES (CONTINUED)

Figure Number	Title
16	Flange Load, Hertz Stress and Lubricant Film Thickness vs. Contact Angle
17	Frictional Heat Generation Rates vs. Contact Angle
18	Flange Hertz stress, Lubricant Film Thickness and Heat Generation Rate vs. Roller End Sphere Radius
19	Bearing-Shaft and Housing Assembly Dimensions
20	Bearing Boundary Conditions and Lubrication Scheme
21	Lubrication Schemes Examined in the AL73P010 Bearing Optimization Study
22	Flange Lubricant Temperature and Frictional Heat Generation Rate vs. Lubricant Flow Rate
23	Inner Raceway Lubricant Temperature and Friction Heat Generation Rate vs. Lubricant Flow Rate
24	Outer Raceway Lubricant Temperature and Frictional Heag Generation Rate vs. Lubricant Flow Rate
25	Lubricant Mean Temperature and Frictional Heat Generation Rate Due to Lubricant Churning vs. Lubricant Mass Flow Rate
26	Flange Lubricant Temperature and Frictional Heat Generation Rate vs. Lubricant Flow Rate
27	Inner Raceway Lubricant Temperatures at Center and Small End Side of Race and Fric tional Heat Generation Rate vs. Lubricant Flow Rate
28	Outer Raceway Lubricant Temperature at Center and Small End Side of Race and Frictional Heat Generation Rate vs. Lubricant Flow Rate

LIST OF FIGURES (CONTINUED)

Figure Number	Title
29	Lubricant Bulk Tmperature and Frictional Heat Generation Rate v. Lubricant Flow Rate
30	Inner Race Lubricant Temperature, Lubricant Mean Temperature and Cage Slip Percent vs. Radial Load
31	Bearing Fatigue Life vs. Radial Load

LIST OF ENCLOSURES

Enclosure Number	Title
1	Bearing Specifications and Operating Conditions
2	Optimized Bearing Design

NOMENCLATURE

Symbol		Description
A	=	Component of roller raceway interference at aximuth j; m (in.)
A	=	Area, m^2 (in^2 or ft^2)
a	=	Semi-major axis of a contact ellipse; m (in.)
a	=	Bearing fatigue life adjustment factors
b	=	Semi-minor axis of a contact ellipse; m (in.)
C_k	=	Viscosity constants = 1, 2 and 3
CD	=	Crown drop; m (in.)
C_d	=	Drag coefficient
CF	=	Centrifugal force
c	=	Constant; $c_1 = 1$, $c_2 = -1$
CP	=	Specific heat - BTU/lb.°F
D	=	Rolling element or general diameter; m(in)
d	=	Cage rail and ring land diameters;m(in)
E	=	Young's modulus; psi
e	=	Pitch diameter; in.
e	=	Surface emissivity
$\bar{F}$	=	Friction Force; N(lb)
F	=	Applied force or moment; N(lb) or N-m(in.-lb)
F	=	Shaft and housing fits; m tight (in. tight)

NOMENCLATURE (CONTINUED)

Symbol		Description
G	=	Gyroscopic moment; N-m(in.-lb)
g	=	Gravitational constant; m/sec^2 (in./sec^2)
$\dot{H}$	=	Heat generation rate; Watts (Btu/hr.)
H	=	Height of the roller end flange contact above the inner raceway measured along a line defining the flange contact angle; m(in)
h	=	Lubricant film thickness; m(in)
h	=	Convective heat transfer coefficient; Watts/m^2°K, (BTU/Hr-ft^2°F)
J	=	Mass moment of inertia; m-Kg-sec^2, (in-lb-sec^2)
J	=	Mechanical to heat energy conversion factor
K	=	Thermal conductivity; watts/m-°K (BTU/hr-ft-°F)
K	=	Ratio, Roller sphere end radius to rearing apex length
K	=	Lubricant mass flow rate proportionality factor
K	=	Integration constant
L	=	Roller total length or a general length; m(in or ft)
Lcm	=	Length from roller small end to the center of mass; m(in)
L_{10}	=	Bearing fatugue life, at which 90 percent of the bearings survive (Hr) or revolutions

NOMENCLATURE (CONTINUED)

Symbol		Description
ℓ	=	Roller raceway effective contact length; m(in.)
M	=	Moment; N-m(in-lb)
$\dot{M}$	=	Fluid mass flow rate; Kg/Hr, (lb/Hr)
N	=	Total number of roller/raceway lamina jets, under race flow paths
N	=	Rotational speed; RPM
N	=	Rotational speed factor $1/m^2$ ($1/in^2$)
NRe	=	Reynolds Number
P	=	Decimal fraction volume of lubricant/volume of bearing cavity
P	=	Shaft/inner ring, housing/outer ring, external pressures N/m^2 (psi)
P*	=	Change in fit pressure due to ring inertia; N/m^2 (psi)
Pr	=	Prandtl Number
Pd	=	Diametral clearance; m, (in)
Q	=	Contact normal load; n (lb)
Qc	=	Raceway dynamic capacity; N (lb)
Qe	=	Raceway equivalent load N (lb)
Q	=	Heat transfer rate; watts (BTU/Hr)
Q*	=	Heat generated at a given temperature node; Watts (BTU/Hr)

NOMENCLATURE (CONTINUED)

Symbol		Description
q	=	Load per unit length; N/m lb/in
R	=	Radius; m (in)
$\bar{R}$	=	Roller/raceway equivalent radius; m (in)
Rsph	=	Roller end sphere radius m(in)
r	=	Radius; m (in)
r_f^*	=	Radius from roller axis of rotation to the center of the roller end flange contact; m (in)
S	=	Dimensionless speed factor
s	=	$y/a \quad o \leq s \leq 1$
T	=	Temperature; °K (°F)
$\bar{T}$	=	Bearing shaft andhousing mean temperatures; °K (°F)
t	=	$z/b \quad o \leq t \leq 1$
U	=	Radial portion of contact deformation in a roller/raceway contact; m (in)
U	=	Uniform radial displacement; m (in)
$\bar{U}$	=	Dimensionless entrainment velocity
u	=	Mean value of contact surface velocities; m/sec (in/sec)
v	=	Sliding velocity; m/sec, (in/sec)
V	=	Fluid velocity; m/sec (in/sec)

NOMENCLATURE (CONTINUED)

Symbol		Description
W	=	Width or thickness; in
$\bar{X}$	=	Dimensionless factor to adjust bearing shaftor housing shaft rigidity accounting for unequal bearing ring and shaft and housing effective widths
$\bar{Y}$	=	Dimensionless factor to adjust bearing shaft or housing seat rigidity accounting for shaft and housing shoulders
Z	=	Number of rollers
α	=	Contact angle or roller included angle; degrees or radians
α	=	Coefficient of thermal expansion; $\frac{m}{m}/^{\circ}K$, $(\frac{in}{in\ ^{\circ}F})$
β	=	$\alpha_f + \frac{\alpha_o+\alpha_i}{2} - \frac{\pi}{Z}$ degrees or radians
γ	=	$\frac{D\ Cos\alpha m}{e}$
γ'	=	$\frac{D}{e}$
γ_{60}	=	Lubricant specific weight at 60°F
Δ	=	Designates change
Δ_K	=	Inner ring displacements relative to outer ring; m(in) $K = 1-5$.
δ	=	Roller raceway deflection; m(in)
δ^{α}	=	Difference between ring radial displacements at a common boundary due to rotational speed; m(in)
ϵ	=	Exponent for calculating raceway equivalent load

NOMENCLATURE (CONTINUED)

Symbol		Description
ϵ	=	Lubricant scoop or jet efficiency
φ	=	Roller pitch angle degrees or radians
η	=	Absolute viscosity; N-sec/m^2 (lb_f - sec/in^2)
η'	=	Absolute Viscosity; Kg/Hr-m lb/Hr-ft
Θ	=	Time; seconds
Λ	=	Ratio; lubricant film thickness to composit surface roughness
λ	=	Pressure coefficient of viscosity; m^2/N (in^2/lb_f)
λ	=	Heat transfer coefficient; watts/°K . (BTU/Hr °F)
ν	=	Constants ν_1 = o ν_2 = 1
ξ	=	Poissons Ratio
ρ	=	Density; Kg/m^3 (lb/in^3)
σ	=	Pressure; N/m^2 (psi)
σ'	=	Surface roughness; m(in)
σ	=	Composite roller/raceway surface roughness
$\Sigma\rho$	=	Curvature sum; 1/m (1/in)
τ	=	Shear stress; N/m^2 (psi)
ϕ	=	Ellipcitivity Factor
φ	=	Roller aximuth angle; degrees or radians

NOMENCLATURE (CONTINUED)

Symbol		Description
φ	=	Ratio of jet travel to roller length
ψ	=	Ratio of lubricant flow rates through under-race flow paths.
Ω	=	Inner or outer ring rotational speed radians/sec
ω	=	Rotational speed relative to cage speed; radians/sec
ω_c	=	Cage rotational speed; radians/sec
ω_o	=	Roller orbital speed; radians/sec

Subscripts

B	=	Refers to lubricant distribution
cold	=	refers to shaft and housing fits at 293°K (68°F)
CR	=	Cage Rail
c	=	Refers to cage
d	=	Refers to lubricant hydrodynamic drag
F	=	Refers to lubricant distribution
(F,Q)	=	Refers to ring radial displacement due to fits and uniform rolling element loads.
f	=	Refers to flange
H	=	Refers to housing
Hl	=	Refers to the housing outer ring equivalent section at the roller flange end side of the bearings
	=	Ratio of lubricant flow rates through under race symbol flow paths

NOMENCLATURE (CONTINUED)

Symbol		Description
H2	=	Refers to the housing outer ring equivalent section at the roller small end side of the bearing
Hot	=	Refers to shaft and housing fits at operating temperature
I	=	Refer to inner ring
i	=	Refers to inner ring, internal pressure or to a temperature node
J	=	Refers to jet
j	=	refers to a roller azimuth location, or to a temperature node
k	=	Refers to a laminum location or to a temperature node
LL	=	Refers to ring radial expansion which occurs, starting with loose fit, up to the speed at which the fit becomes tight
LT	=	Refers to ring radial expansion which occurs, starting with a loose fit, at the total ring speed
m	=	m 1 refers to the outer raceway m 2 refers to the inner raceway m 3 Refers to the flange
n	=	n=1 refers to the roller large end side of the bearing n=2 refers to the small end side

NOMENCLATURE (CONTINUED)

Symbol		Description
o	=	Refers to outer ring or external pressure
O	=	Refers to outer ring
R	=	Refers to roller
S	=	Refers to shaft
S	=	Refers to scoop
S1	=	Refers to inner ring shaft equivalent section at the roller large end side of the bearing
S2	=	Refers to the inner ring shaft equivalent section at the roller small end side of the bearing
SP	=	Refers to speed related lubricant distribution
TL	=	Refers to ring radial expansion which occurs; starting with a tight fit, up to the speed at which the fit becomes loose
T	=	Refers to total specified ring space
$\bar{T}$	=	Refers to ring radial displacement which results from changes in temperature from 293°K (68°F)
TOT	=	Refers to total ring radial displacement which results from fit, temperature, rolling element load and rotational effects

NOMENCLATURE (CONTINUED)

Symbol		Description
x	=	Refers to a distance measured in the x direction
y	=	Refers to a distance measured in the y direction
z	=	Refers to a distance measured in the z direction
Ω	=	Refers to rotational speed
1	=	Refers to outer raceway, x direction, or roller large end side of the bearing
2	=	Refers to inner raceway, y direction, or the roller small end side of the bearing
3	=	Refers to flange or z direction
4	=	Refers to the XZ plane
5	=	Refers to XY plane

1. SUMMARY

The purpose of this effort was to develop a tool for the analysis of high speed tapered roller bearings. The tool developed is SKF Computer Program AE71Y001 which has the following capabilities.

1) Bearing loads may be applied and bearing deflections determined in three distinct linear directions and two angular directions.

2) Hydrodynamic cage and roller drag friction and elasto-hydrodynamic concentrated contact (EHD) friction forces are considered.

3) Cage web/roller loading is determined.

4) Bearing thermal performance is determined on the basis of heat generation, dissipation rates and temperature mapping.

5) Bearing geometry changes which occur from cold to operating conditions are determined as affected by thermal gradients, shaft and housing fits, ring centrifugal growth, and rolling element - raceway normal loads.

As previously available to SKF, the computer program had capabilities 1, 2 and 3. Under Contract NAS3-15700 capabilities 4 and 5 were added.

The complete computer program was used to optimize the design of a tapered roller bearing having the external dimensions and operating conditions listed below.

Bearing Boundary Dimensions:

Outer ring O.D. - 2061375 mm (8.125 in)
Inner ring I.D. - 120.650 mm (4.750 in)
Total Width - 47.625 mm (1.875 in)

Operating Conditions:

Axial Load - 8896-53389 N (200-12000 lb)
Radial Load - 8896-26678 N (2000-6000 lb)
Shaft Speed - 12500 RPM

Lubricant Data:

Type-MIL-L-23699
Input Temperature - 364°K (195°F)
Maximum Lubricant Flow Rate - .017 $\frac{m^3}{min}$ (4.5 gal/min)

Based on the maximum load conditions, the optimum internal geometry was developed as follows:

Outer Raceway Half Angle	23° 57' 36"
Inner Raceway Half Angle	18° 20'
Roller Included Angle	5° 40'
Roller Large End Diameter	23.609mm (0.9295 in)
Roller Length	27.742mm (1.0922)
Roller End Sphere Radius	196,850mm (7.75 in)
Number of Rollers	20

The bearing half angles are biased by 2' 24" such that roller large end pinching is promoted. This bias is relieved at operating conditions.

The bearing lubrication scheme was also studies and optimized. Recommended lubricant flow rates are 227 Kg/Hr (500 lb/Hr or about 1 gal/min) introduced to the inner raceway undercut at the roller large end and 227 Kg/Hr via jets, to the inner race impinging at the roller small end side of the bearing. The lubricant is to be scavenged at both sides of the bearings.

Under the maximum load conditions and with the recommended lubrication scheme, the predicted lubricant temperatures within the bearing are less than 422°K (300°F).

For the optimized bearing at the maximum load conditions, the bearing L_{10} life is 765 hours. This includes a 2.55 miltiplicative factor which reflects practically full EHD films in the roller raceway contacts. A material life multiplier of 1.0 was assumed. Cage speed is predicted to deviate from eppicylic by less than 6 percent. Under the same conditions the roller end flange contact performance parameters are as follows:

Maximum Hertz stress -3.01 x 10^9 N/m^2 (43,750 psi)
Maximum Sliding speed 22.85 m/sec (900 in/sec)
Maximum Rolling Speed 49.50 m/sec (1950 in/sec)
Minimum EHD film thickness 0.965 m x 10^{-6}, (38 microinches).

A "Z" configuration cage which is guided by the outer ring I.D. at the roller small end side of the bearing and at the inner ring flange at the roller large end side of the bearing was selected as optimum because the lubricant flow to and from the bearing is less restricted than it would be with either the strictly inner or outer ring land riding cage.

2. INTRODUCTION

The purpose of this effort was two fold:

1. To develop a mathematical model in the form of a computer program for the determination of the kinetic and thermal performance characteristics of lubricated high speed tapered roller bearings.

2. To use the mathematical model to optimize the internal geometry of a tapered roller bearing whose boundary dimensions and operating conditions are presented in Enclosure 1.

The basis for the model was embodied in the SKF developed Computer program AE71Y001, "The Analysis of Dynamic Performance Characteristics of Tapered Cylindrical and Spherical Roller Bearings Under Radial Axial and Moment and/or Misalignment Loading". Under the sponsorship of NASA, a heat dissipation, temperature mapping analysis was developed, and incorporated into this roller bearing computer program. In addition, an SKF developed model which predicts the change in bearing geometry from the "off the shelf" state, to operating conditions was incorporated into the program. As finally constructed, computer program AE71Y001 can analyze total bearing performance when the bearing is subjected to general loading, high speed rotation and various combinations of jet and through-race lubrication.

The methods of analysis used are extensions of previous work. The bearing load deflection analysis was first developed by Jones ref. (1). Harris expanded the load deflection analysis to include the effects of hydrodynamic (HD) and elastohydrodynamic (EHD) lubrication on rolling element bearing performance, refs. (2 and 3). Crecelius and Harris utilized a temperature mapping heat dissipation model in conjunction with a bearing dynamics model, to optimize the design of an ultra high speed ball bearing, ref. (4). The analysis presented herein offers further refinements to the previous work by providing better definition of lubricant distribution within the bearing cavity, and a more complete analysis of the changes in bearing geometry which occur as a bearing reaches steadystate operating conditions.

It is expected that these models will be further refined as analytical methods improve and comparisons between analytical

predictions and experimental results become available.

Interest in high speed tapered roller bearings has been provided by the need for greater load carrying capacity in moderately high speed gearbox applications, typically serviced by ball bearings. The immediate need for high speed, high torque gearboxes has been generated by the helicopter industry. Additionally, tapered roller bearings are being evaluated for use as mainshaft bearings in small gas turbines.

Results from several high speed tapered roller bearing experimental programs (ref. 5 and 6) have been used in the bearing design optimization portion of this effort. It became clear as a result of this optimization study, that additional experimental and theoretical work would be required to develop a complete model defining acceptable roller-end-flange contact. This analysis provides various operating characteristics realized at that contact such as:

- Load
- Hertz Stress
- Sliding Speed
- Rolling Speed
- EHD Film Thickness
- Lubricant and Surface Ambient Temperatures

However, a unifying theory describing a successful REFC, in terms of the above variables does not exist.

The bearing performance data includes load/deflection data in the form of spring constants for each of the bearing's five degrees of freedom. This data is useful for rotor dynamics studies, and its presentation was an explicit requirement of this effort.

Throughout this analysis English Units are used. Where data is presented in International Standard Units, it was obtained by conversion utilizing ref. (7).

3.0 ANALYSIS

3.1 Mathematical Models

The mathematical model has four major segments which are interdependent but sufficiently distinct to allow them to be discussed separately. The four analytical segments and their major subsegments are as follows:

1. Bearing dynamic performance
    a. Applied loading, bearing deflection and inner ring force and moment equilibrium.
    b. Lubricant related friction forces and roller and cage equilibrium.
2. Thermal performance
    a. Temperature mapping
    b. Heat dissipation
    c. Lubricant distribution
3. "Off the shelf" to operating geometry analysis.
4. Bearing raceway fatigue life

The size and diversity of this analytical presentation has required some designations to be used with several meanings. Therefore, in the required instances, their meanings are presented immediately subsequent to their use.

3.1.1 Bearing Dynamic Model

A major portion of the following presentation is taken directly from a publication, Rolling Element Bearing Dynamics by Harris and Mindel, ref. (8). That work is not included in its entirety as an appendix because it deals with ball, as well as roller bearings. In addition, Rolling Element Bearing Dynamics presents a more detailed analysis of the cage-roller interaction than is used in computer program AE71Y001. In particular, the AE71Y001 analysis assumes zero friction at the roller/cage web contact.

3.1.1.1 Roller Analysis

The nature of the tapered roller bearing dynamics problem is such that it is most easily understood if the action of a rolling element is examined, first, then, the interaction of each rolling element with the cage, rings and lubricant will be developed.

3.1.1.1.1 Normal Forces and Deformations

The tapered roller bearing and the individual roller coordinate systems are given in Figure 1.

A roller may be characterized by Figure 2; it rotates about an axis inclined to the x-axis and its lateral surface is a portion of a curved surface of revolution. This surface is arbitrarily shaped, and for the purpose of analysis a roller is divided into a number of laminae, each having identical width W_m. It is assumed that there are no abrupt pressure changes along the width of the contact and thus no shear effects are assumed to occur between laminae and each laminum deflects independently of its neighbors.

In the following equations, the sub-scripts take on the following meaning:

- j - refers to a particular roller j = 1..Z
  where Z is the total number of rollers in the bearing
- m - refers to a particular raceway
  m = 1 outer raceway
  m = 2 inner raceway
- k - refers to a particular laminum location k=1...N where N is at most 20.

Lundberg ref. (9) developed the following load-deflection relationship for a roller in contact with a raceway such that a uniform load per unit length occurs along the length of contact:

$$\delta_{mj} = \frac{2 Q_{mj} (1-\xi^2)}{\pi E l_{mj}} \ln\left[\frac{\pi E l_{mj}^2}{Q_{mj}(1-\xi^2)(1+C_m Y_m)}\right] \qquad 3.1.1.1$$

In terms of load per unit length acting on a particular laminum, Eq. 3.1.1.1 becomes:

$$\delta_{mj} = \frac{2q_{Kmj}(1-\xi^2)}{\pi E} \ln\left[\frac{\pi E \ell_{mj}}{q_{Kmj}(1-\xi^2)(1+c_m\gamma_m)}\right] \qquad 3.1.1.2$$

where ℓ_{mj} is the actual length of contact. The roller load is:

$$Q_{mj} = W_m \sum_{K=1}^{K=N} q_{Kmj} \qquad 3.1.1.3$$

ξ is Poisson's ratio, E is the modulus of elasticity. Both roller and raceway materials are assumed to be steel.

$$\gamma_m = \frac{D}{e}\cos\alpha_m \qquad 3.1.1.4$$

where D is the roller diameter, e is the pitch diameter, α_m is the raceway contact angle and $c_1 = +1$, $c_2 = -1$.

3.1.1.1.1.1 Roller Alignment

In a tapered roller bearing, rollers are constrained by the raceways and guide flange to move in a prescribed path and the inner and outer raceway contact angles are substantially constant. However, a roller axis can pitch through a small angle ζ; relative to the contact angle to achieve a balance of moments about the roller centroid in a plane passing simultaneously through the roller and bearing axes of rotation. The maximum normal displacement owing to roller pitch is equal to $\ell_{mj}\zeta_j$. The skew angle is assumed zero.

3.1.1.1.1.2 Crowning

When a tapered roller is pressed into a reacway of different axial length, stress concentrations develop at the contact extremities as shown by Figure 3. To relieve these stresses, crowning, shown by Figure 4, is used. The crown radius is usually large compared to the roller diameter, so that the crown drop at the roller ends is slight, but sufficient to minimize edge loading.

3.1.1.1.1.3 Contact Deformation with Roller Pitch and Crowning

At a given azimuth angle φ_j (see Figure 1), the contact deformation varies as a function of laminum position. Assuming

a contact is divided into N laminae, each of width Wm ($\ell_m = WmN$), the contact deformation at the axial mid point of a given laminum is

$$\delta_{kmj} = U_{mj} - c_m W_m \left(k - \tfrac{1}{2}\right)\left[\gamma_m\left(\Delta_4 \cos\varphi_j + \Delta_5 \sin\varphi_j + \zeta_j\right)\right] - CD_{km}$$

$$\delta_{kmj} \geq 0 \qquad 3.1.1.5$$

$$\gamma_1 = 0 \quad \gamma_2 = 1$$

Δ_4 and Δ_5 are angular displacements (misalignment) of the bearing inner raceway relative to the outer raceway. Figure 5 illustrates the components of Eq. (3.1.1.5.). The variables U_{mj} are the relative normal displacements of the roller axis toward the bearing raceways.

At a given azimuth, φ_j, contact deformation varies with laminum location in the contact zone. The interference at the midpoint of the contact is a function of bearing inner ring displacements relative to the outer ring and may be equated to the sum of the inner and outer contact deformations.

$$A_j = \sum_{m=1}^{m=2} \delta_{kmj} \qquad 3.1.1.6$$

3.1.1.1.2 EHD Lubrication

The lubricant is assumed to be a Newtonian fluid which implies that the shear stress, viscosity, and velocity gradient are related as follows:

$$\tau = \eta \frac{\partial u}{\partial z} \qquad 3.1.1.7$$

Since, in EHD contacts, the lubricating film is extremely thin, the lubricant velocity gradient is assumed linear. Therefore, Eq. 3.1.1.7 becomes:

$$\tau = \eta \frac{v}{h} \qquad 3.1.1.8$$

Where v is the roller/raceway or roller/flange sliding velocity, and h is the film thickness. For most lubricants the viscosity-temperature-pressure relationship can be presented in the form of Figure 6. For a given temperature, an approximation to the curves similar to those of Figure 6 is:

$$\eta = C_1 e^{\sqrt{C_2 + C_3 \sigma}} \qquad 3.1.1.9$$

Where σ represents pressure and C_1, C_2 and C_3 are constants calculated from input pressure-viscosity data using a least squares fit procedure.

For a given laminum, the pressure distribution in the y direction is given by:

$$\sigma_{kmj} = \frac{2 q_{kmj}}{\pi b_{kmj}} \sqrt{1 - t^2} \qquad 3.1.1.10$$

$$b_{kmj} = \sqrt{\frac{8 q_{kmj} (1 - \xi^2)}{\pi E \Sigma \rho_{km}}} \qquad 3.1.1.11$$

With y measured from the center of the contact,

$$t = y / b_{kmj} \qquad 3.1.1.12$$

$$\Sigma \rho_{km} = \frac{2}{D_k (1 + c_m \gamma_{km})} + \frac{1}{r_R} - \frac{1}{r_m} \qquad 3.1.1.13$$

r refers to the roller and raceway crown radii.

At the roller-end-flange contact, (REFC), the contact shape is assumed elliptical and the pressure distribution is assumed to form an ellipsoid. At any point within the contact pressure can be given by:

$$\sigma_j = \frac{3Q_{fj}\sqrt{1-s^2-t^2}}{2\pi a_j b_j} \qquad 3.1.1.14$$

Where:

$$s = y/a_j \qquad 3.1.1.15.1$$

$$t = z/b_j \qquad 3.1.1.15.2$$

Given the principal radii of the flange and roller end surfaces;

for the roller;

$$R_y = R_z = R_{SPH} \qquad 3.1.1.16$$

for the flange;

$$R_z = \infty \qquad 3.1.1.17.1$$

$$R_y = \frac{r_f}{\sin(\alpha_f - \frac{\pi}{2})} \qquad 3.1.1.17.2$$

the semi-major (aj) and semi-minor (bj) axes of the contact ellipse can be determined according to the methods of ref. 3. Using Eq. (3.1.1.9, 10 and 14) viscosity can be expressed as a function of pressure.

The sliding velocity, v_{kmj} at any laminum in a raceway contact, depends upon roller speed, raceway speed and geometry of the deformed bodies. Palmgren, ref. 10 states that 2/3 of the contact deformation occurs in the roller and 1/3 in the raceway body. Therefore,

$$v_{kmj} = \frac{1}{2}\left\{\left[e_k + C_m\left(D_k + \frac{1}{3}\delta_{kmj}\right)\right]\omega_m - \left(D_k - \frac{2}{3}\delta_{kmj}\right)\omega_j\right\} \qquad 3.1.1.18$$

The sliding velocity at the center of the REFC is assumed to act at each point within the contact ellipse and is given by:

$$v_{fj} = r_f\omega_i - \left(\frac{D}{2} - H\right)\omega_j \qquad 3.1.1.19$$

r_f and H are defined in Figure 2

$$\omega_m = \Omega_m - \omega_c \qquad 3.1.1.20$$

3.1.1.1.2.1 EHD Film Thickness

EHD films are assumed to be developed in the line contacts at both raceways and at the point contact of roller end flange.

3.1.1.1.2.1.1 Raceway Film Thickness

According to Dowson et al (11), the lubricant film thickness in a rolling line contact is defined by:

$$h_{mj} = 1.6\left(\frac{\lambda_o E}{1-\xi^2}\right)^{0.6} \frac{\bar{U}_{mj}^{0.7}\bar{R}_m}{\bar{Q}_{mj}^{0.13}} \qquad 3.1.1.21$$

$$\bar{U}_{mj} = \frac{\eta_o(1-\xi^2)}{4E\bar{R}_m}\left[\omega_{mj}\left(\frac{1}{\gamma'} + C_m \cos\alpha_{mj}\right) + \omega_j\right] \qquad 3.1.1.22$$

$$\bar{Q}_{mj} = \frac{Q_{mj}(1-\xi^2)}{l_{mj} E \bar{R}_m} \qquad 3.1.1.23$$

$$\bar{R}_m = \frac{D}{2}(1 + C_m \gamma_m) \qquad 3.1.1.24$$

$$\gamma' = D/e \qquad 3.1.1.25$$

η_o and λ_o are based on lubricant bulk temperature.

Others have developed formulae similar to the foregoing; however, Eq. (3.1.1.21) is used herein.

3.1.1.1.2.1.2 Flange-Roller End Film Thickness

For an elliptical point contact Archard et al ref. (12) have developed Eq. (3.1.1.26) to describe the lubricant film thickness

$$h_j = 2.04 \left(\frac{\lambda_o \eta_o U_{fj}}{\left[1 + \frac{2}{3}\frac{\bar{R}_{yj}}{\bar{R}_{zj}}\right]^{1.26}} \left[\frac{E}{Q_{fj}(1-\bar{\gamma}^2)}\right]^{0.1} \right)^{0.407} \bar{R}_{yj} \qquad 3.1.1.26$$

$$U_{fj} = r_f \omega_i + (D/2 - H)\omega_j \qquad 3.1.1.27$$

$$\bar{R}_z = R_{SPH} \qquad 3.1.1.28$$

$$\bar{R}_y = \left[\frac{1}{R_{SPH}} + \frac{\sin\left(\frac{\pi}{2} - \alpha_f\right)}{r_f}\right] \qquad 3.1.1.29$$

For use in Eq. (3.1.1.21, 22 and 26), the terms η_o and λ_o can be developed from Eq. (3.1.1.9).

$$\eta_o = (\eta)_{\sigma=0} = C_1 e^{\sqrt{C_2}} \qquad 3.1.1.30$$

$$\lambda_o = \left(\frac{\partial \eta}{\partial \sigma}\right)_{\sigma=0} = \frac{C_1 C_3 e^{\sqrt{C_2}}}{2\sqrt{C_2}} \qquad 3.1.1.31$$

3.1.1.1.2.1.3 Raceway Traction

Using Eq. (3.1.1.8, 9, 10, 18 and 21), the raceway traction forces are obtained by numerically integrating Eq. (3.1.1.32).

$$\bar{F}_{mj} = 2 W_m \sum_{K=1}^{K=N} b_{Kmj} \int_0^1 \tau_{Kmj}\, dt \qquad 3.1.1.32$$

3.1.1.1.2.4 Roller End Flange Traction

Using Eq. (3.1.1.8, 9, 14, 19 and 26) the roller end flange traction force is obtained by numerically integrating Eq. (3.1.1.33).

$$\bar{F}_{fj} = a_{fj} b_{fj} \int_{-1}^{+1} \int_{-\sqrt{1-s^2}}^{+\sqrt{1-s^2}} \tau_{fj} \, dt \, ds \qquad 3.1.1.33$$

$\bar{F}_{fj}$ is assumed to act at the center of the contact in the direction of sliding at that point.

3.1.1.1.3 Lubricant Hydrodynamic Drag Force

In fluid-lubricated roller bearings, the rollers orbit the bearing axis, moving through space filled with a lubricant-gas mixture. This mixture and orbital motion effect a drag force on the roller which can be described empirically as follows:

$$\bar{F}_{oj} = \frac{\rho C_d D L e^2 \omega_{oj}^{1.95}}{8g} \qquad 3.1.1.34$$

Approximate values of the drag coefficient can be obtained from ref. (13). In Eq. (3.1.1.34), fluid density ρ is the mixture density. It is approximated by the quantity (lubricant weight contained within the bearing boundary dimensions) ÷ (the free space volume within the boundary dimensions), expressed as a decimal fraction, designated P.

3.1.1.1.4 Roller-Cage Normal Force

A roller exerts a force Q_{cj} on the cage, if in the absence of the cage web constraint, it would tend to orbit the bearing axis faster than cage speed, ω_c. Conversely, the cage pushes the roller with a force $-Q_{cj}$ if in the absence of the cage web constraint, the roller orbiting speed tends to be less than cage speed. As noted earlier, the roller-cage forces are neglected as are any roller-cage web forces which would result from skew moments.

3.1.1.1.5 Inertial Forces and Moments

Eq. (3.1.1.35) is used to calculate roller centrifugal force at the roller center of mass.

$$CF_j = \frac{1}{2} m e \omega_{oj}^2 \qquad 3.1.1.35$$

m is the roller mass.

Roller gyroscopic moment in the XZ plane is given by:

$$G_j = J\omega_{oj}\omega_j \sin\left[\frac{1}{2}(\alpha_1+\alpha_2)\right] \qquad 3.1.1.36$$

where J is the roller mass moment of inertia. The gyroscopic moment is counteracted by the roller raceway contacts.

3.1.1.1.6 Skewing (Yaw) Moments

Owing to axial variation of frictional stresses acting on the roller/raceway contacts and REFC friction, a skewing moment occurs about the roller centroid, tending to cause yaw or skew of the roller axis. This skewing moment is resisted by the cage web elements, the REFC normal load and the restoring moment generated at the outer raceway, or all elements in consort. The magnitude of the skewing moment is:

$$M_{sj} = Z\sum_{m=1}^{m=Z} W_m^Z \sum_{k=1}^{K=N} \left\{ b_{Kmj}\left[K-\frac{1}{2}\left(N+1\right)\right]\int_0^t \tau_{Kmj}\,dt \right\} - \frac{1}{2}\left(L-L_{cm}\right)\bar{F}_{fj} \qquad 3.1.1.37$$

By allowing the roller to adopt a non zero skew angle, Eq. (3.1.1.37) may be equilibrated to zero. However allowing the skew angle to be non zero makes the roller equilibrium problem twice as complex as it is presently formulated. Since the skew moment is generated by friction forces which for well lubricated contacts are at least two orders of magnitude lower than their respective contact loads, exclusion of the skew moment from the roller equilibrium solution should not have a major effect on the accuracy of the total bearing kinetic solution.

3.1.1.1.7 Equilibrium of Forces and Moments

In each principal direction, the forces acting on a roller constrained by raceways, guide flange or cage equilibrate to zero. If the roller does not contact the cage web, an acceleration or deceleration results in the y-direction. From Figure 2 the

three equilibrium equations are:

$$\sum_{m=1}^{m=Z} C_m Q_{mj} \cos\alpha_m - CF_j + Q_{fj} \cos\alpha_f = 0 \qquad 3.1.1.38$$

$$\sum_{m=1}^{m=Z} C_m Q_{mj} \sin\alpha_m - Q_{fj} \sin\alpha_f = 0 \qquad 3.1.1.39$$

$$\sum_{m=1}^{m=Z} C_m \bar{F}_{mj} + \bar{F}_{dj} - Q_{cj} - \bar{F}_{fj} = \frac{1}{2} m e \omega_{oj} \frac{d\omega_{oj}}{d\varphi} \qquad 3.1.1.40$$

When cage/roller contact is absent, $Q_{ej}=0$; when such contact occurs $\omega_{oj}=\omega_c$.

For fluid-lubricated bearings, friction moments about the roller axis are obtained by integration of the product of friction stress and the corresponding roller radius:

$$M_{mj} = W_m \sum_{K=1}^{K=N} b_{Kmj} D_K \int_0^1 \tau_{Kmj}\, dt \qquad 3.1.1.41$$

Using Eq. (3.1.1.41) the following moment balance about the roller axis is obtained:

$$\sum_{m=1}^{m=Z} M_{mj} - \bar{F}_{fj} r_f^* = J \omega_{oj} \frac{d\omega_j}{d\varphi} \qquad 3.1.1.42$$

$$r_f^* = \frac{D}{2} - H \cos\beta \qquad 3.1.1.43$$

$$\beta = \alpha_f + \left(\frac{\alpha_i + \alpha_o}{2}\right) - \frac{\pi}{2} \qquad 3.1.1.44$$

Additionally, the moments in the XZ plane must balance. Therefore:

$$\sum_{m=1}^{m=Z} C_m W_m^2 \sum_{K=1}^{K=N} q_{Kmj} \left[K - \tfrac{1}{2}(N+1)\right] - G_j - \left[(r_f^* \cos\beta - (L - L_{cm}) \sin\beta\right] Q_{fj} = 0 \qquad 3.1.1.45$$

Eq. (3.1.1.6, 38, 40, 42, 45) can be solved for the unknown values of U_{mj}, ζ_j, Q_{ij}, ω_j, ω_{oj} and Q_{oj}, if values of bearing ring relative displacements and cage speed are known or assumed.

3.1.1.2 Bearing Ring Loading and Displacements

3.1.1.2.1 Applied Loading

As shown by Figure 1 axial (thrust) loading F_1 can be applied to the bearing along the X-axis. Additionally, radial load applied in the YZ-plane can be resolved into components F2 and F_3 acting along the Y-axis and Z-axis respectively. If axial load is applied at a distance from the X-axis, an overturning moment results, the components of which are F_4 and F_5 in the XZ plane and XY plane respectively. Similarly, moments resulting from eccentrically applied radial loading can be resolved into F_4 and F_5 components.

3.1.1.2.2 Displacements

Owing to applied loading, the bearing inner ring is displaced relative to the outer ring as shown by Figure 7. Five displacements Δi corresponding to the five loading directions are required to define the position, assumed by the inner ring, necessary to achieve an internal distribution of load which equilibrates the applied loading.

Interference

Figure 5 illustrates roller bearing interference at a given azimuth.

$$A_{1j} = \Delta_1 + \frac{1}{2}(e-D)\left(\Delta_4 \left|\cos\varphi_j\right| + \Delta_5 \left|\sin\varphi_j\right|\right) \qquad 3.1.1.46$$

$$A_{2j} = \Delta_2 \sin\varphi_j + \Delta_3 \cos\varphi_j - \frac{1}{2}Pd \qquad 3.1.1.47$$

$$A_j = A_{1j} \sin\left[\frac{1}{2}(\alpha_1+\alpha_2)\right] + A_{2j} \cos\left[\frac{1}{2}(\alpha_1+\alpha_2)\right] \qquad 3.1.1.48$$

A_{1j} is the axial interference, A_{2j} is the radial interference and A_j is the total ring roller interference at the center laminum according to Eq. (3.1.1.6).

3.1.1.2.3 Equilibrium

The bearing applied loads, F_i must equilibrate the summation of the individual rolling element loads according to Eq. (3.1.1.49-53).

$$F_1 = \sum_{j=1}^{j=z} (Q_{zj} \sin\alpha_z + Q_{fj} \sin\alpha_f) \qquad 3.1.1.49$$

$$F_2 = \sum_{j=1}^{j=z} (Q_{zj} \cos\alpha_z - Q_{fj} \cos\alpha_f) \sin\varphi_j \qquad 3.1.1.50$$

$$F_3 = \sum_{j=1}^{j=z} (Q_{zj} \cos\alpha_z - Q_{fj} \cos\alpha_f) \cos\varphi_j \qquad 3.1.1.51$$

$$F_4 = \sum_{j=1}^{j=z} \left\{ \frac{e}{2} Q_{zj} \sin\alpha_z + W_z^2 \cos\alpha_z \sum_{j=1}^{j=z} q_{kzj} \left[K - \tfrac{1}{2}(N+1) \right] + \left(r_f \sin\alpha_f - \tfrac{1}{2} L \cot\alpha_f \right) Q_{fj} \right\} \cos\varphi_j \qquad 3.1.1.52$$

$$F_5 = \sum_{j=1}^{j=z} \left\{ \frac{e}{2} Q_{zj} \sin\alpha_z + W_z^2 \cos\alpha_z \sum_{j=1}^{j=z} q_{kzj} \left[K - \tfrac{1}{2}(N+1) \right] + \left(r_f \sin\alpha_f - \tfrac{1}{2} L \cot\alpha_f \right) Q_{fj} \right\} \sin\varphi_j \qquad 3.1.1.53$$

3.1.1.3 Cage Speed

3.1.1.3.1 Cage Rail/Ring Land Force

Four basic cage types are used in the tapered roller bearing:

1. Roller riding (RR)
2. Inner ring land riding (IRL)
3. Outer ring land riding (ORL)
4. Inner and outer ring land riding "Z" configuration.

These are illustrated schematically by Figure 8. RR cages are usually not used in critical high speed applications. The choice of an IRL, ORL or "Z" cage depends largely upon the application and designer preference. With inner ring rotation, an IRL cage is driven by a force between the cage rail and inner ring land as well as by the rolling elements. ORL cage speed is retarded by cage rail/outer ring land drag force. The "Z" cage is driven at the inner ring and retareded at the outer ring. The magnitude of the drag or drive force between the cage rail and ring land depends upon the resultant of the cage/rolling element loading, the eccentricity of the cage axis of rotation and the speed of the cage relative to the ring on which it is piloted. If the cage rail/ring land normal force is substantial, hydrodynamic short bearing theory (Ref. (14)) might be used to establish the friction force $\bar{F}_{cl}$. For a properly balanced cage and a very small resultant cage/rolling element load, which are assumed here, Petroff's law can be applied to both cage rail-land surfaces; e.g.,

$$\bar{F}_{CL\eta} = \frac{\eta_o W_{cR} C_m D_{cR} (\omega_c - \Omega_m)}{1 - \frac{D_1}{D_2}} \qquad 3.1.1.54$$

where D_2 is the larger of the cage rail and ring land diameters and D_1 is the smaller.

$$\bar{F}_{CL} = \sum_{n=1}^{n=2} \bar{F}_{CL\eta} \qquad 3.1.1.55$$

n = 1 refers to the roller large end side
n = 2 refers to the small end side

3.1.1.3.2 Cage Torque Balance

For steady state operation, the sum of the torques acting on the cage is zero. Therefore:

$$e \sum_{j=1}^{j=Z} Q_{cj} \pm D_{cR} \bar{F}_{CL} = 0 \qquad 3.1.1.56$$

3.1.1.4 Bearing System Solution

For tapered roller bearings, Eq. (3.1.1.49-53) and Eq. (3.1.1.56) can be solved for the displacements Δ_i and cage speed, ω_c. This solution is obtained for a given set of bearing and lubricant temperatures and bearing diametral clearance or end play. As demonstrated in section 3.1.3 diametral clearance is a function of bearing operating temperatures, ring speeds and rolling element loads. It is essential that (1) the temperatures assumed for operating clearance, lubricant film thickness and traction calculations be consistent with actual operating temperatures and (2) that assumed clearance based on assumed rolling element loads be consistent with actual internal loading.

If calculated temperatures and rolling element loads are not consistent with the original assumptions, then the entire calculation or procedure must be repeated using new values of temperature based on the last set of calculated temperatures. This process is continued until a consistent set of kinetic and thermal conditions has been determined.

3.1.2 Temperature Mapping Heat Dissipation Model

At high operating speeds the performance characteristics of rolling element bearings tend to deviate substantially from the characteristics which would be expected based on an extrapolation of slow speed behavior. Cage and rolling element speeds tend to be lower and bearing frictional heat generation tends to be higher than predictions based on slow speed extrapolations. These effects are, at least in part, caused by hydrodynamic forces generated as the lubricant is pushed out of the roller paths and/or is forced to move with the roller set at high speed. These lubricant related forces are highly viscosity dependent and viscosity in turn is highly temperature dependent. The temperature dependence of viscosity is important in both hydrodynamic (HD) and elastohydrodynamic (EHD) lubrication. Accurate temperature predictions result in more accurate viscostiy predictions and thus more accurate friction force and bearing performance predictions.

Temperatures have an additional effect on bearing performance. Radial temperature gradients across the bearing tend to alter the bearing diametral clearance and thus the distribution of loading

among the rolling elements. Axial temperature gradients can cause a pinching of the roller at one end, and thus alter the distribution of load over a roller profile.

The effects of bearing assembly and lubricant temperatures should be an integral part of a bearing dynamic performance analysis when temperature gradients are large. The tapered roller bearing dynamic analysis has provision to account for both of these temperature effects. The operating geometry analysis Section 3.1.3, accounts for the effect of temperature on component dimensions and lubricant viscosity is determined for local lubricant temperatures.

Most bearing analysis precedes bearing manufacture and most bearing tests are not instrumented sufficiently to yield all of the temperatures required for accurate analysis. To allow the extrapolation of experimental temperature data or to allow temperature estimates to be made without experimental information, a temperature mapping heat dissipation analysis has been developed. The analysis uses numerical methods of finite differences as demonstrated by Dusinberre ref. (15). System temperatures are predicted using the frictional heat generation rates calculated by bearing kinetic analysis and consider the following system variables;

- Bearing assembly dimensions and materials
- Ambient air temperature and velocity
- Circulating fluid coolant through the housing
- Lubrication scheme

The numerical method of solution requires the bearing system to be divided into discrete mass segments, each represented by a node point. A map of the nodal points is presented in Figure 9. Figure 9 represents a plane through the bearing axis of rotation, and it is assumed that all the system temperatures may be represented by such a single plane, i.e., the system is symmetric about the bearing axis. High bearing speeds and large lubricant mass flow rates make this assumption reasonably accurate. This assumption implies that each temperature node is a circumferential ring around which no heat may flow.

3.1.2.1 Lubricant Distribution Analysis

The lubricant distribution model is not purported to be the result of a rigorous mass transport analysis. It is a starting point which can be modified and improved as more definitive data become available. It is based on simplifying assumptions, many of which are intuitive. Although the distribution model was developed primarily to give better definition to the thermal analysis and provide a method to optimize a lubrication scheme, it was believed that the concept would prove useful in additional areas of bearing analysis including starvation and transient analyses in which the lubricant supply is terminated.

In high speed, fluid lubricated, rolling element bearings practically full EHD films exist and all frictional heat generation is assumed to result from EHD and HD lubricant shearing. To effectively model the bearing heat dissipation and bearing temperatures by the finite difference method, the temperature grid must be sufficiently fine to represent the real situation. It is obvious that at least three lubricant temperature nodes are required to coarsely represent the heat generated by a tapered roller bearing, ome at each raceway and one at the flange. It was conceived that the lubricant might enter the bearing cavity at four distinct locations; through the inner raceway at both ends of the roller path and by jet to one or both sides of the bearing. Continuity requires at least one node to which all lubricants can flow for exit. Thus, eight lubricant nodes are required as a minimum to define a relatively coarse system. With more than two lubricant nodes which simply define entrance and exit, a model must be developed which apportions the lubricant distribution such that continuity is maintained.

As finally conceived, the tapered roller bearing lubricant node grid has a maximum of 23 nodes, 6 within the bearing which act as the originating points for all of the generated frictional heat. Referring to Figure 9 and 10 these six nodes are numbered 3, 4, 5, 12, 13 and 14. Three nodes represent lubricant entrance to the bearing cavity via jets, nodes 8 and 11, and via the scoop, node 20. The scoop delivers lubricant through flow paths in the shaft and inner ring to both sides of the inner raceway at nodes 15 and 17. Nodes 9 and 10 represent the lubricant which is jetted to but does not enter the bearing. Heat can be convected from the roller ends to these nodes. Nodes 2 and 6 accept all lubricant

which is rejected by or exits from the bearing cavity. Nodes 1 and 7 represent scavenges at which no heat convection takes place.

By its nature the model is complex. In an effort to avoid further complexity, it was decided that the lubricant flow rate to each node would be defined by specifying linear combinations of the lubricant input rates. If this were not done but instead the rollers were allowed to transport lubricant from the outer to the inner race, an iterative solution would be required along with inherent additional complexity. It is necessary therefore that a portion of the lubricant at each and every input node, nodes 8, 11, 15 and 17, be distributed to each of the inner raceway lubricant nodes 12, 13 and 14. All six bearing lubricant nodes will receive some flow since it is assumed that centrifugal force will drive the lubricant at the inner race nodes to their counterparts at the outer races, nodes 3, 4 and 5 respectively. The lubricant flow rate entering the bearing from each of the nodes 8, 11, 15 and 17 is divided into three auxiliary components designated $\dot{M}_{sp}$, $\dot{M}_F$ and $\dot{M}_B$ for the scoop and two components $\dot{M}_{sp}$ and $\dot{M}_B$, for the jets. In a high speed bearing the major portion of lubricant flow is comprised of $\dot{M}_B$. From the jet nodes 8 and 11 $\dot{M}_B$ is defined to be the flow rate of the oil distributed to the nodes at the inner race as a function of the lubricant velocity leaving the jet. The jet velocity reflects the lubricant's ability to penetrate into the bearing. From the through race entrance nodes, 15 and 17, 95 percent of $\dot{M}_B$ enters the lubricant nodes at the edges of the inner race, nodes 12 and 14 respectively. Node 12 accepts all of the frictional heat generated at the roller end flange contacts. 5 percent of $\dot{M}_B$ is assumed to exit the bearing.

From node 15 and 17 $\dot{M}_F$ is distributed to all six of the lubricant nodes within the bearing. From nodes 8, 11, 15 and 17 $\dot{M}_{sp}$ is distributed to the lubricant nodes at the inner race, nodes 12, 13 and 14. $\dot{M}_{sp}$ decreases with increasing cage speed. The effect of high cage speed is to increase the relative amount of lubricant distributed to the inner race lubricant node nearest the jet and results in corresponding decreases in the amount of lubricant reaching the more distant nodes. The same effect is realized with through race lubrication. In addition high speed results in less lubricant distributed to the inner race nodes in favor of the outer race. The lubricant distributed by the terms $\dot{M}_{sp}$ and $\dot{M}_F$ represent the lubricant transported by random splash and surface

wetting. These terms insure that at least a small portion of lubricant is distributed to each and every bearing internal lubricant node from each lubricant inlet source.

A detailed description of the determination of $\dot{M}_B$, $\dot{M}_{SP}$ and $\dot{M}_F$ as well as the flow rates from node to node is presented below. Figures 10.2 and 10.3 give a graphical summary of the lubricant distribution assumptions for the lubricant supplied by under race cooling and for the lubricant supplied by direct jetting respectively.

3.1.2.1.1 Under Race Lubrication

As indicated in Figures 9 and 10, the under race lubrication is admitted to the bearing via a scoop and a set of flow paths; the number of channels which comprise given flow path is specified at input. The scoop efficiency, i.e., that fraction of the lubricant input to the scoop which actually enters the bearing, must be input to the analysis. When both under race flow paths are used, the ratio of the lubricant velocities flowing through paths 1 and 2 is obtained by equating the ratios of the pressure heads developed by the centrifugal pump effect, to the ratios of the negative pressure heads attributable to friction:

$$\frac{V_1}{V_2} = \frac{L_2 D_1^2 (R^2_{EXIT} - R^2_{ENTRANCE})}{L_1 D_2^2 (R^2_{2EXIT} - R^2_{2ENTRANCE})} \qquad 3.1.2.1$$

Where V refers to the lubricant velocity

D refers to the flow path channel diameter
R refers to the radial distance of the flow path entrance and exit points from the shaft centerline.
L is the total length of each respective flow path.

Knowing the ratio of the velocities at which the lubricant is flowing, the ratio of the lubricant mass flow rates may be obtained, referring to Figure 9, 10.1 and 10.2.

$$\psi = \frac{\dot{M}_{20,25}}{\dot{M}_{20,19}} = \frac{V_1 N_1 D_1^2}{V_2 N_2 D_2^2} \qquad 3.1.2.2$$

The designation $\dot{M}_{ij}$ refers to the lubricant mass flow rate from node i to node j. $\dot{M}_{20,19}$ and $\dot{M}_{20,25}$ may be obtained from Eq. (3.1.2.2 and 3). N refers to the number of radial channels spaced around the circumference for each flow path

$$\dot{M}_{20,19} = \epsilon_s \dot{M}_s / (1+\Psi) \qquad 3.1.2.3$$

$$\dot{M}_{20,25} = \epsilon_s \dot{M}_s / (1+\tfrac{1}{\Psi}) \qquad 3.1.2.4$$

$\dot{M}_s$ is the total mass flow rate to the scoop. From Figure 10

$$\dot{M}_{20,6} = (1-\epsilon_s)\dot{M}_s \qquad 3.1.2.5$$

$\dot{M}_{20,6}$ is the rate at which the lubricant is rejected from the scoop.

Continuity requires,

$$\dot{M}_{22,15} = \dot{M}_{20,25} \qquad 3.1.2.6$$

and

$$\dot{M}_{18,17} = \dot{M}_{20,19} \qquad 3.1.2.7$$

From nodes 15 and 17, the under race lubricant is assumed to be distributed symmetrically to the bearing surfaces such that;

$$\frac{\dot{M}_{15,12}}{\dot{M}_{22,15}} = \frac{\dot{M}_{17,14}}{\dot{M}_{18,17}} \qquad \dot{M}_{22,15} \neq 0 \text{ AND } \dot{M}_{18,17} \neq 0 \qquad 3.1.2.8$$

$$\frac{\dot{M}_{15,4}}{\dot{M}_{22,15}} = \frac{\dot{M}_{17,14}}{\dot{M}_{18,17}} \qquad 3.1.2.9$$

Therefore, $\dot{M}_{17,K}$ is fully defined if $\dot{M}_{15,j}$ is fully defined. K and j are symmetric about a surface through nodes 4 and 13.

What follows is an explanation of all $\dot{M}_{15,j}$ mass flow rate terms. To ease the explanation, we will temporarily define a term $\dot{M}$ equal to $M_{22,15}$ and a speed dependent variable S:

$$S = \sqrt{\frac{2g}{e\omega_c^2 + 2g}} \qquad 3.1.2.10$$

The purpose of the variable S is to account for the effect of speed and the centrifugal force field. High speed tends to limit the amount of lubricant which is transported from one side of the inner race to the other. Due to centrifugal force, the major portion of the lubricant is flung to the inside surface of the outer ring and from there flows out of the bearing cavity. As noted earlier, we will define several auxiliary terms:

$$\dot{M}_{SP} \equiv S\dot{M} \qquad 3.1.2.11$$

$$\dot{M}_F \equiv 0.27\,\dot{M}(1-S) \qquad 3.1.2.12$$

$$\dot{M}_B \equiv 0.73\,\dot{M}(1-S) \qquad 3.1.2.13$$

The lubricant flow rates from node 15 to the other nodes within the system are assumed to be given by the following linear combinations of the quantities $\dot{M}_{SP}$, $\dot{M}_F$ and $\dot{M}_B$ with the nodes nearest node 15 receiving proportionately more lubricant than the more distant nodes. Referring to Figure 10;

$$\dot{M}_{15,2} = 0.05\,\dot{M}_B \qquad 3.1.2.14$$

To the outer raceway

$$\dot{M}_{15,3} = 0.333\,\dot{M}_F \qquad 3.1.2.15$$

$$\dot{M}_{15,4} = 0.222\,\dot{M}_F \qquad 3.1.2.16$$

$$\dot{M}_{15,5} = 0.111\,\dot{M}_F \qquad 3.1.2.17$$

To the inner raceway

$$\dot{M}_{15,12} = 0.167\,\dot{M}_F + 0.5\,\dot{M}_{SP} + 0.95\,\dot{M}_B \qquad 3.1.2.18$$

$$\dot{M}_{15,13} = 0.112\,\dot{M}_F + 0.333\,\dot{M}_{SP} \qquad 3.1.2.19$$

$$\dot{M}_{15,14} = 0.055\,\dot{M}_F + 0.167\,\dot{M}_{SP} \qquad 3.1.2.20$$

Examination of Eq. (3.1.2.10-20) and Figure 10.1 and 10.2 reveals that at high speed, the major portion of the under race lubricant entering the bearing cavity at node 15 flows to the large end flange, node 12, and then to the outer race. Relatively small portions of the lubricant are assumed to be splashed or transported to the inner ring surface. As noted earlier, the lubricant flows from nodes 15 and 17 are assumed symmetric one with the other, thus Eq. (3.1.2.10-20) also describe the under race lubricant distribution from the roller small end side of the inner race.

3.1.2.1.2 Jet Lubricant Distribution

Just as the lubricant distribution from nodes 15 and 17 was assumed symmetrical, the distribution from the jets, nodes 8 and 11, is also assumed symmetric. To reduce repetition, only the equations for the distribution from node 11 at the roller small end side of the bearing will be developed.

The lubricant is assumed to be jetted between the cage and the inner ring. However, the lubricant's free access to the bearing cavity is limited by two considerations;

1. The radial gap between the cage and inner ring may be smaller than the jet diameter, and
2. A portion of the annular gap between the cage and inner ring is occupied by the roller ends.

In Eq. (3.1.2.20) the first and second terms account for these respective considerations.

$$\epsilon_J = \left\{ Z \left[\frac{\Delta d \sqrt{D_J^2 - \Delta d^2} + D_J^2 \operatorname{Tan}\left(\frac{\Delta d}{\sqrt{D_J^2 - \Delta d^2}} \right)}{\pi D_J^2} \right] \right\} \left\{ \left[1 - \frac{1.732\,DZ}{\pi (e - D/2)} \right] \right\} \qquad 3.1.2.21$$

It is assumed that the jet is directed at a point midway between the inner raceway and the pitch diameter. ϵ_J is the jet efficiency, defined as the ratio of the amount of lubricant which actually enters the bearing, to the amount which is jetted to the bearing. Dj refers to the jet diameter. Δd is the radial gap between the cage rail I.D. and the inner ring and O.D. Jet efficiency can also be specified at input, in which case Eq. (3.1.2.20) is not used.

The set of auxiliary variables is used to describe the distribution of the under race lubricant and will be redefined in terms of the jet lubricant flow rate $\dot{M}$ which enters the bearing. (Refer to Figure 10.3).

$$\dot{M} = \epsilon_J \dot{M}_J \qquad 3.1.2.22$$

$$\dot{M}_{SP} \equiv (0.18 + 0.82S)\dot{M} \qquad 3.1.2.23$$

where S is defined in Eq. (3.1.2.10)

$$\dot{M}_B \equiv 0.82(1-S)\dot{M} \qquad 3.1.2.24$$

The lubricant flow rate $\dot{M}_B$ is distributed across the bearing inner race according to a function of several variables.

1. The lubricant velocity leaving the jet
2. The cage speed and cage type
3. The bearing geometry

The time available for the jet to penetrate between rollers is given by .

$$\Theta = \frac{2\pi}{\omega_c}\left[\frac{1}{Z} - \frac{0.433D}{e - D/2}\right] \qquad 3.1.2.25$$

A second variable φ is a ratio of the distance the jet can travel during the time Θ, to the length of the roller

$$\varphi = \frac{V_J \Theta}{L} \qquad 3.1.2.26$$

where V_J is the velocity of the jet;

$$V_J = \frac{\dot{M}_J}{\rho A_J N_J} \qquad 3.1.2.27$$

ρ is the lubricant weight density
A_J is the cross sectional area of a jet at the roller small end side
N_J is the number of jets at the roller small end side.

If the cage is outer race guided, φ is limited to 1. If the cage is inner race guided, φ is limited to 0.666. The distribution of the lubricant from the jets at the roller small end side of the bearing to the nodes at the inner race may now be determined as follows:

For $0.75 < \varphi \leq 1.0$

$$\dot{M}^*_{11,12} = \left(1 - \frac{3}{4\varphi}\right)\dot{M}_B \qquad 3.1.2.28.1$$

$$\dot{M}^*_{11,13} = \frac{1}{2\varphi}\dot{M}_B \qquad 3.1.2.29.1$$

$$\dot{M}^*_{11,14} = \frac{1}{4\varphi}\dot{M}_B \qquad 3.1.2.30.1$$

for $0.25 < \varphi \leq 0.75$

$$\dot{M}^*_{11,12} = 0. \qquad 3.1.2.28.2$$

$$\dot{M}^*_{11,13} = \left(1 - \frac{1}{4\varphi}\right)\dot{M}_B \qquad 3.1.2.29.2$$

$$\dot{M}^*_{11,14} = \frac{1}{4\varphi}\dot{M}_B \qquad 3.1.2.30.2$$

for $0.0 < \varphi \leq 0.25$

$$\dot{M}^*_{11,12} = 0 \qquad 3.1.2.28.3$$

$$\dot{M}^*_{11,13} = 0 \qquad 3.1.2.29.3$$

$$\dot{M}_{11,14} = \dot{M}_B \qquad 3.1.2.30.3$$

The flow rates in the three equations Eq. (3.1.2.28, 29 and 30) are supplemented by additional flow rates which are not related to the velocity of the lubricant leaving the jet. This is done to insure that some lubricant reaches nodes 12 and 13 even if the jet velocity is insufficient to penetrate to these nodes. These flow rates are assumed as follows:

$$\dot{M}^{**}_{11,12} = \frac{1}{6}\dot{M}_{SP} \qquad 3.1.2.31$$

$$\dot{M}^{**}_{11,13} = \frac{1}{3}\dot{M}_{SP} \qquad 3.1.2.32$$

$$\dot{M}^{**}_{11,14} = \frac{1}{2}\dot{M}_{SP} \qquad 3.1.2.33$$

and

$$\dot{M}_{11,j} = \dot{M}^{*}_{11,j} + \dot{M}^{**}_{11,j} \quad j = 12, 13, 14 \qquad 3.1.2.34$$

The lubricant flow rate which is jetted to, but does not directly enter the bearing, is

$$\dot{M}_{11,10} = (1-\epsilon_J)\dot{M}_J \qquad 3.1.2.34$$

3.1.2.1.3 Free Lubricant Distribution

The distribution of the lubricant from the jets and from the under race entrance points has been examined. It remains to define the flow rates from the inner ring to the outer ring nodes and finally from the outer ring nodes to the scavenges.

All of the lubricant which has flowed to a given inner race node is assumed to leave the node by flowing radially outward to the corresponding node at the outer race.

$$\dot{M}_{12,3} = \sum_{i=8}^{i=17} \dot{M}_{i,12} \qquad 3.1.2.36$$

$$\dot{M}_{13,4} = \sum_{i=8}^{i=17} \dot{M}_{i,13} \qquad 3.1.2.37$$

$$\dot{M}_{14,4} = \sum_{i=8}^{i=17} \dot{M}_{i,14} \qquad 3.1.2.38$$

The flow of the lubricant out of the bearing along the outer race is governed first by the presence or absence of scavenges. Referring to Figure 10, if scavenges exist at both sides of the bearing, the lubricant flow direction for a tapered roller bearing is assumed, from node 5 to 4 to 3 to 2 to 1 and from 6 to 7. If on the other hand, scavenges exist only at one side of the bearing, all of the flow is toward that side. The scavenges are represented in the system by nodes 1 and 7.

It is significant to note that the rate at which lubricant enters a given lubricant node can be determined simply by:

$$\dot{M}_i = \sum_{j=1}^{j=28} \dot{M}_{j,i} \qquad 3.1.2.39$$

All $M_{j,i}$ terms not specifically defines are set to zero.

3.1.2.2 Heat Dissipation and Temperature Mapping

At steady state conditions, heat generation rates are constant and for a given temperature node, heat flow to a node must equal heat flow from the node. Referring to Figure 9;

$$\sum_{j=1}^{j=69} \dot{Q}_{j,i} + \dot{Q}^*_i - \dot{Q}_{KA} = 0 \qquad \begin{matrix} i = 1-69 \\ K = 28-32 \end{matrix} \qquad 3.1.2.40$$

$\dot{Q}_{j,i}$ refers to heat flow from neighboring temperature nodes. The subscripts j,i indicated flow from node j to node i.
$\dot{Q}^*_i$ refers to the frictional heat which is generated at node i
$\dot{Q}_{KA}$ refers to heat transfer with ambient air.

All $\dot{Q}_{j,i}$ and $\dot{Q}_{KA}$ terms are temperature dependent. This enables the system of equations, developed from Eq. (3.1.2.40) to be solved for the individual nodal temperatures.

3.1.2.2.1 Heat Sources

As noted earlier, the heat sources in this model are all assumed to result from hydrodynamic or elastohydrodynamic friction

forces, i.e., lubricant shear.

A segment of the bearing containing one roller contains five sources of frictional heat generation. Three of these are calculated on the basis of EHD lubricant shear. The hydrodynamic friction results from the rollers plowing through the lubricant and also from the cage rotating centrically on the inner and/or outer ring land.

3.1.2.2.1.1 EHD Frictional Heat Generation Rate

For a given roller in a tapered roller bearing there exists three EHD lubricated contacts. The frictional heat generation rates in these contacts may be obtained by combining Eq. (3.1.1.18 and 32) for the raceway contacts:

$$\dot{H}_{mj} = \frac{2 W_m}{J} \sum_{k=1}^{k=N} V_{kmj}\, b_{kmj} \int_0^t \tau_{kmj}\, dt \qquad 3.1.2.41$$

$m = 1$ refers to the outer raceway contact $m = 2$ to the inner raceway. Eq. (3.1.1.19 and 33) may be combined to obtain the heat generation rates for each roller end flange contact.

$$\dot{H}_{fj} = \frac{a_{fj} b_{fj} V_{fj}}{J} \int_{-1}^{+1} \int_{-\sqrt{1-s^2}}^{+\sqrt{1-s^2}} \tau_{fj}\, dt\, ds \qquad 3.1.2.42$$

In the above equations J converts heat generation rates in lbf-in/sec to BTU/Hr.

The assumed axial symmetry allows heat to be input to the model as though the heat were generated at a single segment, such that for the three EHD contacts;

$$\dot{H}_m = \sum_{j=1}^{j=2} \dot{H}_{mj} \qquad 3.1.2.43$$

m = 1 Outer Race
m = 2 Inner Race
m = 3 Flange

3.1.2.2.1.2 Roller Drag

The rollers, as they orbit within the bearing cavity, displace and shear the lubricant and thus generate heat according to the semi-empirical relationship from Ref. 4 (refer to Eq. 3.1.1.34).

$$\dot{H}_a = \frac{z\rho D L C_d \bar{e}^3 \omega_c^{2.76}}{16gJ} \qquad 3.1.2.44$$

If there is a substantial amount of lubricant within the bearing cavity, and the cage orbital speed is high $\dot{H}_a$ has been found to be several times higher than the sum of all heat generated in the EHD contacts.

3.1.2.2.1.3 Cage Drag

Assuming negligible cage rail to ring land force, the frictional heat generated at the cage rail-ring land contacts may be estimated by Petroff's equations as follows:

$$\dot{H}_s = \sum_{n=1}^{n=2} \frac{\eta_o (|\omega_m| - |\omega_c|)^2 A_n d_n}{\Delta d_n J} \qquad 3.1.2.45$$

where the subscript 1 refers to the roller large end side of the bearing and 2 refers to the small end side. A is the area at the cage rail/ring land interface. d is the land diameter and Δd is the radial gap between the cage rail and ring land.

3.1.2.2.2 Frictional Heat Distribution

The lubricant churning heat Eq. (3.1.2.44) is assumed to be generated primarily as the roller set pushes the bulk lubricant around the outer raceway, thus the churning heat is distributed to the three lubricant nodes at the outer race. Also, it is assumed that the amount of churning heat distributed to each of the three lubricant nodes is proportional to the amount of lubricant at each of the three nodes. The total lubricant per hour at a given outer raceway node j is given by:

$$\dot{M}_j = \sum_{i=1}^{i=25} \dot{M}_{ij} \qquad 3.1.2.46$$

A proportionality constant Kn can be developed.

$$K_n = \frac{\dot{M}_n}{\sum_{k=3}^{k=5} \dot{M}_k} \qquad n = 3, 4, 5 \qquad 3.1.2.47$$

Heat from all sources is distributed according to Eq. (3.1.2.48-52.2)

$$\dot{Q}_4^* = \tfrac{1}{2}\dot{H}_1 + K_4\dot{H}_4 \qquad 3.1.2.48$$

$$\dot{Q}_{13}^* = \tfrac{1}{2}\dot{H}_2 \qquad 3.1.2.49$$

For an outer ring land riding cage, Fig. 8;

$$\dot{Q}_K^* = K_K\dot{H}_4 + \tfrac{1}{4}(\dot{H}_1 + 2\dot{H}_5)\quad K=3,5 \qquad 3.1.2.50.1$$

$$\dot{Q}_{12}^* = \dot{H}_5 + \tfrac{1}{4}\dot{H}_2 \qquad 3.1.2.51.1$$

$$\dot{Q}_{14}^* = \tfrac{1}{4}\dot{H}_2 \qquad 3.1.2.52.1$$

For an inner ring land riding cage:

$$\dot{Q}_K^* = \tfrac{1}{4}\dot{H}_1 + K_K\dot{H}_4 \quad K=3,5 \qquad 3.1.2.50.2$$

$$\dot{Q}_{12}^* = \dot{H}_3 + \tfrac{1}{4}\dot{H}_2 + \tfrac{1}{2}\dot{H}_5 \qquad 3.1.2.51.2$$

$$\dot{Q}_{14}^* = \tfrac{1}{4}\dot{H}_2 + \tfrac{1}{2}\dot{H}_5 \qquad 3.1.2.52.2$$

For the "Z" configuration cage $\dot{Q}_K^*$ is defined as follows:

$\dot{Q}_3^*$ by Eq. (3.1.2.50.2)

$\dot{Q}_5^*$ by Eq. (3.1.2.50.1)

$\dot{Q}_{12}^*$ by Eq. (3.1.2.51.2)

$\dot{Q}_{14}^*$ by Eq. (3.1.2.52.1)

3.1.2.2.3 Heat Transfer

3.1.2.2.3.1 Ambient Convection and Radiation

For the housing external surface, considering convection and radiation ref. (16) gives,

$$\dot{Q}_{KA} = 0.848\, W D^{0.75} (T_K - T_A)^{1.25} + 0.543\, DW e \left[\left(\frac{T_K+460}{100}\right)^4 - \left(\frac{T_A+460}{100}\right)^4\right] \qquad 3.1.2.53$$

$K = 28-32$

T - refers to temperature in degrees Farenheit
w - refers to the nodal cylindrical surface width-feet
D - refers to the diameter of the surface-feet
e - is the housing emmissivity.
$\dot{Q}_{KA}$ - is the heat flow rate in BTU/Hr.

Eq. (3.1.2.53) may be modified by miltiplication of the entire right hand side by Φ to account for forced convection at the housing. According to the data of ref. (17);

$$\Phi = 1 + \frac{V_A^{0.666}}{T_K^{0.321}} \qquad 3.1.2.54$$

where V_A is the air velocity in ft/sec.

3.1.2.2.3.2 Conduction

Between adjacent nodes in the (bearing, shaft, housing) assembly, heat is transferred by conduction such that;

$$\dot{Q}_{ij} = \frac{A_{ij} K}{L_{ij}} (T_j - T_i) \qquad 3.1.2.55$$

A_{ij} is the area of normal to the heat transfer path between nodes i and j, ft^2
L_{ij} is the linear distance between nodes i and j, ft
K is the thermal conductivity of the material between nodes i and j, BTU/ft Hr°F

If, between nodes, heat must flow serially through two distinct materials having thermal conductivities K_1 and K_2 and thicknesses L_1 and L_2 then an equivalent heat transfer coefficient must be determined such that:

$$Q_{ij} = \lambda_{ij} (T_j - T_i) \qquad 3.1.2.56$$

and

$$\lambda_{ij} = A_{ij}\left(\frac{K_1 K_2}{L_1 K_1 + L_2 K_2}\right) \qquad 3.1.2.57$$

Note: $\lambda_{ij} < \frac{A_{ij} K_1}{L_1}$ and $\lambda_{ij} < \frac{A_{ij} K_2}{L_2}$ and the distance between nodes is $L_{ij} = L_1 + L_2$

If, between nodes, heat must flow through parallel paths of two distinct materials having thermal conductivities K_1 and K_2 and areas normal to heat flow of A_1 and A_2, then an equivalent heat rransfer coefficient λ is calculated such that;

$$\lambda_{ij} = \frac{1}{L_{ij}} (A_1 K_1 + A_2 K_2) \qquad 3.1.2.58$$

Note: that the cross sectional area normal to heat flow is

$A_{ij} = A_1 + A_2$ $\lambda_{ij} > \frac{A_1 K_1}{L_{ij}}$ and $\lambda_{ij} > \frac{A_2 K_2}{L_{ij}}$

3.1.2.2.3.3 Convection

Eq. (3.1.2.59) describes the convective heat transfer between two adjacent temperatures nodes, one in the assembly, node j, and one in the lubricant or fluid coolant, node i.

$$Q_{ij} = A_{ij} h_{ij} (T_{mi} - T_j) \qquad 3.1.2.59$$

h - is the convective heat transfer coefficient. BTU/(hr ft^2 °F).

Tm - is the mean temperature of the lubricant at node i defined as follows:

$$T_{Mi} = \frac{1}{2}\left[T_i + \frac{\sum_{K=1}^{K=25} \dot{M}_{Ki} T_K}{\sum_{K=1}^{K=25} \dot{M}_{Ki}} \right] \qquad 3.1.2.60$$

A - is the heat transfer area normal to heat flow ft^2.

Three relationships for the convective heat transfer coefficient are used in this analysis.

1. Laminar flow in the coolant and in each under race flow path.
2. Laminar flow in the housing and on the shaft.
3. Turbulent flow within the bearing cavity.

3.1.2.2.3.3.1 Laminar Flow in Tubes

For Laminar flow within the helically wound outer ring coolant tube and also for the under race lubricant flow paths, Eq. (3.1.2.61) from ref. (18) is adapted to describe the heat transfer coefficient.

$$h = 1.86 \frac{K}{D} \left(\frac{\eta_b}{\eta_w} \right)^{0.14} \left(\frac{4\dot{M} C_p}{\pi K L} \right)^{1/3} \qquad 3.1.2.61$$

Where D is the flow path diameter, ft

L is the flow path length, ft
M is the fluid mass flow rate
Cp is the fluid specific heat
η is the fluid dynamic viscosity. The subscript b refers to the evaluation of the viscosity at the fluid bulk temperature W refers to wall temperature.
K is the fluid thermal conductivity BTU/Hr-ft °F

Of the terms within Eq. (3.1.2.61) K, cp and η are temperature dependent. However the temperature dependenceof K and Cp is weak, therefore, the values of K and Cp are determined for the lubricant based only on the inlet temperature. From ref. (19);

$$C_p = \frac{0.388 + 0.00045\,T}{\gamma_{60}} \qquad 3.1.2.62$$

$$K = \frac{0.0676}{\gamma_{60}}\left[1 - .0003\,(T-32)\right] \qquad 3.1.2.63$$

Where γ_{60} is the lubricant specific weight at 60°F.

Eq. (3.1.2.62 and 63) are valid for typical lubricating oils.

Since the housing coolant may be any fluid, the coolants thermal conductivity, specific heat, and viscosity are input to the model.

To simplify Eq. (3.1.2.61), the term $(\eta_b/\eta_w)^{0.14}$ is set to 1.0. This is justified since T_b and T_w will not be substantially different. Also, with such a small exponent on the viscosity ratio, even if T_w is several hundred degrees higher than T_b such that (η_b/η_w) is 5, $5^{0.14}$ is only 1.25.

3.1.2.2.3.3.2 Laminar Flow Unrestricted

There are nodes within the assembly adjacent to which the lubricant is not forced to move at high speed. Referring to Figure (9), these nodes are numbered 1, 2, 6, 7, 8, 11 and 20. At these nodes, an adaptation of the convective heat transfer coefficient for laminar flow over a flat plate is used such that:

$$h = 0.332\,K\,Pr^{1/3}\left(\frac{\rho\,\omega_c}{g\,\eta}\right)^{1/2} \qquad 3.1.2.64$$

$\frac{\rho\,\omega_c}{g\,\eta}$ must have units of ft^2 when K has units of BTU/Hr-ft°F ω_c must be set to its absolute value. Pr represents the dimensions prandtl number, defined as:

$$Pr = \frac{\eta' CP}{K} \qquad 3.1.2.65$$

must be expressed in units of lb/hr-ft.

3.1.2.2.3.3.4 Turbulent Flow

Referring again to Figure 9 , the lubricant at nodes 3, 4, 5, 12, 13 and 14 is forced to travel over the bearing internal surfaces at relatively high speeds. The bulk lubricant is assumed to be carried between rollers at the cage rotational speed.

Determining the Reynolds number for a 120 mm bore tapered roller bearing lubricated with a MIL-L-23699 lubricant at 363°K (200°F), rotating at a shaft speed of 12500 rpm, a Reynolds number may be estimated from Eq. (3.1.2.66) to be, 7.5 X 10^5, well into the range of turbulent flow.

$$NRe = \frac{LV\rho}{\eta g} = \frac{e^2 \omega_c \rho}{4 \eta g} \qquad 3.1.2.66$$

In the turbulent region Kent, ref. (16), gives Eq. (3.1.2.67) to describe the convective heat transfer coefficient for oil.

$$h = C \frac{V}{\eta^{1\,0.63}} \qquad 3.1.2.67$$

V - is the relative lubricant/surface velocity ft/sec.
has units of lb/hr-ft
C is a constant having a value of 122 if the lubricant is being heated or 91.5 if the lubricant is being cooled.
h has units of BTU/hr-ft^2-°F. Inspection of Eq. (3.1.2.67) indicates that typical convection heat transfer coefficients for oil in turbulent flow are of the order of 5000 BTU/hr-ft^2-°F. Coefficients of this magnitude effectively help bring the bearing surface temperatures into near equilibrium with the adjacent lubricant temperature.

Eq. (3.1.2.64) and Eq. (3.1.2.67) are viscosity dependent and as stated earlier, viscosity is temperature dependent. The temperature viscosity relationship assumed, is:

$$\eta = e^{\left[\ln \eta_1^* - (\ln \eta_1^* - \ln \eta_2^*) \frac{(\ln T_1^* - \ln T_m)}{(\ln T_1^* - \ln T_2^*)}\right]} \qquad 3.1.2.68$$

Where η_1^*, T_1^* and η_2^*, T_2^* are input to the analysis. η_1^* is the lubricant viscosity at temperature T_1^* and η_2^* is the viscosity at T_2^* both at atmospheric pressure.

3.1.2.2.3.3.5 Heat Flow by Mass Transfer

Heat transfer between fluid temperature nodes occurs entirely through mass transport. It is necessary to develop an additional temperature, T_{Ii}, for each node in the lubricant, which is the temperature of the lubricant entering a given node.

$$T_{Ii} = \frac{\sum_{j=1}^{j=25} \dot{M}_{ji} T_j}{\sum_{j=1}^{j=25} \dot{M}_{ji}} \qquad 3.1.2.69$$

Values of $\dot{M}_{ji}$ are determined by the lubricant distribution analysis. With T_{Ii} thus defined Eq. (3.1.2.60) may be simplified

$$T_{Mi} = \frac{1}{2}\left(T_i + T_{Ii}\right) \qquad 3.1.2.70$$

Within the lubricant, the rate of heat transfer, from all nodes, to node i is given by $\dot{Q}_{ji}$ such that

$$\dot{Q}_{ji} = C_P \sum_{j=1}^{j=25} \dot{M}_{ji} T_j \qquad 3.1.2.71$$

3.1.2.2.4 System Boundary Conditions

A portion of the system boundary conditions has already been mentioned i.e., the ambient air temperature and velocity. In addition, the temperatures at the shaft and housing ends must be specified. If the effective shaft and housing widths are suitably long, the end temperatures may be set to the ambient air temperature. If these widths are short, the end temperatures must be estimated. Specification of boundary temperatures in this way allows the bearing and lubrication system to be a heat sink.

The remaining boundary conditions are the lubricant and coolant mass flow rates and temperatures at input.

3.1.2.2.5 Heat Dissipation

In addition to determining all assembly and lubricant temperatures, the thermal model also yields the rates of heat dissipation via:

- Lubricant
- Radiation and convection to ambient air
- Outer ring housing coolant
- To the shaft and housing end, nodes.

3.1.2.3 Significant System Temperatures

For use within the bearing dynamic analysis four lubricant temperatures are required.

The temperature of the lubricant at the flange is taken to be the temperature at node 12, at the outer raceway node 4, and at the inner raceway node 13, the bulk temperature, i.e. the mean lubricant temperature within the cavity is given by Eq. (3.1.2.73)

$$T_{MEAN} = \frac{\sum_{K=3}^{K=5} \dot{M}_K T_K}{\sum_{K=3}^{K=5} \dot{M}_K} + \frac{\sum_{K=12}^{K=14} \dot{M}_K T_K}{\sum_{K=12}^{K=14} \dot{M}_K} \qquad 3.1.2.73$$

As noted in Section 3.1.3 on operating geometry an effective temperature must be calculated for all assembly components. For instance, the equivalent temperature of the inner ring portion of section S1, refer to Fig. 9 and 11, is given by

$$\bar{T}_{IS1} = \frac{\sum_{K=49}^{K=51} T_K + \sum_{K=56}^{K=58} T_K}{6.} \qquad 3.1.2.74$$

3.1.2.4 Closure

The thermal analysis provides temperatures throughout the bearing assembly and lubricant. The analysis is easily adaptable to ball and cylindrical roller bearings. For all bearing types the analysis is meant to model high speed bearing operation where full EHD films are expected, the assumption of axial symmetry is valid.

3.1.3 Bearing Geometry Change Analysis From Cold Unmounted to Mounted Operating Conditions

3.1.3.1 Introduction

As a bearing is taken from the shelf, mounted in a housing and on a shaft, turned up to speed and subjected to operating loads and temperature, the internal geometry of the bearing will change. To accurately analyze the dynamic performance of a bearing, its operating geometry must be known. An analysis has been developed to account for the following effects:

1. Temperature changes and gradients.
2. Initial and operating shaft and housing fits.
3. Rotation induced ring radial growth.
4. Uniform radial components of the rolling element-raceway normal loads.

In conducting the analysis each bearing ring is conceptually divided into two parts by a radial plane perpendicular to the axis of rotation. These planes pass through the center of each raceway rolling path. By considering changes in roller path radii for the two sections the change in raceway contact angles and therefore the amount of roller pinching, as well as the change in bearing diametral clearance can be estimated.

The basis for the major portion of this analysis is taken from Timoshenko, ref. 20 . The bearing rings are treated as thick walled circular cylinders of constant wall thickness subjected to the action of uniformly distributed internal and external pressure.

The external pressure arises in the case of the outer ring from a press fit into the bearing housing. The internal pressure on the outer ring arises from the discrete roller loads which are regarded as uniform internal pressure acting on the outer ring. Similarly for the inner ring the press fit on the shaft provides a uniform internal pressure and the roller loads are regarded as a uniform external pressure. Fig. 11.1 shows the idealized sections used in the analysis.

3.1.3.2 Bearing Shaft and Housing Equivalent Sections

Timoshenko's analysis requires that a ring be fully defined by specification of only internal and external radii. If two concentric rings are pressed together the analysis assumes that the rings are of equal width. Referring to Fig. 11.2 it is obvious that the outside surface of the actual inner ring section can not be defined by a single radius. However, a single radius may be found such that the cross sectional areas of the real and equivalent rings are equal.

The equal area criterion may be applied to all four assembly aections S1, S2, H1 and H2. Fig. 11.1 presents the equivalent sections for a tapered roller bearing assembly. Assembly refers to the bearing shaft and housing components.

A second significant dimension associated with each of the four ring sections is the radius of the roller path at each section. Ultimately, it is the change in these four roller path radii, in addition to a change in the rolling element diameter, which permit a change in the bearing diametral clearance and a change in the inner and outer ring contact angles to be calculated. These radii are shown on Fig. 11.1 and are the radii to the actual inner and outer ring roller paths.

The bearing geometry change problem requires the solution to similar problems for each of the four bearing sections. To help eliminate repetition and cumbersome subscripting, only section S1, will be covered thoroughly. However, differences in analysis which occur from section to section will be noted.

3.1.3.3 Internal and External Equivalent Pressures

Each of the four sections consists of either a solid or hollow shaft and inner ring and outer ring and housing respectively. The rings may or may not be in intimate contact. Intimate contact occurs when due to any of several factors, the outside radius of the inside ring is greater than the inside radius of the outside ring. A pressure is developed at that interface, which tends to expand the outside ring and collapse the inside ring. Although the pressure acting on the actual interfering surfaces are identical, the use of equivalent geometrical sections requires the use of equivalent pressure, such that the calculated pressure acting to collapse the inside ring will not be identical to the

pressure acting to expand the outside ring.

The equivalent pressure concept allows the effect of unequal component width to be considered as well as the effect of shaft and housing shoulders. Both of these effects tend to increase the bearing seat stiffness above the value which could be determined by considering only the shaft and housing diameters at the bearing seats.

The effect of unequal inner ring and shaft width is the same for both sections S1 and S2. The same is true for the outer ring and housing section H1 and H2. This effect is taken into account by the factor X which applies to the pressure where, referring to Fig. 11.2

$$0.5 \leq \left(X_S = \frac{w_I}{w_S}\right) \leq 2. \qquad (3.1.3.1)$$

$$0.5 \leq \left(X_H = \frac{w_O}{w_H}\right) \leq 2. \qquad (3.1.3.2)$$

Where w denotes the element width and the subscripts I, O, S and H refer to inner, outer, shaft and housing respectively.

The effect on equivalent pressure resulting from shaft and housing shoulders is applicable at sections and housing shoulders is applicable at sections S1 and H2 and is accounted for with the factor Y. Referring to Fig. 11.2

$$Y_{S2} = Y_{H1} = 1. \qquad (3.1.3.3)$$

$$Y_{S1} = \left[\left(\frac{b^2+a^2}{b^2-a^2} - \xi_S\right) \Big/ \left(\frac{d^2+a^2}{d^2-a^2} - \xi_S\right)\right] \qquad (3.1.3.4)$$

$$Y_{H2} = \left[\left(\frac{g^2+f^2}{g^2-f^2} + \xi_H\right) \Big/ \left(\frac{g^2+h^2}{g^2-h^2} + \xi_H\right)\right] \qquad (3.1.3.5)$$

Where ξ is Poisson's ratio.

Assuming multiplicative effects;

$$P_{s_o} = \overline{X}_s Y_s P_{I_i} \qquad (3.1.3.6)$$

$$P_{H_i} = \overline{X}_H Y_H P_{o_o} \qquad (3.1.3.7)$$

where P_{s_o} denotes the pressure on the shaft O.D. as related to the pressure on the inner ring P_{I_i}, P_{H_i} and P_{o_o} are similarly defined. The pressures (P) in Eq. (3.1.3.6 and 7) are non zero only if an interference fits exists at the section in question. An interference fit may exist under cold mounted conditions but due to thermal gradients and high speed rotation, clearance may develop at operating conditions.

To account for the elastic effect of the uniform radial components of the rolling element loads on the ring dimensions, an equivalent inner ring external pressure and outer ring internal pressure are calculated based on the minimum radial component of the rolling element loads, such that for the inner ring;

$$P_{I_o} = \frac{Z\,(Q_{1,J} \cos \alpha_{1,J})_{MIN}}{2\pi\, C\, W_I} \qquad (3.1.3.8)$$

where Z is the total number of rolling elements

$Q_{i,j} \cos \alpha_{i,j}$ is the smallest rolling element raceway radial load component at the inner raceway

W_I is the inner ring total width.

The external pressures thus calculated are assumed equal on both inner ring sections. An expression corresponding to Eq. (3.1.3.8) can be developed for the internal pressure acting to expand the outer ring. In fact, for a tapered roller bearing, P_{I_o} will exist only when the applied load is predominantly

axial or the bearing is preloaded, but the internal pressure acting on the outer ring, P_{o_i} , will always exist to some extent, as a result of rolling element centrifugal force.

3.1.3.4 Temperature Effects

The effect of temperatures which occur at operating conditions is considered in two ways. A bulk effect based on the radii to the rolling paths (R) is calculated from Eq. (3.1.3.9)

$$U = R \alpha \bar{T} \qquad (3.1.3.9)$$

where

U - is the change in rolling path radius

α is the component coefficient of thermal expansion,

$\bar{T}$ - is the difference between the component effective temperature and 68°F.

A similar expression may be written for the change in roller diameter. Referring to Fig. 9 for Section S1;

$$\bar{T}_{SI} = \frac{\left[\sum_{K=49}^{K=51} T_K + \sum_{K=56}^{K=58} T_K\right]}{6} - 68^\circ F \qquad (3.1.3.10)$$

$$\bar{T}_{S_S} = \frac{\left[\sum_{K=56}^{K=58} T_K + \sum_{K=63}^{K=65} T_K\right]}{6} - 68^\circ F \qquad (3.1.3.11)$$

The second effect of temperatures is the change in interference fit from cold to operating conditions such that the interference fit as a result of the initial fit and the temperature difference between the two components can be calculated. Cold (293°K, (68°F)), shaft and housing fits Fcold are input to the analysis. A positive value reflects an interference fit. The analysis neglects asperity crushing, and, the fits for both sections of a given ring are assumed to be identical referring to Fig. 11 for section S1; the fit $(F_{HOT})_{S1}$ at operating temperature is given by

$$(F_{HOT})_{S1} = (F_{COLD})_{S1} + 2b\left(\alpha_S \bar{T}_{S_1} - \alpha_i \bar{T}_{I_1}\right) \qquad (3.1.3.12)$$

F_{hot} is the fit considering operating temperatures.

3.1.3.5 Ring Radial Displacement Considering Surface Pressures

At this point we consider the problem of evaluating thick walled cylinder, (ring) radial displacements as a function of the ring radial dimensions, physical properties, and uniform internal and external pressures. Timoshenko develops Eq. (3.1.3.13) for determining the ring/radial displacement (U), as a function of a general radius (r) to any point within the ring when considerations of ring rotation are omitted.

$$\frac{d^2U}{dr} + \frac{1}{r}\frac{dU}{dr} - \frac{U}{r^2} = 0. \qquad (3.1.3.13)$$

The general solution to this equation is

$$U = K_1 r + \frac{K_2}{r} \qquad (3.1.3.14)$$

The expression for normal stress in the ring is given by:

$$\sigma_r = \frac{E}{1-\varphi}\left[K_1\left(1+\varphi\right) - K_2\left(\frac{1-\varphi}{r^2}\right)\right] \qquad (3.1.3.15)$$

The constants of integration K_1 and K_2 can be determined from Eqs. (3.1.3.16 and 17) which make use of the boundary conditions at the inner and outer surfaces of the ring. Note that the dimensions of inner ring sections S1, Fig. 11.1, are used in Eq. (3.1.3.16-19). These equations, however, are general expressions and are valid for all rings.

$$(\sigma_r)_{r=c} = -P_{I_o} = \frac{E_I}{1-\varphi_I^2}\left[K_1\left(1+\varphi_I\right) - K_2\left(\frac{1-\varphi_I}{c^2}\right)\right] \qquad (3.1.3.16)$$

$$(\sigma_r)_{r=b} = -P_{I_i} = \frac{E_I}{1-\varphi_I^2}\left[K_1\left(1+\varphi_I\right) - K_2\left(\frac{1-\varphi_I}{b^2}\right)\right] \qquad (3.1.3.17)$$

Where E and ξ are the modulus of elasticity and Poisson's ratio respectively. The negative sign associated with P_{I_o} and P_{I_i} reflect the sign convention, wherein a positive normal stress indicates tension. Solving Eqs. (3.1.3.16-17) for K_1 and K_2 and substituting the results into Eqs. (3.1.3.14 and 15) gives the general expressions for normal stress and radial deflection as functions of the internal and external pressures acting on the ring:

$$\sigma_r = \frac{b^2 P_{I_i} - c^2 P_{I_o}}{c^2 - b^2} - \frac{(P_{I_i} - P_{I_o}) c^2 b^2}{r^2 (c^2 - b^2)} \qquad (3.1.3.18)$$

$$U_{IR} = \frac{1 - \xi_I}{E_I} r \frac{b^2 P_{I_i} - c^2 P_{I_o}}{c^2 - b^2} + \frac{1 + \xi_I}{r E_I} \left[\frac{b^2 c^2 (P_{I_i} - P_{I_o})}{(c^2 - b^2)} \right] \qquad (3.1.3.19)$$

Using the appropriate dimensions and pressures, Eq. (3.1.3.19) can express the inward displacement of the shaft and the outward displacement of the inner ring when assembled with a interference fit F_{HOT}.

$$U_{Ib} - U_{Sb} = F_{HOT} \qquad (3.1.3.20)$$

$$U_{Ib} = \frac{1 - \xi_I}{E_I} b \left(\frac{b^2 P_{I_i} - c^2 P_{I_o}}{c^2 - b^2} \right) + \frac{1 + \xi_I}{b E_I} \left[\frac{b^2 c^2 (P_{I_i} - P_{I_o})}{(c^2 - b^2)} \right] \qquad (3.1.3.21)$$

$$U_{Sb} = \frac{-b P_{S_o}}{E_S} \left[\frac{a^2 + b^2}{b^2 - a^2} - \xi_S \right] \qquad (3.1.3.22)$$

P_{S_i} and P_{H_o} are assumed zero. Using Eq. (3.1.3.8) to obtain P_{I_o}, the following expression may be developed for P_{I_i} which accounts for all variables in the interference fit problem exacept for the effect of ring and shaft rotation.

$$P_{Ii} = \frac{F_{HOT} + 2\left(\frac{1-\xi_I}{E_I}\right)\left(\frac{bc^2 P_{Io}}{c^2-b^2}\right)}{\left(\frac{1-\xi_I}{E_I}\right) b\left(\frac{b^2+c^2}{c^2-b^2}\right) + \frac{b\Sigma Y}{E_S}\left(\frac{a^2+b^2}{b^2-c^2} + \xi_S\right)} \quad (3.1.3.23)$$

Note, P_{Ii} may not be negative, i.e. the effect of fitting one ring on another can not result in placing the common surfaces in tension.

Having determined P_{Ii} and P_{Io}, Eq. (3.1.3.19) may be used to determine $U_{IR(F,Q)}$ by replacing the general radius (r) with the radius to the roller path, R. $U_{IR(F,Q)}$ is defined as the change in rolling path radius resulting from:

- The initial fit
- The change in fit resulting from a temperature gradient
- The effect of the rolling element load.

3.1.3.6 Ring Rotation

We must now examine the effect on the rolling path which results from high speed rotation. If the rotational speed is less than 100 rpm the rolling path radius is assumed to be unaffected.

Timoskenko presents Eq. (3.1.3.24) to define ring displacement U in terms of a general radius (r), the weight density of the ring material, (ρ), and the ring angular velocity (Ω)

$$\frac{d^2U}{dr^2} + \frac{1}{r}\frac{dU}{dr} - \frac{U}{r^2} + \left(1-\xi^2\right)\frac{\rho\Omega^2 r}{gE} = 0 \quad (3.1.3.24)$$

Using the notation;

$$N = \left(1-\xi^2\right)\frac{\rho\Omega^2}{gE} \quad (3.1.3.25)$$

the general solution to Eq. (3.1.3.24) may be written:

$$U = -N\frac{r^3}{8} + K_1 r + \frac{K_2}{r} \qquad (3.1.3.26)$$

The general expression for the normal stress is given by:

$$\sigma_r = \frac{E}{1-\xi^2}\left[\frac{-3+\xi}{8} N r^2 + (1-\xi)K_1 - (1-\xi)K_2\frac{1}{r^2}\right] \qquad (3.1.3.27)$$

Using Eqs. (3.1.3.26 and 27) and the principle of superposition, the effects of ring rotation can be considered. In this case, superposition allows a set of integration constants K_1 and K_2 to be calculated for a ring based on a change in pressure (P*) at the internal and external surfaces. Eq. (3.1.3.27) may be written for the four specific surfaces of section S1, as follows;

Inner Ring External Surface

$$\frac{E_I}{1-\xi_I}\left[\frac{-3+\xi_I}{8} N_I c^2 + (1+\xi_I)K_{1I} - (1-\xi_I)K_{2I}\frac{1}{c^2}\right] = -P^*_{Io} = 0 \qquad (3.1.3.28)$$

Inner Ring Internal Surface

$$\frac{E_I}{1-\xi_I}\left[\frac{-3+\xi_I}{8} N_I b^2 + (1+\xi_I)K_{1I} - (1-\xi_I)K_{2I}\frac{1}{b^2}\right] = -P^*_{Ii} \qquad (3.1.3.29)$$

Shaft External Surface

$$\frac{E_S}{1-\xi_S}\left[\frac{-3+\xi_S}{8} N_S b^2 + (1+\xi_S)K_{1S} - (1-\xi_S)K_{2S}\frac{1}{b^2}\right] = -P^*_{So} \qquad (3.1.3.30)$$

Shaft Internal Surface

$$\frac{E_S}{1-\xi_S}\left[\frac{-3+\xi_S}{8} N_S a^2 + (1+\xi_S)K_{1S} - (1-\xi_S)K_{2S}\frac{1}{a^2}\right] = -P^*_{Si} = 0 \qquad (3.1.3.31)$$

From Eq. (3.1.3.6)

$$P^*_{So} = \bar{X}\bar{Y}P^*_{Ii} \qquad (3.1.3.32)$$

An additional useful relationship derived from Eq. (3.1.3.26) defines the difference δ^* between the inner ring and shaft displacement at their common surface, as a result of their rotational speed, in terms of the four integration constants of Eq. (3.1.3.28-31).

$$K_{1I}b + \frac{K_{2I}}{b} - N_I\frac{b^3}{8} - K_{1S}b - \frac{K_{2S}}{b} + N_S\frac{b^3}{8} = \delta^* \qquad (3.1.3.33)$$

Under press fit conditions $\delta^* = 0$.

We will now examine the application of Eq. (3.1.3.28-31) in determining the ring behavior as a function of rotational speed.

The following conditions might be encountered.

1. A tight fit remains tight
2. A tight fit loosens
3. A loose fit remains loose
4. A loose fit tightens

For all four conditions, $P^*_{Si} = 0.$ and $P^*_{Io} = 0.$, i.e. it is assumed that no change in pressure occurs at the internal surface of the shaft or the external surface of the inner ring resulting from ring rotation. Also Ω_I and Ω_S are identical. All four of the integration constants K_{1I}, K_{2I}, K_{1S} and K_{2S} are unknowns. Also, either the change in pressure P^*_{Ii} or the rotational speed, Ω embodied in N_I and N_S are additional unknowns.

Now the formulations of Eq. (3.1.3.28-33) are presented which are required to solve each of the four conditions. Since the equations refer to section S1, the variable $U_{IR_{S1}}$ will be written as U.

3.1.3.6.1 Situation 1 and 2, Initially Tight Fit

In addition to the integration constants, P_{Ii}^* is the unknown, where P_{Ii}^* is the change in inner ring internal pressure resulting from the rotational speed. If P_{Ii}^* is less than P_{Ii} from Eq. (3.1.3.23), situation 1 is realized. The operating fit pressure is the difference between P_{Ii} and P_{Ii}^* and the fit remains tight. The resulting radial displacement at the inner ring roller path is given by:

$$U_\Omega = -N_I \frac{R^3}{8} + k_{1I} R + \frac{k_{2I}}{R} \qquad (3.1.3.34)$$

and the total change in roller path radius at section S1 is given by:

$$U_{TOT} = U_{(F,Q)} + U_T + U_\Omega \qquad (3.1.3.35)$$

U_T is the change in rolling path radius which occurs as a result of a temperature change from 68°F.

If P_{Ii}^* is greater than P_{Ii} the solution to the problem requires several additional steps. Eq. (3.1.3.28), must be re-solved to determine the rotational speed, Ω_{TL} at which the change in fit pressure is just equal to the initial fit pressure and $\delta^* = 0$. This rotational speed is termed the tight fit speed limit and is subscripted with the letter (TL). Using the integration constants thus determined and Eq. (3.1.3.26), U_{TL} may be determined.

Note, the subscripts in parenthesis should be interpreted as follows: The first subscript refers to the state of the initial fit (T-tight) or(L-Loose), the second subscript refers to the rotational speeds (T-Total) or (L-Limit). For instance, U_{TL} refers to the change in inner ring rolling path radius due to the rotational speed at which the initially tight shaft fit is lost.

After determining U_{TL} Eqs. (3.1.3.28-31) are resolved twice for the four integration constants, with P_{Ii}^* set to zero. First, for the full rotational speeds, yielding U_{LT} and then for the tight fit speed limit, yielding U_{LL} . This is accomplished by change in the values of N_I and N_S through a change in the value of Ω in Eq. (3.1.3.25). Utilizing super-position, the change in rolling path radius resulting from rotation is given by Eq. (3.1.3.36).

$$U_\Omega = U_{TL} + (U_{LT} - U_{LL}) \qquad (3.1.3.26)$$

Eq. (3.1.3.26) is presented graphically in Fig. 12. Then is calculated from Eq. (3.1.3.25).

3.1.3.6.2 Situations 3 and 4 Initially Loose Fit

The integration constants K_{1I}, K_{2I}, K_{1S}, and K_{2S} are unknowns. P_{Ii}^*, P_{Io}^*, P_{Si}^* and P_{So}^* are all set to zero, and only Eqs. (3.1.3.28-31) are solved. Using the integration constants thus obtained, Eq. (3.1.3.33) is solved for δ^*. If $\delta^* < |F_{HOT}|$ where F_{HOT} is negative, the loose fit remains loose at operating conditions. The constants K_{1I} and K_{2I} are used to calculate U_Ω . Using Eq. (3.1.3.25), U_{TOT} is calculated. If $\delta^\heartsuit > |F_{HOT}|$, the shaft has expanded further under the effects of rotation than the inner ring, and the initially loose fit becomes tight. This requires additional solutions to Eqs. (3.1.3.28-33).

δ^* is set equal to F_{HOT} and the equations are solved for the integration constants plus the speed at which the initially loose fit becomes tight Ω_{LL}. Using the integration constants K_{1I} and K_{2I} along with Eq. (3.1.3.37), U_{LL} is determined. Eq. (3.1.3.28-33) are again resolved twice at Ω_{LL} and Ω_{LT} for P_{Ii}^* and the integration constants, after setting $\delta^\heartsuit$ to zero. U_{TL} and U_{TT} can be obtained by from Eq. (3.1.3.34) using the two sets of integration constants. The operating fit pressure is then given by;

$$P_{Ii} = P_{Ii\,TT}^* - P_{Ii\,TL}^* \qquad (3.1.3.37)$$

$$U_\Omega = U_{LT} + (U_{TT} - U_{TL}) \qquad (3.1.3.38)$$

and Eq. (3.1.3.35) is used to determine U_{TOT} . Where U_{TOT} represents the total change in the radius to the rolling path of section S1 as the bearing is taken off the shelf at 68°F, mounted on the shaft subjected to load and rotated up to operating speed.

3.1.3.7 Bearing Geometry Changes

The preceeding sections dealt primarily with section S1. However, the equations presented are valid for all four of the assembly sections. For each section a value is determined for U_{TOT} , cold fit pressure, operating fit pressure and the speed at which an initially tight fit loosens. The changes in bearing geometry are calculated by combining the U_{TOT} terms from all four sections.

As noted earlier, Eq. (3.1.3.9) can be used to determine this change in rolling element diameter such that:

$$U_{R\bar{T}} = D(\alpha \bar{T})_R \qquad (3.1.3.39)$$

The change in bearing diametral clearance is given by

$$\Delta Pd = \left[U_{H1} + U_{H2} - U_{S1} - U_{S2} - 2U_{R\bar{T}}\right] \qquad (3.1.3.40)$$

where TOT is omitted from the subscript. The change in contact angle at the outer raceway is given by:

$$\Delta\alpha_o = \mathrm{Tan}^{-1}\left[\frac{2\cos\alpha_o'(U_{H1}-U_{H2})}{L\cos(\alpha_R/2)}\right] \qquad (3.1.3.41)$$

At the inner raceway:

$$\Delta\alpha_i = \mathrm{Tan}^{-1}\left[\frac{2\cos\alpha_i(U_{S1}-U_{S2})}{L\cos(\alpha_R/2)}\right] \qquad (3.1.3.42)$$

3.1.4 Bearing Fatigue Life

Bearing raceway L_{10} fatigue life, at a given laminum as determined by Lundberg-Palmgren, ref. 21 is expressed by Eq. (3.1.4.1).

$$L_{10mk} = \left[\frac{QC_{mk}}{Q_{emk}}\right]^4 \times 10^6 \text{ REV} \qquad (3.1.4.1)$$

QC_{mk} is the raceway laminum dynamic capacity, defined as the load for which the laminum will have a 90 percent assurance of surviving 1 million revolutions. m refers to raceway, k refers to laminum, from ref. 21 .

$$QC_{mk} = 30100 * \left[D_k \quad (1 \pm \gamma \cos\alpha_m)\right]^{1.0740741} W_m^{0.777778} \qquad (3.1.4.2)$$
$$(\gamma \cos\alpha_m)^{0.22222} \Big/ \left[Z*(1 \pm \gamma \cos\alpha_m)\right]^{0.25}$$

The upper sign is used for the outer race, the lower sign refers to the inner race.

Q_{emk} is the raceway laminum equivalent load.

$$Q_{emk} = \left[\frac{1}{Z}\left(\sum_{j=1}^{j=Z} Q_{mkj}^{\epsilon}\right)\right]^{1/\epsilon} \qquad (3.1.4.3)$$

Q_{mkj} is the individual roller contact load. On the k-th laminum and $\epsilon = 4.0$ or $\epsilon = 4.5$ depending respectively upon whether the applied load rotates or is stationary with respect to the raceway in question.

Substitution of Eq. (3.1.4.3) into Eq. (3.1.4.1) yields

$$L_{10mk} = \frac{1}{\left[\frac{1}{Z}\sum_{j=1}^{j=Z}\left(\frac{Q_{mkj}}{Q_{cmk}}\right)^{\epsilon}\right]^{4/\epsilon}} \times 10^6 \text{ REV} \qquad (3.1.4.4)$$

Since a unique lubricant film thickness can be determined for each roller/raceway contact, a unique lubricant life multiplier a_3 is inserted into Eq. (3.1.4.4) to yield

$$L_{10mK} = \frac{Z^{4/\epsilon}}{\left[\sum_{j=1}^{j=2}\left(\frac{Q_{mKj}}{Q_{cmK}}\right)^{\epsilon}\frac{1}{(a_{3m_j})^{\epsilon/4}}\right]^{4/\epsilon}} \times 10^6 \text{ cycles} \qquad (3.1.4.5)$$

The a_3 factor is a function of the EHD contact lubricant film thickness. Tallian, ref. 22 and Skuaka, ref. 23 , have defined the lubrication-life effect in terms of the lubricant film thickness/surface roughness ratio.

$$\Lambda_{m_j} = \frac{h_{m_j}}{\sigma_m} \qquad (3.1.4.6)$$

h is the lubricant film thickness and σ is the composite raceway roller surface roughness.

$$\sigma_m = \sqrt{\sigma'^2_{ROLLER} + \sigma'^2_{RACEWAY}} \qquad (3.1.4.7)$$

The fatigue life data presented herein use the mean between the Tallian-Skurka data as shown by Fig. 13.

The L_{10} life of a raceway is given by

$$L_{10m} = \left[\sum_{K=1}^{K=N}\left(\frac{1}{a_{2m}L_{10mK}}\right)^{9/8}\right]^{-8/9} \qquad (3.1.4.8)$$

a_2 is a material factor. Background into the use of the material factor is presented in ref. 24 . For ease of comparison, the L_{10} life data presented herein, represent an a_2 factor of 1.0.

The bearing fatigue life is given by

$$L_{10} = \left[\sum_{m=1}^{m=2}\left(L_{10_m}\right)^{-9/8}\right]^{-8/9} \frac{166667}{N_{RPM}} \text{ HOURS} \qquad (3.1.4.9)$$

N is the absolute value of the difference between the inner and outer ring speeds in rpm.

3.2 Analytical Procedure

Presently, the greatest value of computer program AE71Y001 is its ability to compare the relative performance of several bearing design or lubrication schemes as the bearing operates under identical load and speed conditions. The program was used in this manner in the bearing optimization phase of this effort.

Use of SKF Computer Program AE71Y001 requires prior definition of the following conditions.

- Bearing design geometry and shaft housing dimensions
- Applied load and/or outer ring angular misalignment
- Shaft and/or housing rotational speed
- Lubricant type, flow rate, input temperature, density, and tabulated viscosity temperature and pressure data
- Ambient thermal conditions.

3.2.1 Bearing Optimization Study Objectives

(1) Based upon successful performance reported in the literature the maximum roller end-flange Hertz stress must not exceed 3.11×10^9 N/M^2, (45,000 psi)

(2) For the given bearing section height and width, fatigue life is maximized to the extent that objective (1) allows.

(3) Bearing heat generation rates must not exceed the bearing and lubrication system's ability to dissipate the heat while maintaining a maximum lubricant temperature of 422°K (300°F) and/or a maximum component temperature of 450°K (350°F).

The bearing design was optimized for the maximum NASA supplied load conditions as presented in Enclosure 1.

- Axial load 53378 N (12000 lb)
- Radial load 26689 N (6000 lb)
- Shaft speed 12500 rpm

- Lubricant input temperature 340°K (195°F)
- Maximum lubricant flow rate 0.017 $\frac{M3}{min}$ (4.5 gal/min)

3.2.2 Roller End-Flange Contact (REFC) Performance Limitations

Computer program AE71Y001 generates the following data which describes the REFC performance for each roller:

- Contact load
- Maximum Hertz stress
- EHD film thickness
- Coefficient of friction
- Heat generation rate
- Rolling and sliding speeds
- Lubricant, flange and roller temperature.

It remained to determine operational limits of the above variables which permit acceptable performance.

Data on sliding speed and smearing load was presented by Cocks et. al. Ref. (25). This data, when extrapolated to the conditions of lower stress and higher temperature and sliding speeds, applicable in the phase of study, indicated that smearing would not occur as long as lubricant supply was adequate.

More recently, Conners et. al. ref. (5) presented data on 25 mm bore tapered roller bearings which were operated at REFC Hertz stresses to 2.69×10^9 N/m^2 (39,000 psi) and at a flange linear speeds to 148 m/sec (3136 oft/min). Data from ref. (5) indicated that satisfactory performance could be obtained at the values of Hertz stress and sliding speed, required as long as the lubricant is readily available to the contacts.

Lemanski, ref. (6), has provided additional data with which roller end flange contact performance could be evaluated. The data

is for a 95.3 mm (3.75 inch) bore bearing operating at 16000 rpm, resulting in a flange linear speed of 101.6m/sec (20,000 ft/min) versus 107 m/sec (21,000 ft/min) for the bearing proposed. Hertz stress values ranged from 1.93×10^9 to 3.65×10^9 N/m2 (28,000 to 53,000 psi) which corresponds very closely to the stress levels encountered in this study. A MIL-L-7808G lubricant was used in the ref. (6) experimental work as compared to the more viscous MIL-L-23699 used in this analysis.

Lemanski's experimental results at a flange linear speed of 101.6m/sec indicate successful REFC performance at the following conditions.

- Hertz stresses from 2.07×10^9 to $3.58 \times 10^9 N/m^2$ (30,000 psi to 52,000 psi).

- Lubricant flow rates of 98 Kg/Hour (215 lb/hour) introduced through the race to the roller large end flange and 47 Kg/hr (105 lb/hr) introduced by jet at the roller small end side.

The data from all three sources were used to establish a basis to judge the roller end flange performance at the various contact angles examined in the optimization study. In particular, a maximum Hertz stress level of $3.1 3 \times 10^9$ N/m2 (45,000 psi) was used as the limiting criteria. Sliding and flange linear speeds encountered in this study have been successfully exceeded in the referenced tests.

3.2.3 Phase I - Preliminary Design Considerations

At the outset of the design study it was anticipated that outer ring contact angle would have two prime effects on bearing performance which would have to be considered in selecting an optimum bearing design.

1) With increasing contact angle bearing raceway fatigue life was expected to increase.

2) The operating conditions at the roller end flange contact (REFC) were expected to become more severe as contact angle increased.

Fatigue life was expected to increase with contact angle due to the two to one ratio of the applied axial to radial load and the reduced roller race normal loads which would result at high-contact angles. The operating conditions at the REFC were expected to become more severe. As contact angle increases the bearing apex length decreases; the REFC principal radii decrease and as a result the Hertz stress increases. Outer ring contact angle the number of rollers and roller dimensions had to be established which would fit within the limits of bearing radial section height and width and in addition, would provide maximum load carrying capacity. An analysis was developed for this purpose and is presented in Appendix A.

Using the methods of appendix A a unique set of roller dimensions, large end diameter, length included angle and number of rollers were determined for various contact angles ranging from 12° to 28°. This data is presented in Table 1.

3.2.4 Outer Ring Contact Angle Determination

Using computer program AE71Y001 and the bearing designs as determined by the methods of Appendix A, bearing performance analyses were made for outer raceway contact angles of 12, 16, 18, 20, 22, 24 and 28 degrees. Fig. (14-17) present the relevant data with which the bearing contact angle was selected. This data was generated using a roller sphere end radius of 90 percent of the apex length for all designs and a constant lubricant temperature of 364°K (195°F).

From Fig. 14, bearing fatigue life increases with increasing contact angle due to the decrease in roller raceway normal loads, apparent from Fig. 15.

Fig. 16 presents a relatively complete picture of the roller end contact performance. REFC Hertz stress increases rapidly with increasing contact angle. Film thickness remains fairly constant. Fig. 17 presents the bearing frictional heat generation rates which increase with increasing contact angle.

Utilizing the data of Figs. (14-17) nominal outer raceway contact angle of 24° was selected as the best compromise between maximizing fatigue life and maintaining an REFC Hertz stress level below 3.11×10^9 N/m^2 (45000 psi).

3.2.5 Cage Design

As a part of this design study, consideration of an optimum lubrication scheme played a prime role. A large quantity of lubricant within the bearing cavity serves only to increase frictional heat generation and to cause increased slip in the roller raceway contacts by increasing the drag force on the rollers.

Efficient lubrication necessitates getting the lubricant to the bearing contacts which must be lubricated and then removing the lubricant as quickly as possible. The "Z" cage, Fig. 8, was selected because it does not impede efficient lubrication.

The "Z" cage is guided by the inner ring land at the roller large end side of the bearing and by the outer race at the small end side. This configuration permits relatively free entrance of jetted lubricant at the small end between inner ring land and cage. Since centrifugal force will drive the lubricant to the outer raceway once it is in the bearing, it is certainly beneficial to aim the jet at the inner raceway. Centrifugal force and the outer raceway taper tend to drive the lubricant to the large end side of the outer race. As a result, undesirable lubricant churning may be minimized if the lubricant is free to exit from the bearing at that point. The "Z" cage allows this to occur since the cage is inner ring land riding at the large end.

3.2.6 Bearing Manufacturing Considerations

The basic roller configuration as presented in Table I for the 24° outer raceway contact angle was reviewed by bearing design specialists who finalized the design, making certain that the bearing could be manufactured and that it would conform to accepted design principles. It was stipulated that the cage be of the "Z" configuration. The following design changes resulted from this review.

1) The roller length was reduced from 33.934 to 27.742 mm (1.3360 to 1.0922 inches)

2) The roller large end diameter was increased from 23,564 to 23.609 mm (0.9277 to 0.9295 inches)

3) The roller included angle was increased from 5° 36' to 5° 40'

4) The number of rollers was increased from 19 to 20.

The "Z" cage was primarily responsible for the most important of these design changes, the reduction of roller length. For this reason, an inner ring land riding cage was examined.

As noted previously, the Z cage was chosen for its ability to permit easy entrance of a jet stream between the cage rail I.D. and the inner ring land O.D. at the small end side of the bearing. An inner ring land riding cage severely limits the jet target and perhaps could cause a lubricant starved condition at the roller small end side of the bearing. Two alternatives exist to circumvent this situation;

1) Introduce lubricant through the race to the undercut at the roller small end side of the inner race.

2) To scavenge the lubricant only at the large end side. The latter may result in inefficient lubrication, and thus was not considered further.

A design review considering through race lubrication to the small end undercut, revealed that undercuts at both the large and small ends of the inner race would have to be substantially over sized in order to guarantee proper placement of the lubrication holes. This situation was caused by the large tolerance stack up alloted to ring machining dimensions. The decrease in inner raceway effective length resulting from the large undercuts approached the reduction in roller length required by the "Z" cage. The "Z" cage was thus retained in the final design.

3.2.7 Roller End Flange Contact Lubrication and Geometry

The roller end flange geometry is of substantial importance in the high speed tapered roller bearing. Since that contact has been shown to be most prone to failure.

The data and conclusions of ref. (5, 6 and 25) all support the need for a copious supply of lubricant at the flange roller end contact. For this reason through race lubrication to the undercut at the roller large end side of the inner race is specified for the proposed optimum design. The through race flow hole diameter and spacing is in accordance with the methods of ref. (6). The amount of lubricant to be supplied will be discussed subsequently.

Also of prime importance in maximizing the chances of survival of the REFC is the roller end geometry. Historically a roller end sphere radius (R_{SPH}) between 95 and 100 percent of the bearing apex length has been used. However, Lemanski encountered problems at high speed operation using an R_{SPH} equal to 97 percent of the Apex length and found optimum results with R_{SPH} equal to 80 percent of Apex. Conners used an R_{SPH} equal to 75 percent of Apex in his tests.

Using Archard's EHD film thickness equation, Lemanski plotted REFC film thickness versus K where:

$$K = \frac{R_{SPH}}{APEX} \qquad 3.2.1$$

He found maximum film thickness between K = 0.75 and 0.80.

Archard developed a term ϕ in his film thickness equation to express the effect of side leakage in an elliptical contact.

$$\phi = \left[1 + \frac{2\bar{R}_y}{3\bar{R}_z}\right]^{-1} \qquad 3.2.2$$

where y is the direction of translation. For a typical line contact $\bar{R}_z$ is infinite and $\phi = 1$. In his theoretical derivation Archard applied an exponent on ϕ of 0.74 in his film thickness equation. However, in his experimental work he found that an exponent of 0.93 yielded a better fit of theoretical to experimental data. As indicated by Eq. (3.1.1.26) the exponent 0.93 has been used in this analysis.

Lemanski's determination of a maximum film thickness at K between 0.75 and 0.80 can be explained by expressing $\bar{R}_y$ and $\bar{R}_g$, Eq. (3.1.1.28 and 3.1.1.29) in terms of K-Apex and then solving the expression dh/dK for K, h is the lubricant film thickness. Using the exponent of 0.74, K is found to be 0.754. With the ϕ exponent of 0.93, K is found to be 0.66.

Lemanski's findings suggest experimental justification for use of a K value less than the historical value of 0.95 to 1.00. Archard's film thickness equation also suggests justification.

Computer Program AE71Y001 was used to obtain data on the roller end flange contact performance characteristics as a function of K for the proposed optimum bearing design. These data are presented in Fig. 18. Based on this data and the experimental results of ref. (5) and (6) the roller end sphere radius equal to 82.5 $\pm$ 2.5 percent of the Apex length was chosen for the proposed bearing design.

3.2.8 Optimum Tapered Roller Bearing Thermal Performances

Of prime interest in this effort was the development of a model to predict the thermal performance of the tapered roller bearing including the effects of the lubrication input and scavenge system.

The bearing-shaft-housing assembly dimensions used in the thermal portion of the analysis are shown in Fig. 19 . The thermal boundary and lubrication conditions studied are shown in Fig. 20. A schematic of the lubrication distribution schemes studied is presented in Fig. 21.

The thermal analysis section 3.1.2 was used to evaluate the various lubricant flow rates to the bearing by jet to the roller small end; and by through race lubrication to the large end undercut. In generating these data the assumption was made that the amount of lubricant within the bearing cavity could be represented as a function of total lubricant flow rate according to Eq. (3.2.3)

$$P = 0.1 + 25.0 \times 10^{-6} \dot{M} \qquad 3.2.3$$

Where P is the decimal fraction of lubricant in the cavity and $\dot{M}$ is the total lubricant input rate to the bearing. Normally P and M are separate inputs to the computer program. This assumption is believed to be conservative, i.e. the heat generation rate predictions which result from the assumption will be high rather than low. Thus, if the assumption is not totally accurate, less rather than more lubricant should be required to maintain desirable system temperatures.

The proposed bearing lubrication scheme consists of lubricant input to the undercut at the large end side of the inner race and by jets to the small end side of the bearing between the cage rail I.D. and the inner ring land O.D. The lubricant is scavenged at both sides of the bearing. With this lubrication scheme, an optimum amount and ratio of through race to jet lubrication was sought. Figs. 22-29 present the heat generation rate and lubricant temperatures at the flange, inner raceway, outer raceway and the average lubricant temperature which results from the various flow rates and flow ratios.

Figs.(21-25) indicate that a jet lubricant flow rate of approximately 340 kg/hr (750 lb/hr) is required to maintain the majority of the lubricant temperatures between 394 and 422°K (250 and 300°F). Only 66.2 percent of the lubricant jetted to the small end side is calculated to enter the bearing. 33.8 percent is rejected to the scavenge. The lubricant input through the race to the large end undercut effectively cools the flange, Fig. 19. However, it is not well distributed throughout the bearing. Fig. 22 indicates that a through race flow rate of 227 kg/hr (500 lb/hr) is sufficient to maintain the temperature of the lubricant at the flange to a desirable 394°K (250°F). The shape of the curves representing the temperature versus through race flow rate in Fig. 22-25 indicate that the cooling ability of the through race lubrication tends to become nominal above a flow rate of 227 Kg/hr. Referring to Fig. 21.2, the lubricant distribution model assumes that the major portion of the lubricant enters at the undercut and moves to the outer race node 3 and then exits from the bearing. Only nominal amounts of lubricant are assumed to be distributed to nodes, 4, 5 13 and 14.where frictional heat is being generated. Referring to Fig. 21.1 only 66.2 percent of the lubricant which is jetted to the bearing is assumed to enter. However, that which does enter is assumed to be better distributed over the inner race than when the lubricant enters through the race.

Fig. 23-24 indicate that despite less lubricant actually in the bearing, a better distribution of the lubricant results in lower lubricant temperatures at inner and outer raceways with jet as opposed to through race lubrication at flow rates greater than 272 kg/hr 600 (lb/hr).

The data presented in Figs. 26-29 was generated to determine the effectiveness of introducing the lubricant via. jets at the small end side of the bearing, versus introducing it directly to the large end flange. Difference in lubricant temperatures at the same total flow rate was used as the measure of effectiveness. Each curve has been generated by holding one of the lubricant input rates constant at 227 kg/hr (500 lb/hr) while varying the other from 56.7 to 227 kg/hr (125 to 500 lb/hr), in increments of 56.7 kg/hr. Along any line parallel to the ordinate the total lubricant flow rate is identical, ranging from 283.5 to 453.6 kg/hr (625 to 1000 lb/hr). The difference in temperature from curve to curve is thus a function only of the method used to introduce the lubricant.

Figs. 27 and 28 show lubricant temperatures at the small end of the inner and outer raceways as well as the center and indicate lower temperature at the small end side of the raceways resulting with increased jet lubrication.

With the beneficial effects realized at the small side of the raceway, the relatively uniform and low temperatures throughout the bearing cavity, and the requirement for lubricant at the small end of the outer raceway for cage lubrication, lubricant flow rates of 227 kg/hr (500 lb/hr) via. jet and through the race were selected for optimum lubrication.

3.2.9 Geometry Change at Operating Conditions

In the optimization study, the geometry change analysis was used to obtain changes in bearing geometry which would be manifested at operating conditions.

A cold shaft fit of 0.114 mm (0.0045 in) tight and a line to line housing fit were assumed. With the recommended lubrication scheme and flow rates, at the heavy load condition, two significant changes in geometry were noted.

1) Changes in raceway and roller diameters result in a decrease in bearing diametral clearance of 0.089 mm (0.0035 in). More appropriate to tapered roller bearings, this corresponds to a reduction in shaft end play of 0.1119 mm (0.0044 in).

2) The outer raceway contact angle is expected to increase by 2.2 minutes and the inner raceway contact angle is expected to decrease by 0.2 minutes.

Sufficient bearing end play must be built into the bearing, shaft housing assembly such that at operating conditions the bearings do not become axially preloaded.

The indicated changes in bearing contact angle would result in a pinching across the small end of the roller. This condition can be alleviated by the bearing design. The optimum bearing design thus has a specified outer raceway contact angle 2.4 minutes less than nominal.

3.3 Analytical Results

Since, in the bearing optimization study, results of one phase were needed to proceed to the next phase a good portion of the analytical results have been presented in the Analytical Procedure Section. However, those results not previously noted are presented herein.

3.3.1 Bearing Material, Lubricant Film Thickness and Bearing Fatigue Life

As noted, in Section 3.1.4 on fatigue life analysis, a multiplicative factor is applied to raceway fatigue life to include the effects of material and lubrication. Throughout, the material factor was set to one. However, as noted, the effect of lubrication as determined by the Λ ratio, varied with EHD film thicknesses. In the preliminary studies in which an optimum contact angle was being sought, the lubricant temperature was set to 364°K (195°F). The resultant inner and outer raceway film thicknesses were typically 127 x 10^{-9} mm (50 microinches) with a Λ ratio of approximately 7, and the life multiplier was 2.85. In the later studies in which the lubricant temperature

was approximately 394°K (250°F), the film thickness dropped to (68.6 x 10^{-9} m) 27 microinches yielding a Λ ratio of 3.85. However, the life multiplier dropped only to 2.58. This data indicates that nearly full EHD films exist in the roller raceway contacts with the proposed design at the proposed lubricant flow rates. Also, a substantial increase in bearing life can not be expected with increasing lubricant film thickness beyond approximately 76.2 x 10^{-9} m (30 microinches).

3.3.2 Contact Load and Cage Slip

The effect of raceway normal loads on cage slip can be noted in Fig. 15. The high contact loads which occur at the 12° contact angle result in the cage speed deviating from epicyclic by less than 1 percent. As the raceway normal loads decrease with increasing contact angle, cage speed deviation from epicyclic is 6.9 percent at 28°. Cage speed deviation from epicyclic (cage slip) is indicative of slip within the roller inner raceway contacts. This slip explains the increase in contact heat generation rates with increasing contact angle evident in Fig. 17.

The decrease in churning heat generation with increasing contact angle simply reflects the decrease in roller frontal area.

The effect of reduced contact loads on cage slip can also be seen in Fig. 30. Fig. 30 is a plot of percentage cage slip versus applied radial load for the proposed bearing. The data of Fig. 30 was generated in order that the performance of the optimum bearing design could be examined at the low and midpoint of the load spectrum with a lubricant flow rate of 454Kg/Hr (1000 lb/Hr), half entering the bearing via. the small end jets and half through the inner ring to the large end undercut, the relatively light loading results in substantial skidding in the inner raceway-roller contacts. The high slip rates under the low load-high speed condition are indicative of too much lubricant within the bearing cavity. This finding indicates

(1) That in order to have the bearing run at an acceptable slip rate, (less than 10 percent), the lubricant supply will have to be reduced with possible higher temperatures resulting.

(2) The relationship used to calculate roller drag Eq. (3.1.1.34) is not totally accurate or the assumed relationship between lubricant flow rate and the amount of lubricant with the cavity Eq. (3.2.3) is not totally accurate.

Most likely, both situations (1) and (2) are true.

The bearing lives at the light and medium load conditions are presented in Fig. 31. These lives include the effect of reduced roller centrifugal force caused by the high slip rates.

4.0 DISCUSSION OF RESULTS

Two prime results have emerged from this effort. The capabilities of computer program AE71Y001 have been enhanced and refined such that it is now a powerful tool for the kinematic and thermal performance analysis of high speed tapered roller bearings.

The second prime result is the proposed optimum tapered roller bearing design, developed by means of the computer program. The complete bearing design is presented in Enclosure 2. The performance characteristics for the bearing with the proposed optimum design and lubrication scheme is presented in Table II.

The plots in Fig. 14-18 which were used in determining the optimum bearing contact angles are discontinuous at an angle between 20° and 22°. Appendix A, which was used to determine the roller geometry at each contact angle, contains three criteria to limit roller size; tests T_1, T_2 and T_3. At a given contact angle, the roller fully utilizes the dimensions of only two of the tests. Roller size was limited at outer raceway contact angles by tests T_1 and T_2, below and including 20°. Tests T_1 and T_3 limited size at angles above and including 22°. This change in criteria appears to be the cause for the discontinuities.

It became apparent from the study that both on the basis of a bearing's load carrying capability and lubrication requirements, a bearing design which would perform optimally at high load conditions, would not necessarily be the design chosen at lower load conditions, especially if the ratio between axial and radial loads were different at the high and low load conditions. The bearing design optimization was directed only at the high end of the load spectrum presented in Enclosure 1. It was reasoned that any bearing which would perform under the most severe load conditions would also perform satisfactorily at lower load conditions. The inverse is probably not true.

Computer program AE71Y001 is capable of analyzing two identical bearings mounted on the same shaft, such that an axial load in either direction will be taken by one or the other bearing. This study, as required, considered only a single bearing. Use of the data in Fig. 30 and 31 was generated using applied radial load only, since the axial loads required to keep the bearing together under the radial load were unknown. In general, only a two bearing system is capable of accepting applied

loading in five distinct directions. Computer program AE71Y001 is capable of analyzing the two bearing assembly, but this capability was not used in this study.

As noted in the introduction, the principle value of computer program AE71Y001 is its ability to compare various bearing designs and lubrication schemes as the bearing operates under identical loading and operating speed conditions. The program's ability to predict absolute magnitudes of bearing performance parameters particularly in the area of heat generation rates and system temperatures must be evaluated as experimental data becomes available. The lubrication scheme and lubricant flow rates recommended will be only as accurate as the assumptions and relationships used in determining heat generation rates and the lubricant distribution. However, as mentioned, the recommended flow rates are believed to be conservative. Even though conservative, the recommended flow rates are well within the system limits as specified in Enclosure 1.

5.0 CONCLUDING REMARKS AND PROPOSED FUTURE EFFORTS

Consistent with the objectives of this effort an analytical method has been developed to predict the thermal and kinetic performance of lubricated tapered roller bearings subject to combined loading. This analysis, [redacted] computer program AE71Y001, provides the user with a powerful tool to analyze new bearings designs (as shown by the bearing optimization study) and to trouble-shoot problem applications.

5.1 Analytical and Experimental Data Correlation

Effort should now be made to compare the program predictions with experimental data. Hopefully an effort in data correlation would result in an analytical expression relating bearing size, speed, and lubricant flow rates to lubricant-imposed resistance to roller motion. A technical break-through in this area is needed and if found could be applied to other bearing types.

A second but as important result of a data match-up program would be knowledge gained of the strong and weak areas of the mathematical model. Weak areas could be subjected to additional analysis and thus strengthened.

5.2 Study of Concentrated Contacts

Another area for future effort is the study of low stress, high sliding rate-contacts such as occur in the roller end-flange contact (REFC). Ideally the objective of this study would be to analytically and experimentally deduce a performance number such as;

$$\Psi = f(h, H_z, v, u, \dot{M}, \phi T) \qquad (5.1)$$

h = lubricant film thickness

H_Z = maximum Hertz stress

$\dot{V}$ = sliding rate

u = lubricant entrainment velocity

$\dot{M}$ = lubricant supply rate

ϕ = Archard's ellipticity factor

T = temperature

Based on experimental results limits of Ψ could be established which would denote excellent, adequate and poor performance. Such a development is essential to the rational design of low stress, high s liding rate-concentrated contacts.

6.0 REFERENCES

6.1 Jones, A., "The Mathematical Theory of Rolling-Element Bearings", Mechanical Design and Systems Handbook, Section 13, McGraw-Hill, 1964, pp. 26-33.

6.2 Harris, T., "An Analytical Method to Predict Skidding in High Speed Roller Bearing", ASLE Transactions, 9, 1966, pp. 229-441.

6.3 Harris, T., Rolling Bearing Analysis, Wiley, 1966.

6.4 Crecelius, W. J. and Harris, T. A., "Ultra High Speed Bearing Analysis", Technical Report NASA CR 120837.

6.5 Conners, T. F., and Morrison, F. R., "Feasibility of Tapered Roller Bearings for Mainshaft Engine Applications", Final Report on Contract DAAJ02-70-C-0047, [redacted] Report AL73P010.

6.6 Lemanski, A. J., Lenski, J. W. and Drago, R. J., Design Fabricate, Test and Evaluation of Spiral Bevel Support Bearings (Tapered Roller) Final Report D210-10561-1, December, 1972 DA.

6.7 Mechtly, E. Q., "The International System of Units Physical Constants and Conversion Factors", NASA SP-4012, 1969.

6.8 Harris, T. A. and Mindel, M. H., "Rolling Element Bearing Dynamics", Wear Vol. 23, February, 1973.

6.9 Lundberg, G. and Sjovall, H., Stress and Deformation in Elastic Contacts, Pub. No. 4, Inst. Theory of Elasticity and Strength of Mat'l., Chalmers Inst. Tech., Gothenburg, Sweden, 1958.

6.10 Palmgren, A., Ball and Roller Bearing Engineering, 3rd Ed., Burbank, 1959.

6.11 Dowson, D. and Higginson, G., "Theory of Roller Bearing Lubrication and Deformation", Proc. Inst. Mech. Eng., London, Vol. 177, 1963, pp. 58-69.

6.12 Archard, J. and Cowking, E., "Elastohydrodynamic Lubrication at Point Contacts", Proc. Inst. Mech. Eng., Vol. 180, Part 3B, 1965-1966, pp. 47-56.

REFERENCES (CONTINUED)

6.13 Streeter, V., Fluid Mechanics, McGraw-Hill, 1951, pp. 313-314

6.14 Sternlicht, B., "Hydrodynamic Lubrication", Mechanical Design and Systems Handbook, Section 12, McGraw-Hill, 1964, pp. 20-22.

6.15 Dusinberre, G. M., Numerical Methods in Heat Transfer, McGraw-Hill, 1949.

6.16 Mackey C. O., "Heat Transmission" Kent Section 3, John Wiley and Sons, Inc., 1950, pp. 3-01 to 3-31.

6.17 PAPCO HEAT INSULATION MANUAL, 1957

6.18 McAdams, W. H., Heat Transmission McGraw-Hill Book Company, Inc., 1954, pp. 184-252.

6.19 McGrew, J. M., Gu, A., Cheng, H. S., Murray, S. F., Elastohydrodynamic Lubrication Preliminary Design Manual Technical Report AFAPL/TR-70-27, November 1970, pp. 36-44.

6.20 Timoshenko, Strength of Materials, Part II, Advanced Theory and Problems, 3rd Edition, D. VanNostrand Co., Inc., 1958.

6.21 Lundberg, G. and Palmgren, A., "Dynamic Capacity of Rolling Bearings", Acta Polytechnica, Mechanical Engineering Series 1, Proceedings of the Royal Swedish Academy of Engineering, Vol. 7, No. 3, 1947.

6.22 Tallian, T., "On Competing Failure Modes in Rolling Contact", ASLE Transactions, Vol. 10, 1967, pp. 418-439.

6.23 Skurka, J., "Elastohydrodynamic Lubrication of Roller Bearings", ASME Transactions, Journal of Lubrication Technology, Vol. 92, 1980, pp. 281-291

6.24 Bamberger, E. N., Harris, T. A., Kacmarsky, W. M., Moyer, C. A., Parker, R. J., Sherlock, J. J., and Zaretsky, E. V., Life Adjustment Factors for Ball and Roller Bearings, The American Society of Mechanical Engineers, 1971.

REFERENCES (CONTINUED)

6.25 Cocks, et al., A Basic Study of the Sliding Contact in Rolling Bearings Prepared under U.S. Navy Contract No. N00019-67-C-0048, SKF Report No. AL69P003.

TABLE I - PRELIMINARY BEARING DESIGNS

Contact Angle (Deg)	½ Roller Included Angle (Deg)	Roller Length (MM)	Roller Length (in)	Roller Large End Diameter (MM)	Roller Large End Diameter (in)	Apex Length (MM)	Apex Length (in)	Number of Rollers
12	1.70	32.994	1.2990	27.960	1.1008	471.22	18.552	15
18	2.33	33.538	1.3204	25.798	1.0157	317.29	12.492	17
20	2.51	33.660	1.3252	25.121	.9890	286.79	11.291	18
22	2.67	33.667	1.3255	24.397	.9605	261.87	10.310	18
24	2.80	33.934	1.3360	23.563	.9277	241.15	9.494	19
28	3.04	33.688	1.3263	22.164	.8726	208.96	8.227	21

TABLE 2

PERFORMANCE PARAMETERS AT MAXIMUM LOAD CONDITIONS FOR
THE PROPOSED OPTIMUM TAPERED ROLLER BEARING
SEE ENCLOSURE 2 FOR DESIGN DETAILS

	Max. Contact Load		Maximum Hertz Stress		Minimum Lub. Film		Sliding Heat Generation		L_{10} Life	Surface Temp.	
	N	LBF	$10^9 N/m^2$	10^5 psi	Microns	Microin.	Watts	BTU/Hr	Hours	°K	°F
Outer Ring	9525.8	2141.5	1.1059	1.604	.7004	27.576	95.49	325.91	1308.	409.62	277.67
Inner Ring	7088.6	1593.6	1.0397	1.508	.6865	27.030	140.51	479.55	1547.	384.80	233.00
Flange	1731.6	389.3	.3013	.437	.9773	38.477	92.51	315.74	-	375.21	215.73

	Max. Cage Load		Rotational Speed RPM	Gyroscopic Moment		Centrifugal Force		Orbital Speed RPM	Skewing Moment	
	N	LBF		N-M	IN-LB	N	LBF		N-M	IN-LB
Roller	85.02	19.113	47450	8.342	73.840	2536.9	570.33	5146.9	.1422	1.2586

	Linear Deflection				Linear Spring Rate						L10 Life	Cage Slip
	X-Axis		Z-Axis		DFX/DX		DFZ/DZ		Torque			
	10^{-3}	10^{-3}IN	10^{-3}M	10^{-3}IN	10^{-6}N/M	10^6LB/IN	10^6N/M	10^6LB/IN	N-M	IN-LB	Hours	%
Bearing	.047	1.882	.0081	.3198	.6244	5.527	2.105	18.628	8.161	72.235	765.2	5.774

Heat Generation Rate	
Watts	BTU/Hr
10688.	36478.

Shaft Speed 12500 rpm
Total lubricant flow rate 454Kg/hr(1000 lb/hr)
Lubricant inlet temperature 364 °K (195°F)
Lubricant type MIL-L-23699
Roller sphere end radius is 80 percent of the apex length

AL73P010

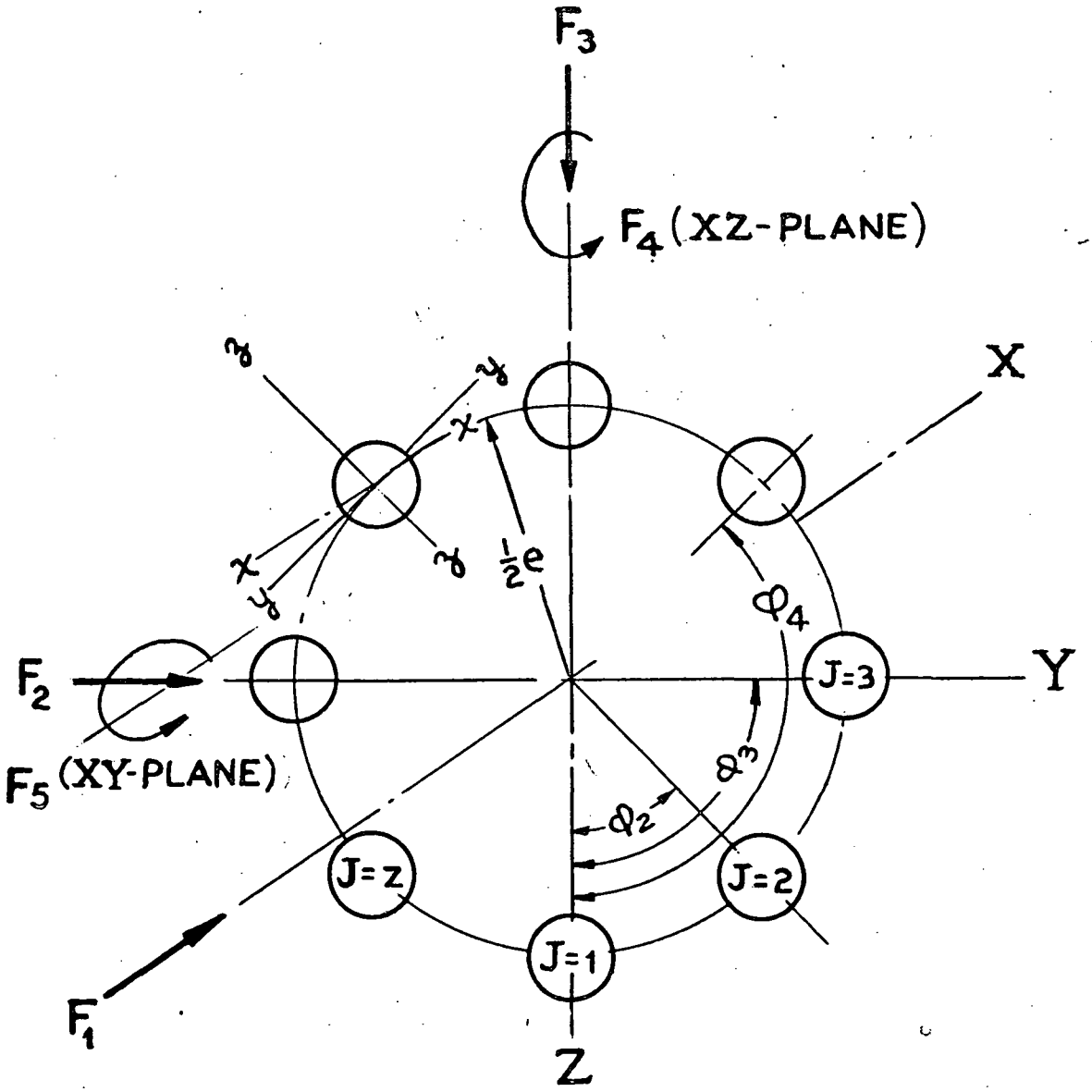

FIG. 1 BEARING OPERATING IN YZ-PLANE

FIG. 2 ROLLER FORCES AND GEOMETRY

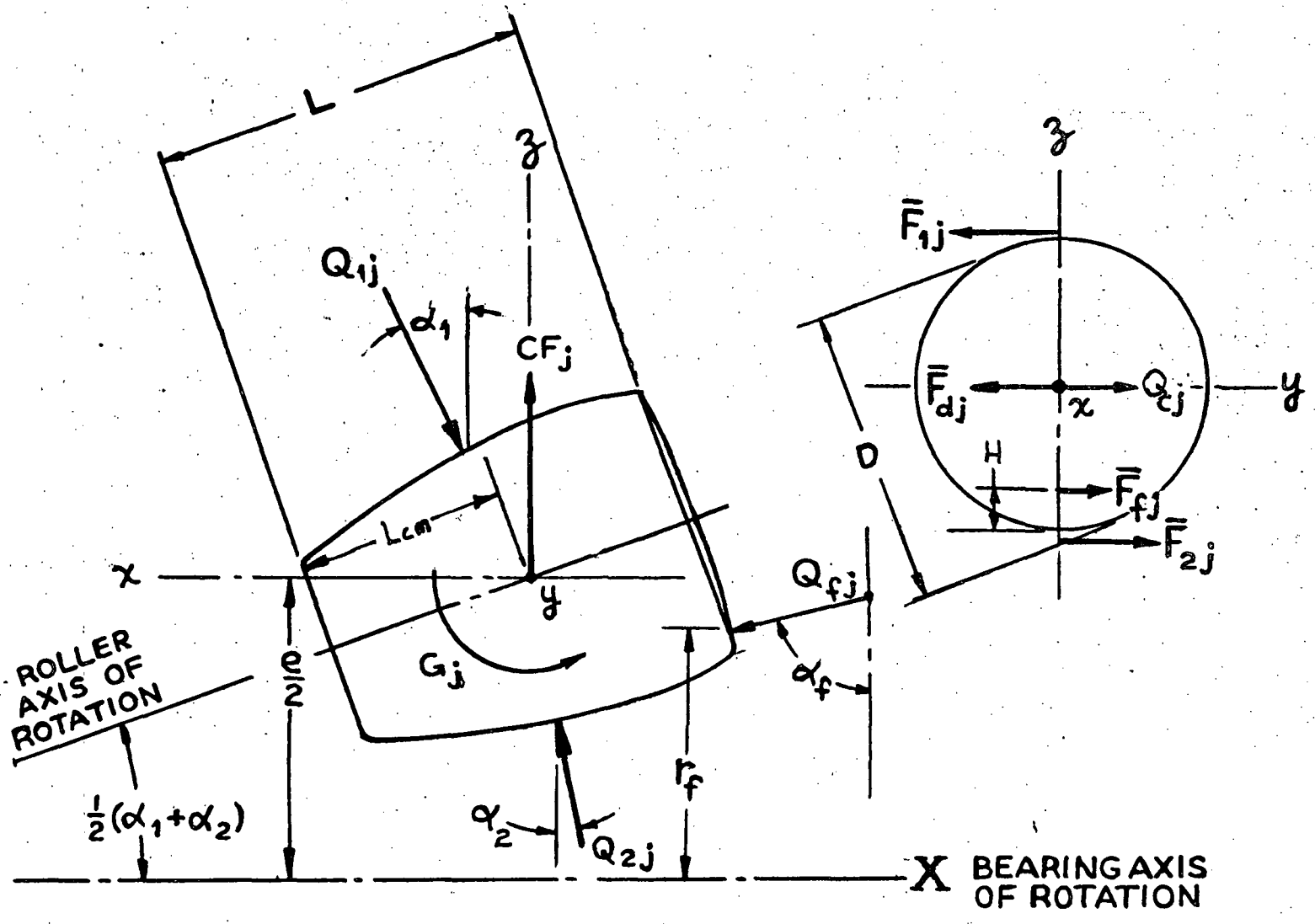

FIG. 3 ROLLER RACEWAY STRESS CONCENTRATIONS

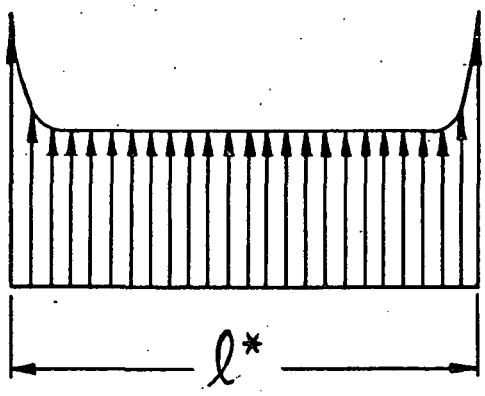

(a) STRAIGHT ROLLER EDGE STRESS CONCENTRATIONS

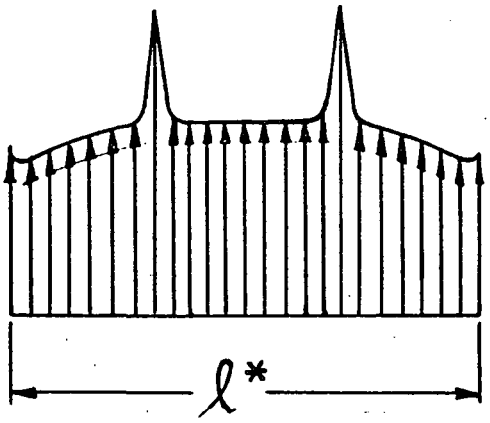

(b) PARTIALLY CROWNED ROLLER STRESS CONCENTRATIONS

* EFFECTIVE LENGTH OF ROLLER - RACEWAY CONTACT

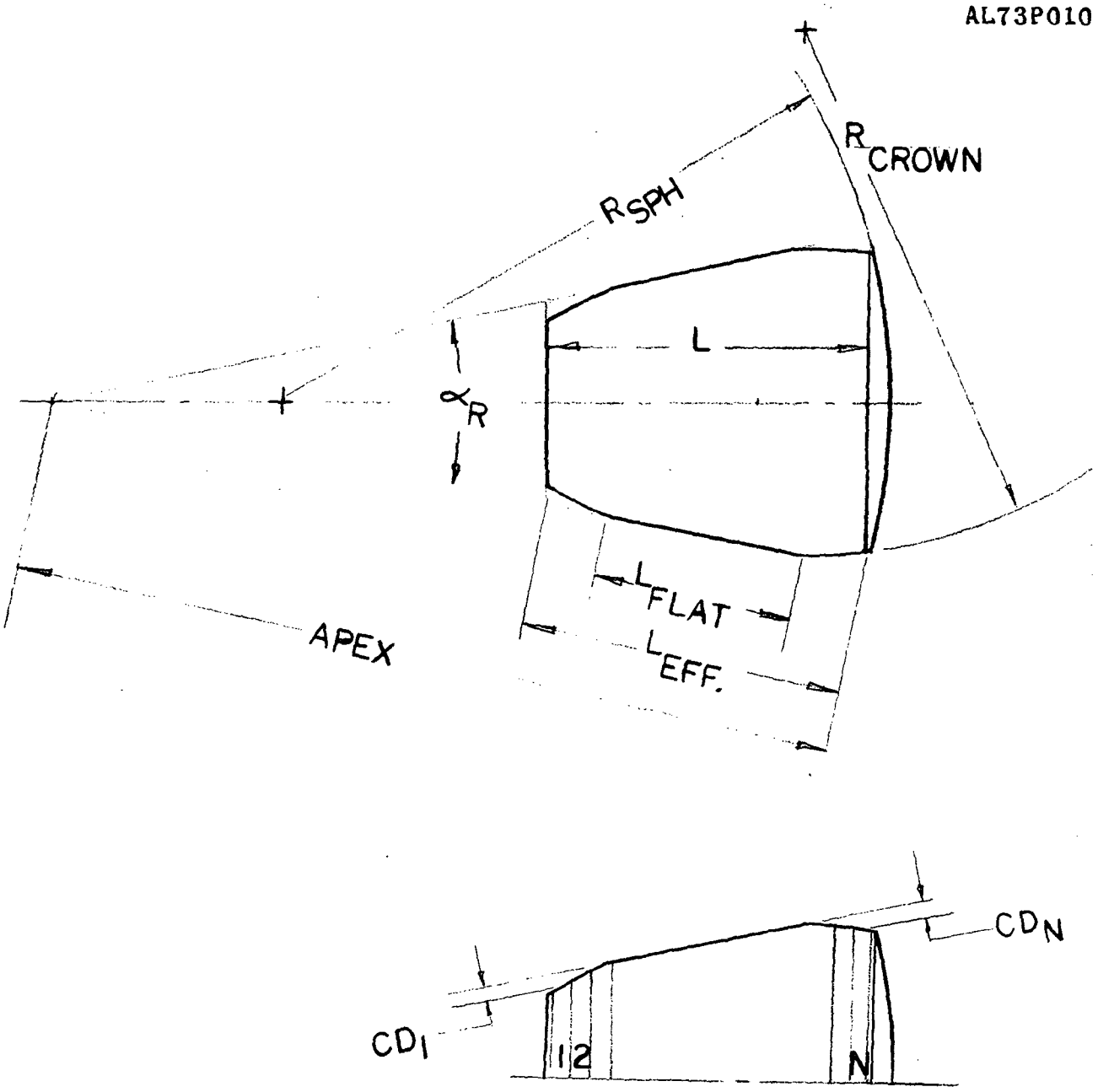

LAMINATED ROLLER STRUCTURE SHOWING

CROWN DROP VERSUS LENGTH

FIG 4 TAPERED ROLLER GEOMETRY

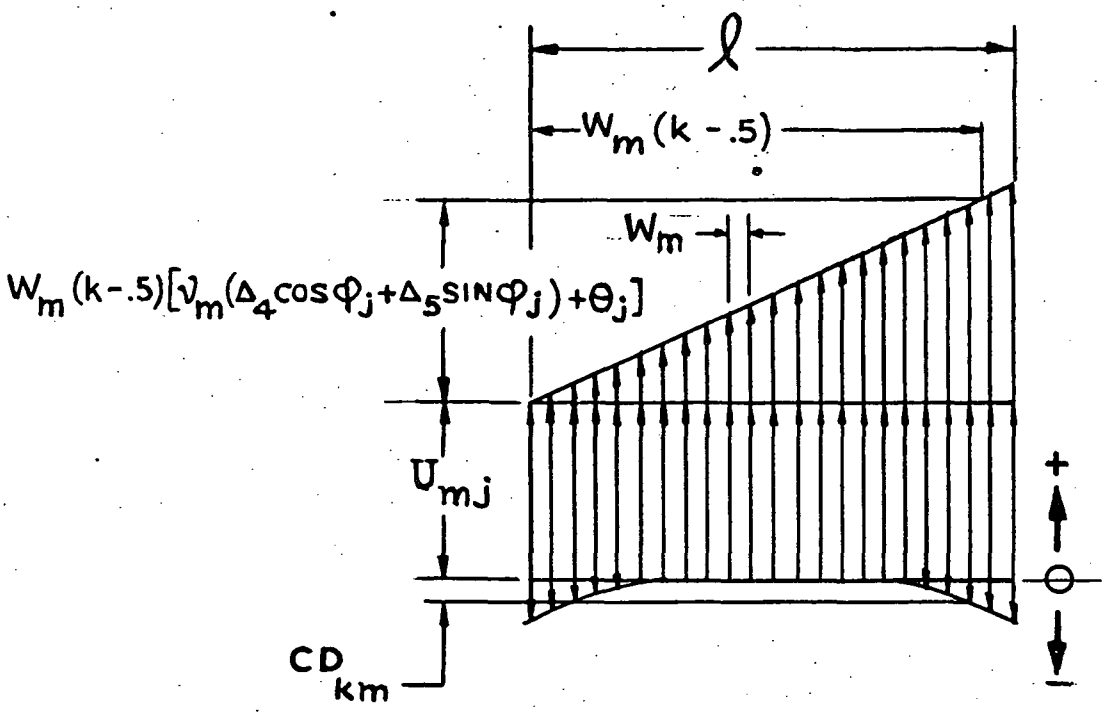

FIG. 5 COMPONENTS OF ROLLER DEFLECTION DUE TO RADIAL LOAD, MISALIGNMENT AND CROWNING

FIG. 6 MIL-L-23699 LUBRICANT VISCOSITY VS PRESSURE AND TEMPERATURE

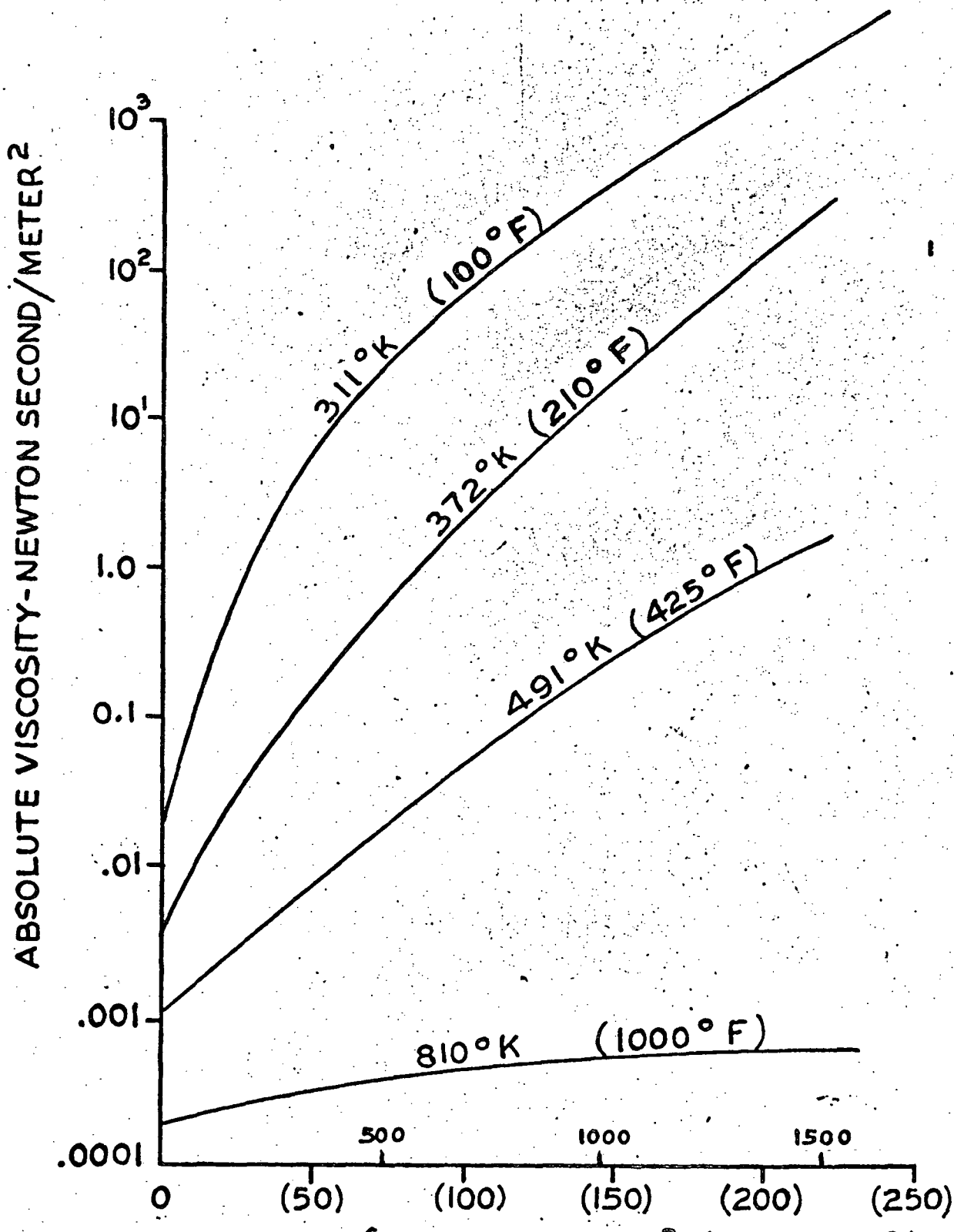

RESEARCH LABORATORY SKF INDUSTRIES, INC.

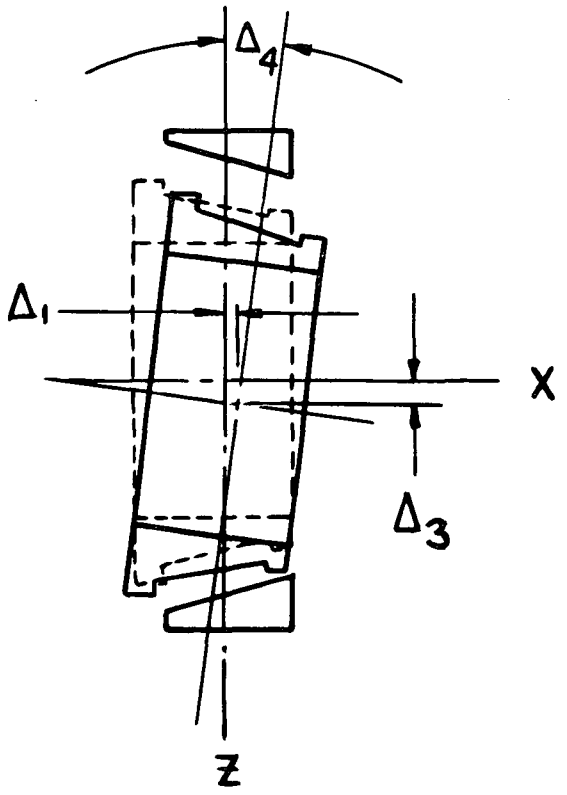

FIG. 7 XZ PLANE INNER RING DISPLACEMENTS

FIG. 8 CAGE TYPES

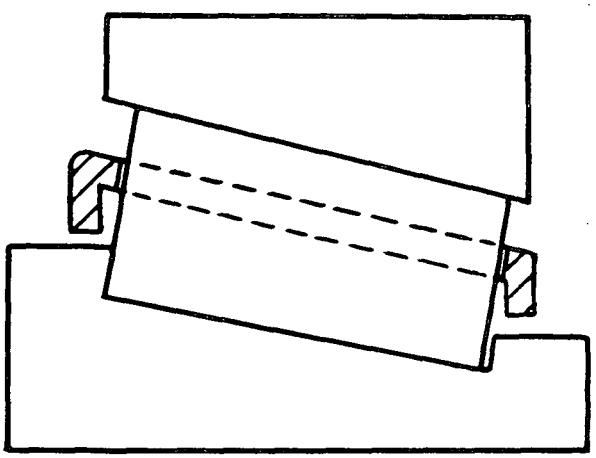

ROLLER RIDING
(RR)

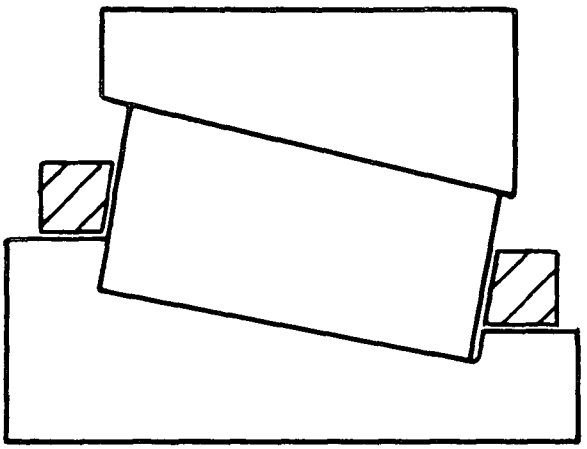

INNER RING LAND RIDING
(IRR)

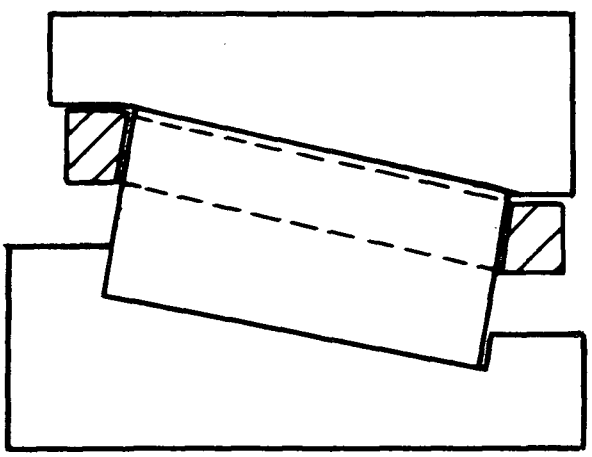

OUTER RING LAND RIDING
(ORR)

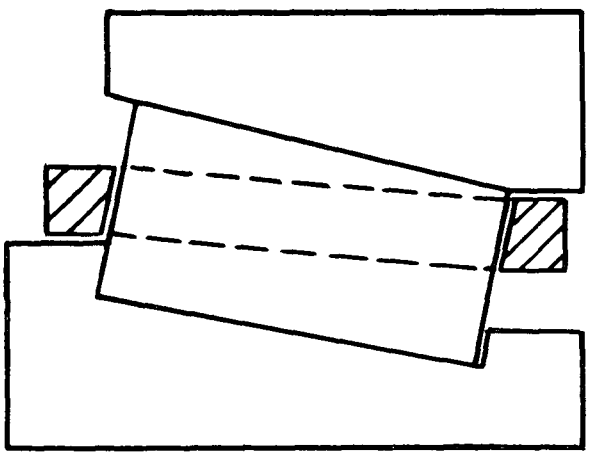

INNER AND OUTER RING
RIDING (Z)

FIG. 9 HEAT DISSIPATION AND TEMPERATURE MAP

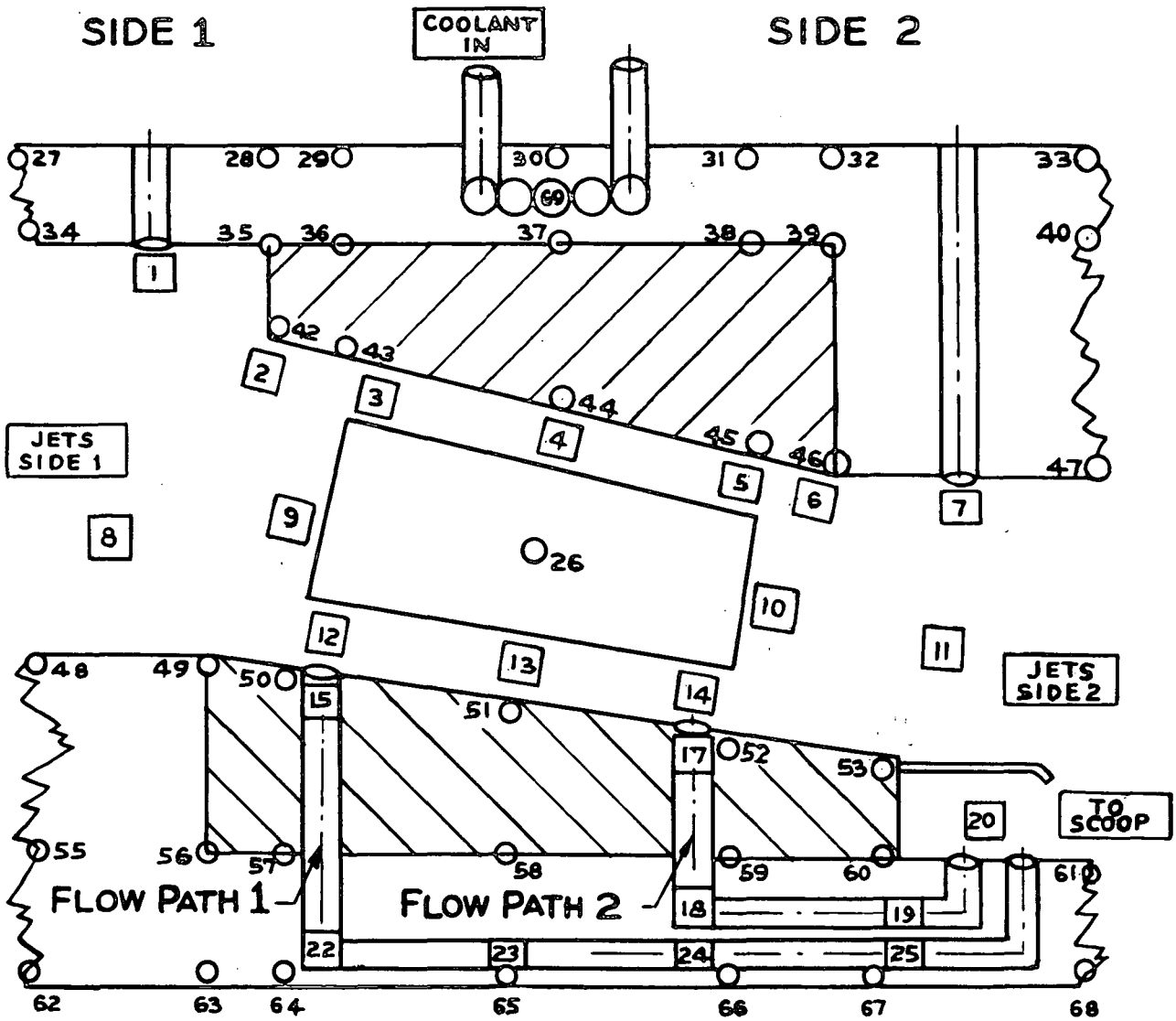

CIRCLES REPRESENT TEMPERATURE NODES IN THE ASSEMBLY COMPONENTS

SQUARES REPRESENT TEMPERATURE NODES IN THE LUBRICANT AND FLUID COOLANT

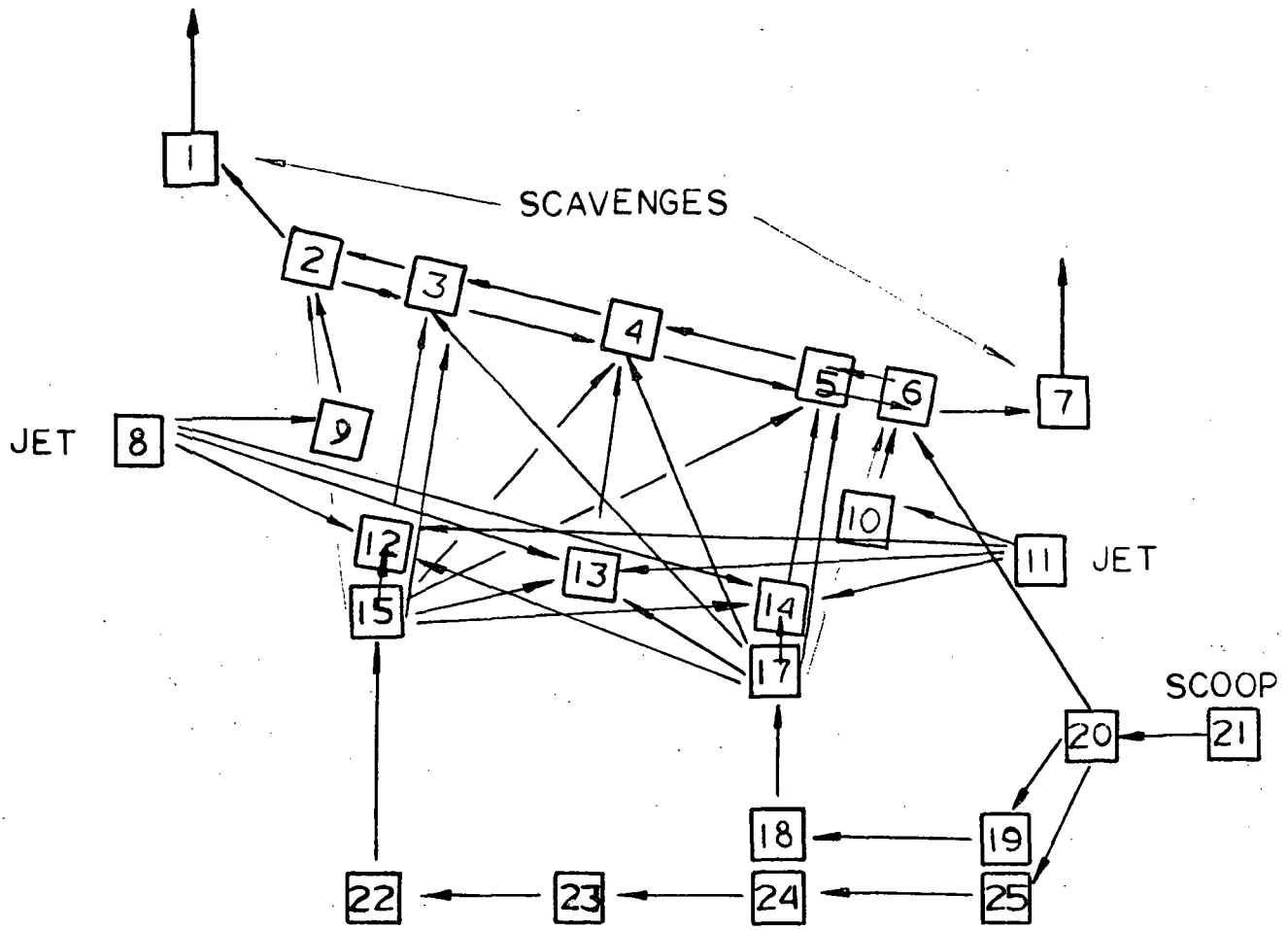

FIG. 10.1 LUBRICANT DISTRIBUTION MODEL

FIG 10.2 LUBRICANT FLOW SCHEME FROM THE JET (NODE 21) WHICH FEEDS THE SCOOP (NODE 20) TO THE LUBRICANT NODES WITHIN THE BEARING CAVITY

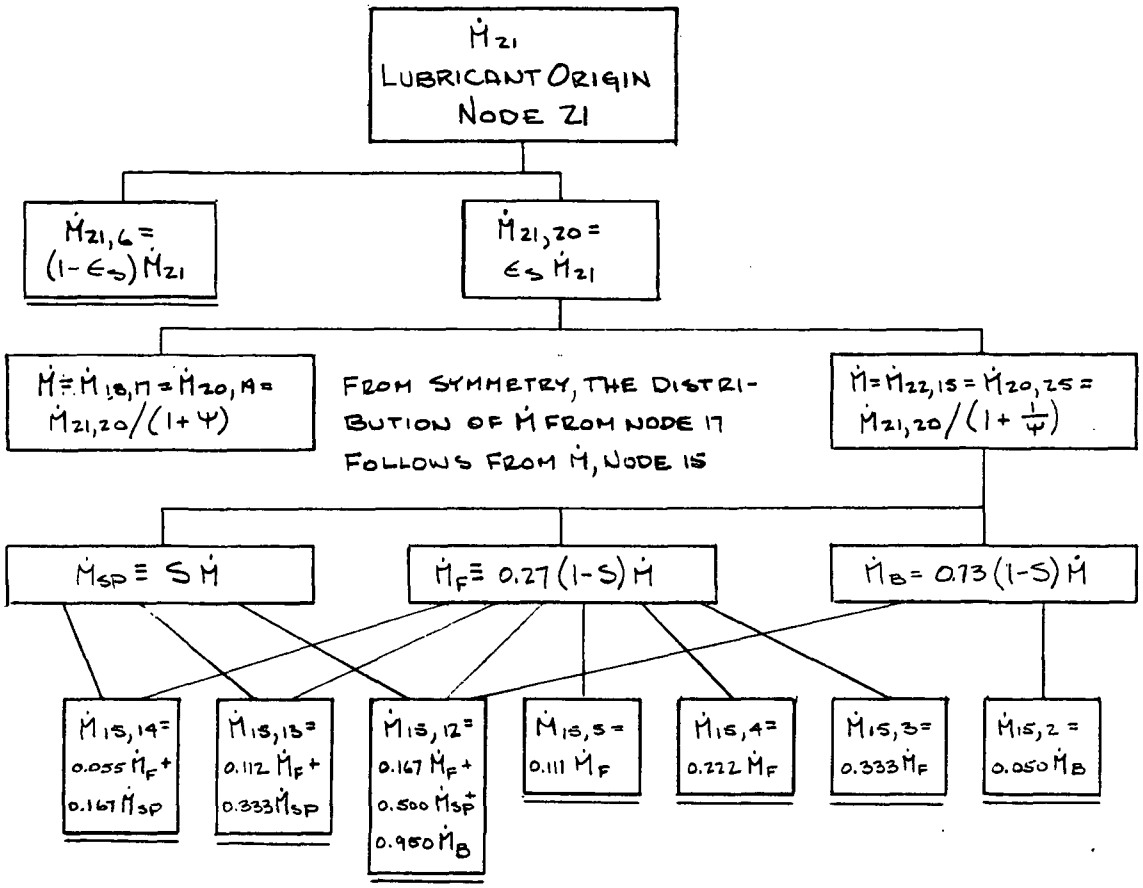

Designates the total mass flow rate from node 21

Designates the rate at which lubricant flows fron node 21 to node j

is the scoop efficience; that fraction of the lubricant jetted to the scoop from node 21 which actually enters the bearing. must be input to the analysis

Is the flow rate from nodes and which enters the bearing vis the scoop flow paths.

Is a function of bearing cage

are auxiliary mass flow rate variables

Is a function of shaft speed, the number of radial under race flow paths and flow path dimensions Eq. (3.1.2.2)

FIG. 10.3 LUBRICANT FLOW SCHEME FROM THE JETS AT SIDE 1 (NODE 11) TO THE LUBRICANT NODES WITHIN THE BEARING CAVITY

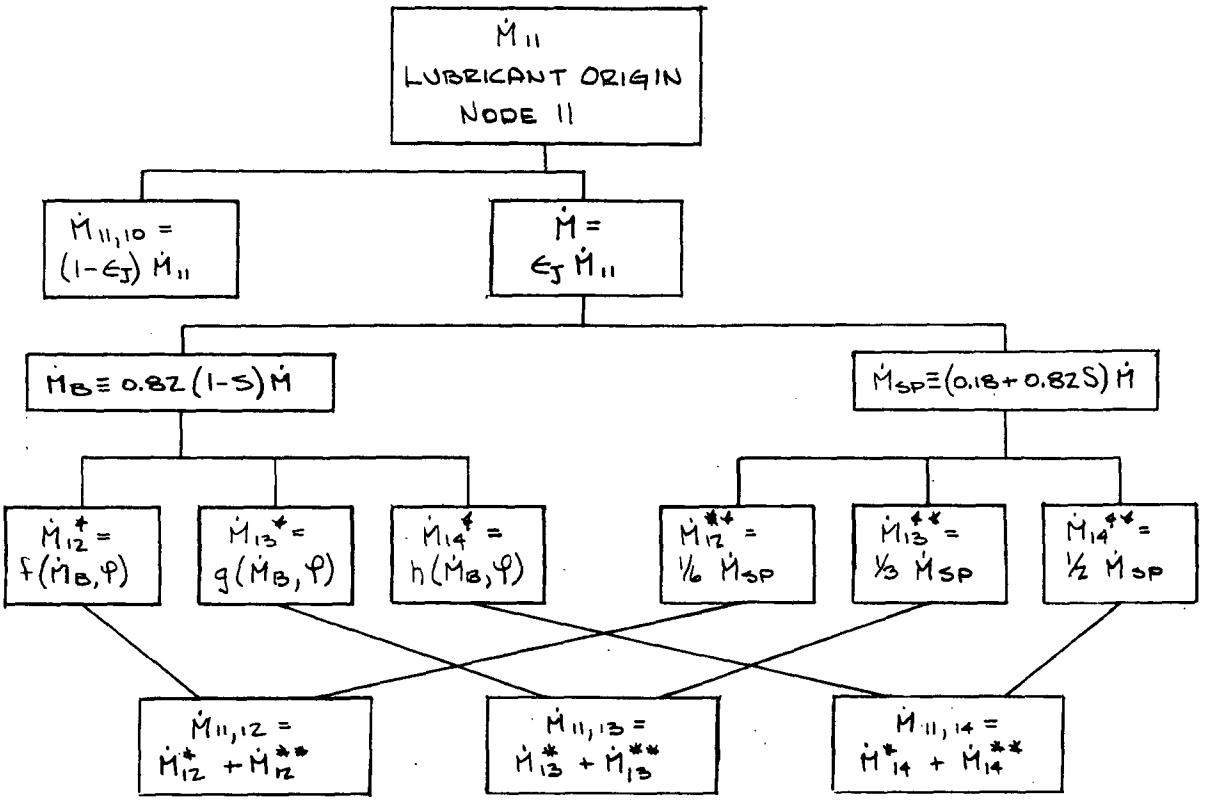

Designates the total mass flow rate through node 11
Designates the rate at which lubricant flows from node 11 to node j
Is the jet efficiency that fraction of the lubricant jetted to the bearing. can be inpute or calculated as a function of jet diameter and bearing design

is the flow rate from nodes 11 which enters the bearing from the jet

are prescribed func ions of and Eq. (3.1.2.38.1 - 3.1.2.30.3)

and are auxiliary mass flow rate variables

is a function of bearing cage speed and jet velocity Eq 3.1.2.26

FIG. II.1 BEARING ASSEMBLY EQUIVALENT SECTIONS

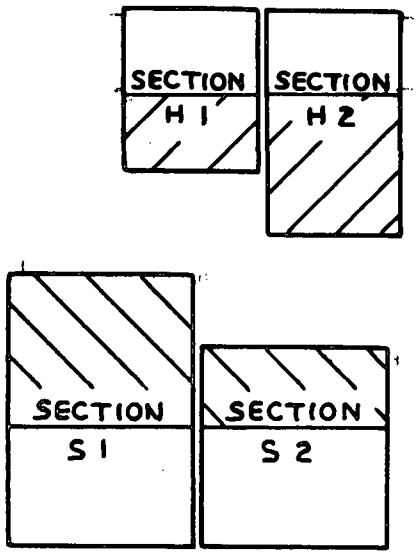

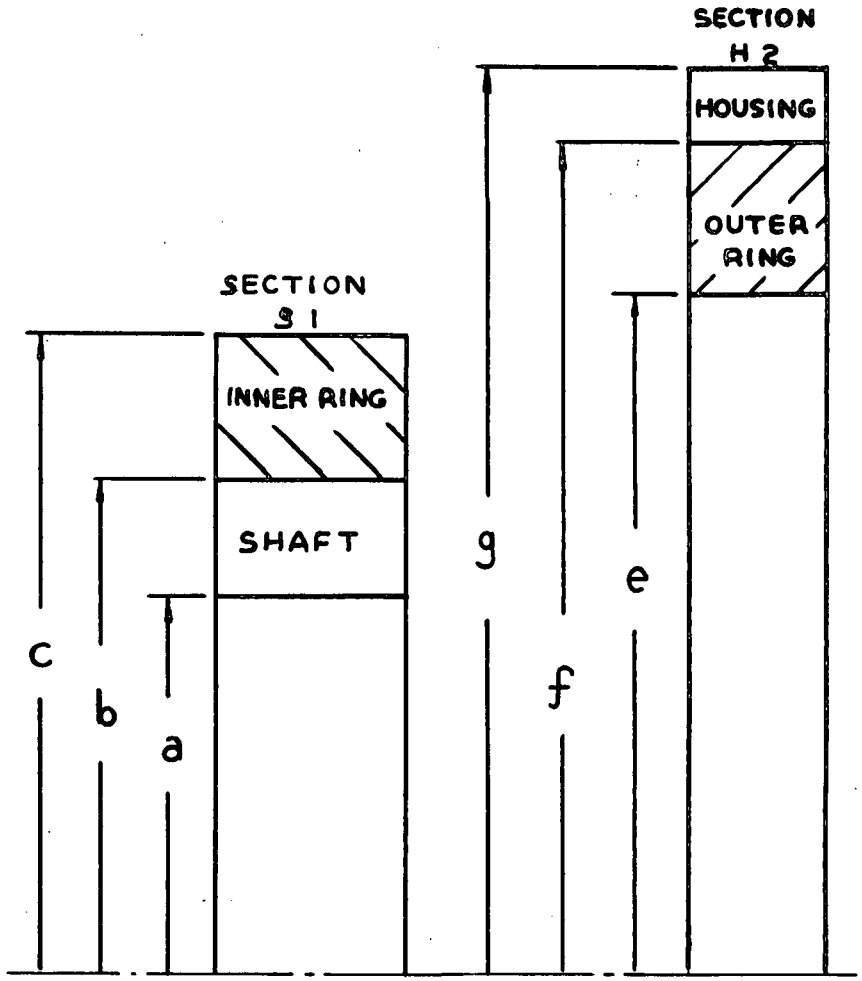

AL73P010

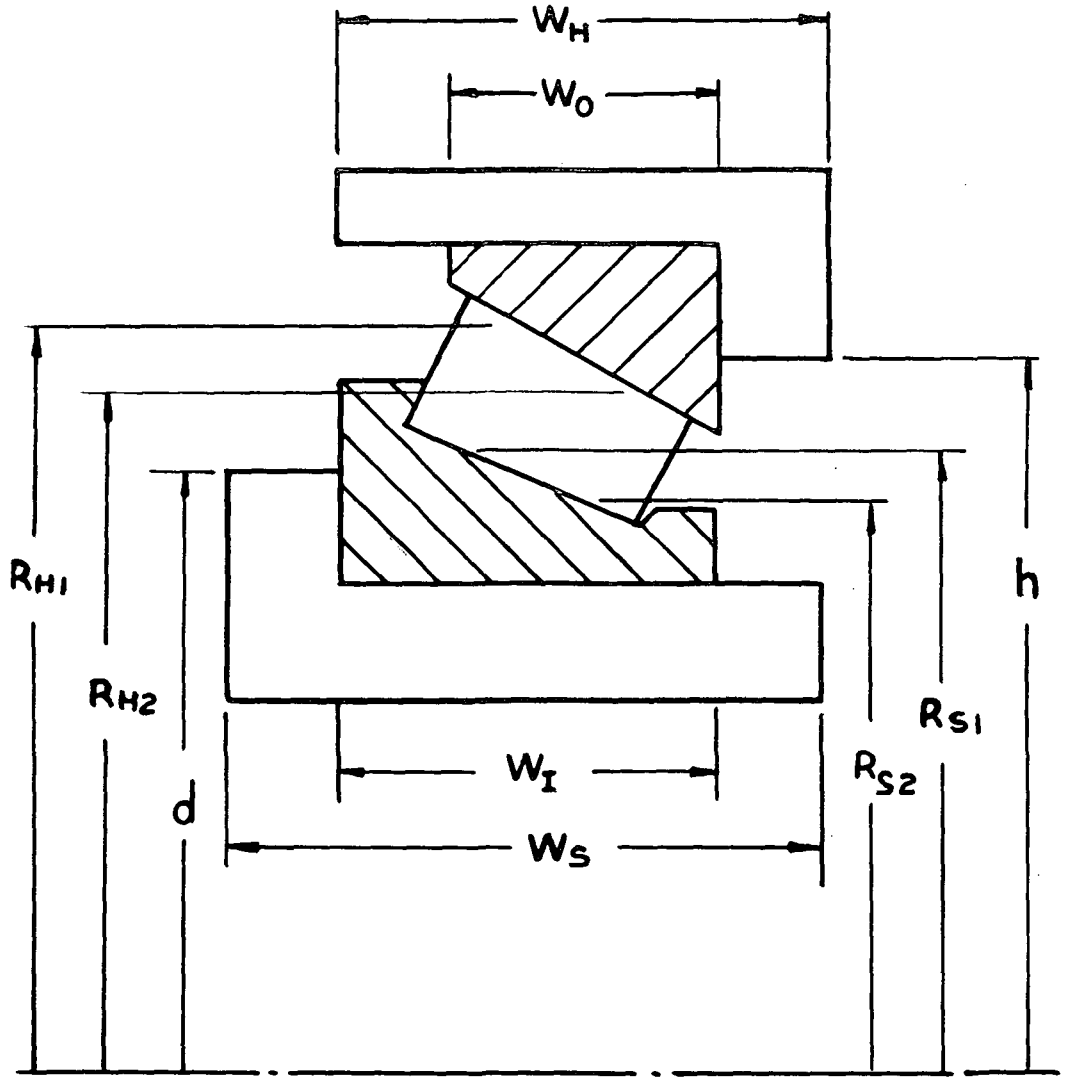

FIG. 11.2 BEARING ASSEMBLY WIDTHS, AND ROLLER PATH RADII

FIG. 12 RING RADIAL EXPANSION
VS
ROTATIONAL SPEED SQUARED

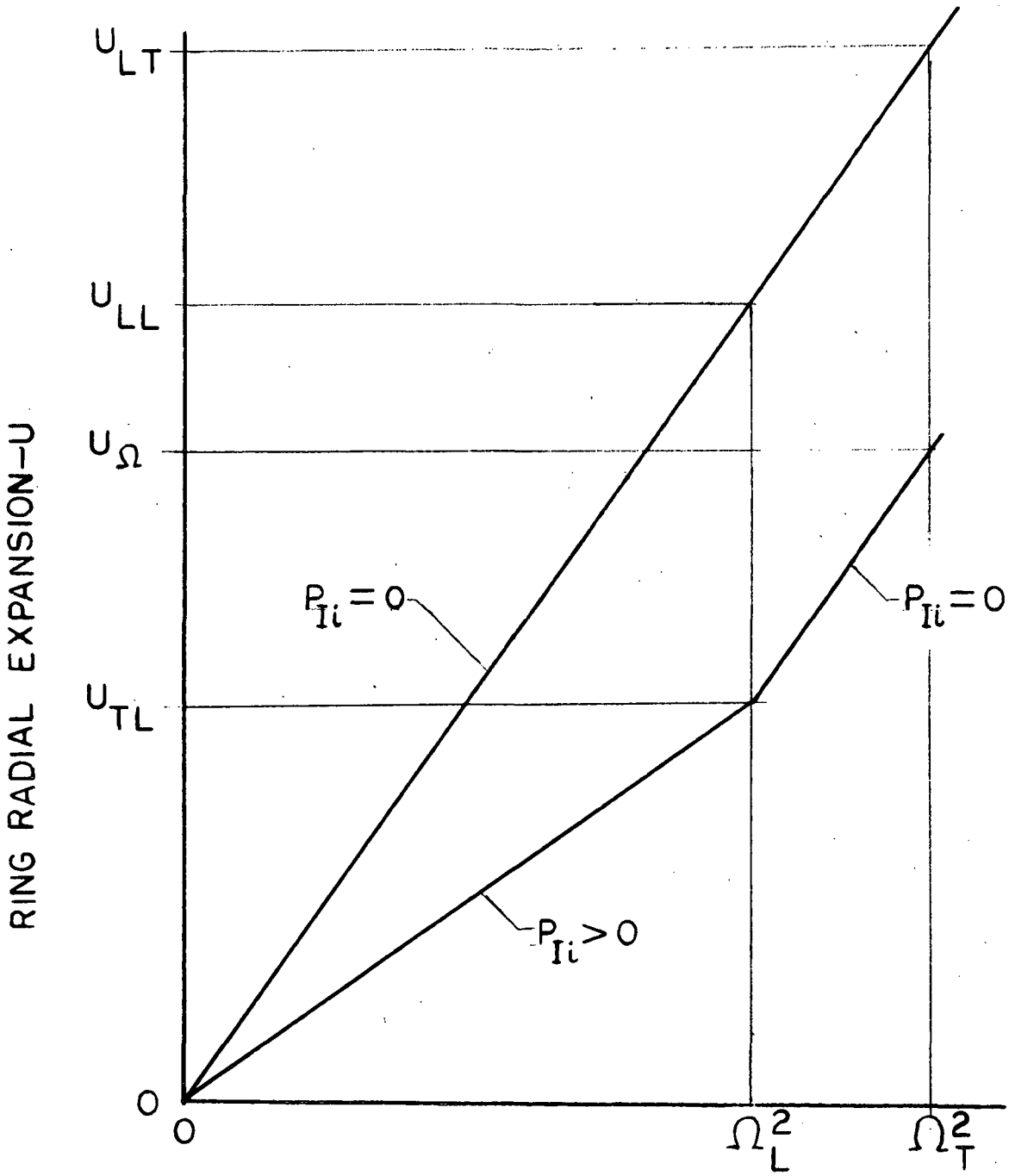

FIG. 13 LIFE ADJUSTMENT FACTOR FOR LUBRICATION a_3
FILM THICKNESS / SURFACE FINISH RATIO Λ

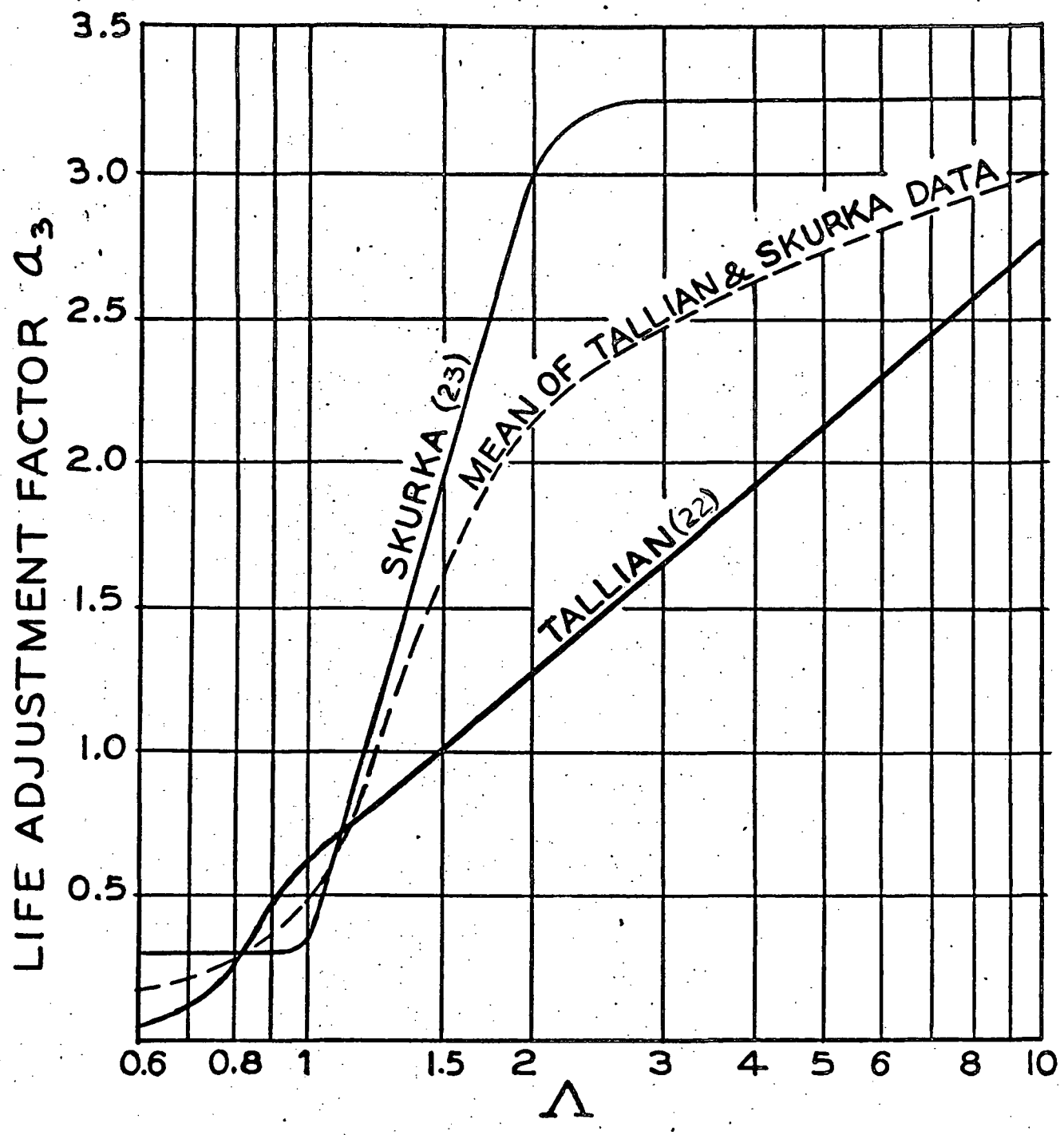

FIG. 14 L-10 FATIGUE LIFE
VS
CONTACT ANGLE

AXIAL LOAD = 53378 N (12000 LBS.)
RADIAL LOAD = 22689 N (6000 LBS.)
SHAFT SPEED = 12500 RPM

SEE TABLE 1 FOR GEOMETRY DATA

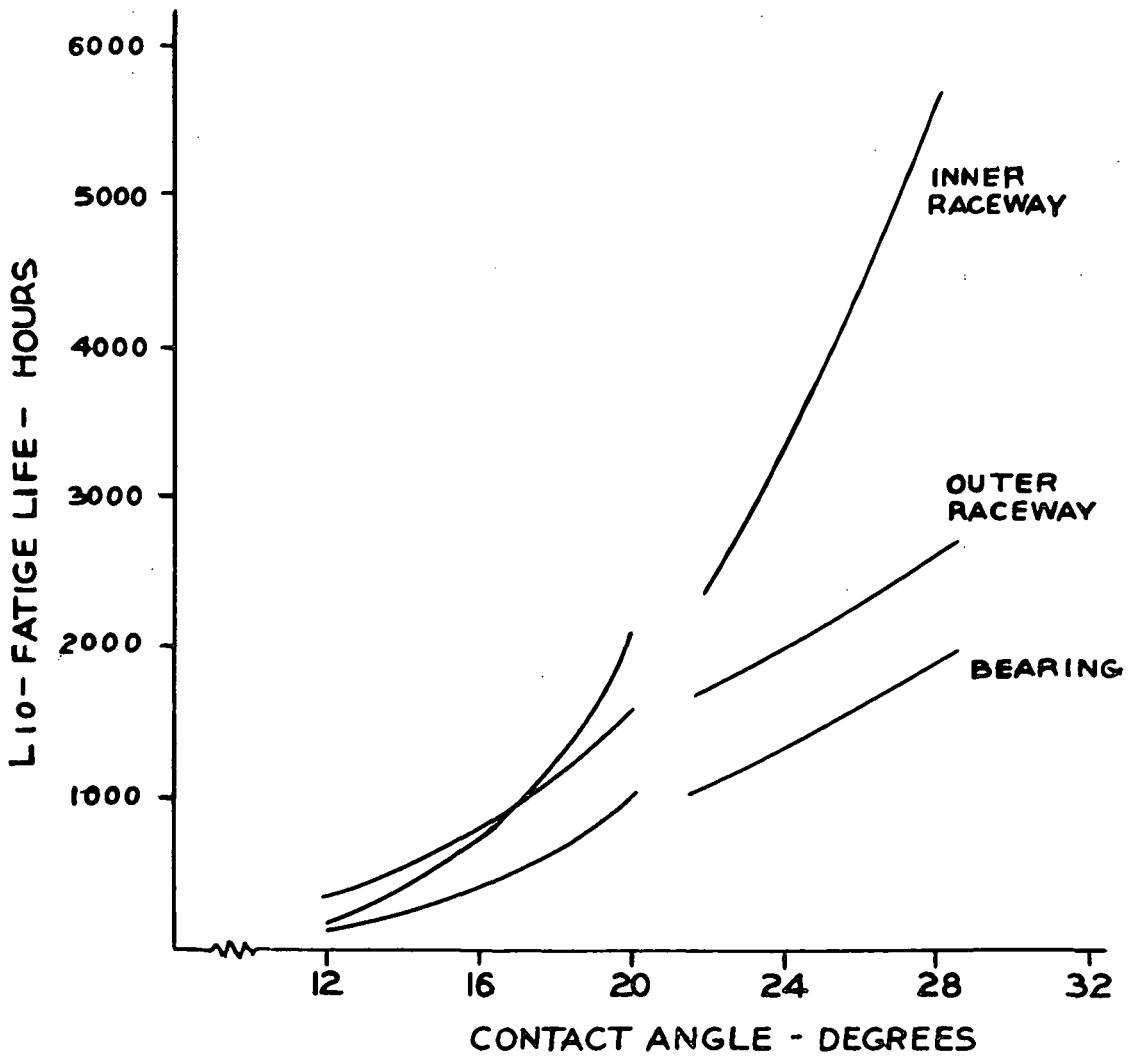

FIG. 15 ROLLER - RING NORMAL LOADS, ROLLER CENTRIFUGAL FORCE AND CAGE SLIP PERCENT VS OUTER RING CONTACT ANGLE

ROLLER END SPHERE RADIUS
90% OF APEX LENGTH

SEE TABLE 1 FOR GEOMETRY DATA

AXIAL LOAD 53378 N (12000 LBS.)
RADIAL LOAD 26689 N (6000 LBS.)
SHAFT SPEED 12500 RPM

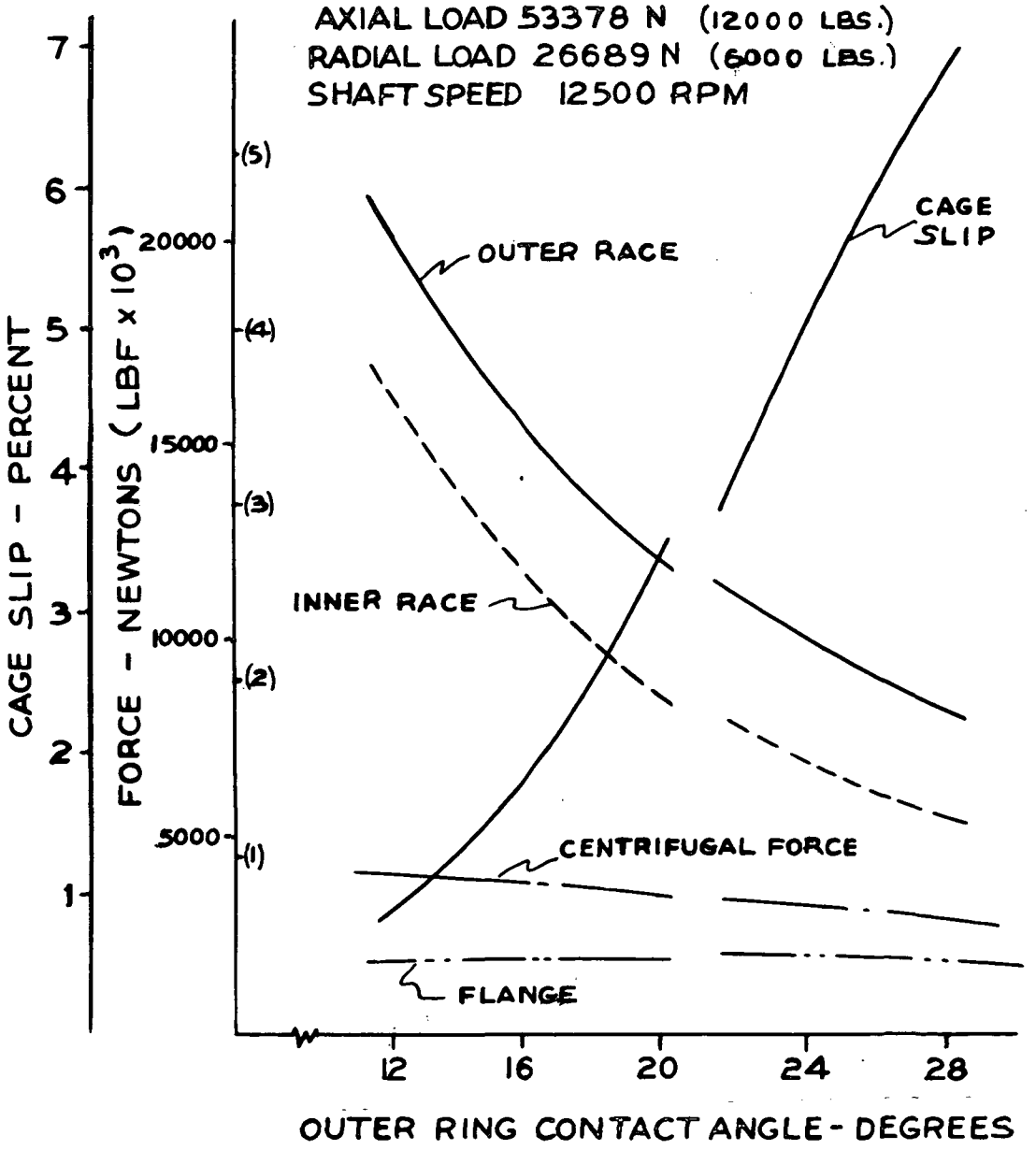

FIG. 16 FLANGE LOAD, HERTZ STRESS AND LUBRICANT FILM THICKNESS VS CONTACT ANGLE

AXIAL LOAD = 53378 N (12000 LB)
RADIAL LOAD = 26689 N (6000 LB)
SHAFT SPEED 12500 RPM
ROLLER END SPHERE RADIUS EQUAL TO 90 % OF APEX
SEE TABLE 1 FOR GEOMETRY DATA

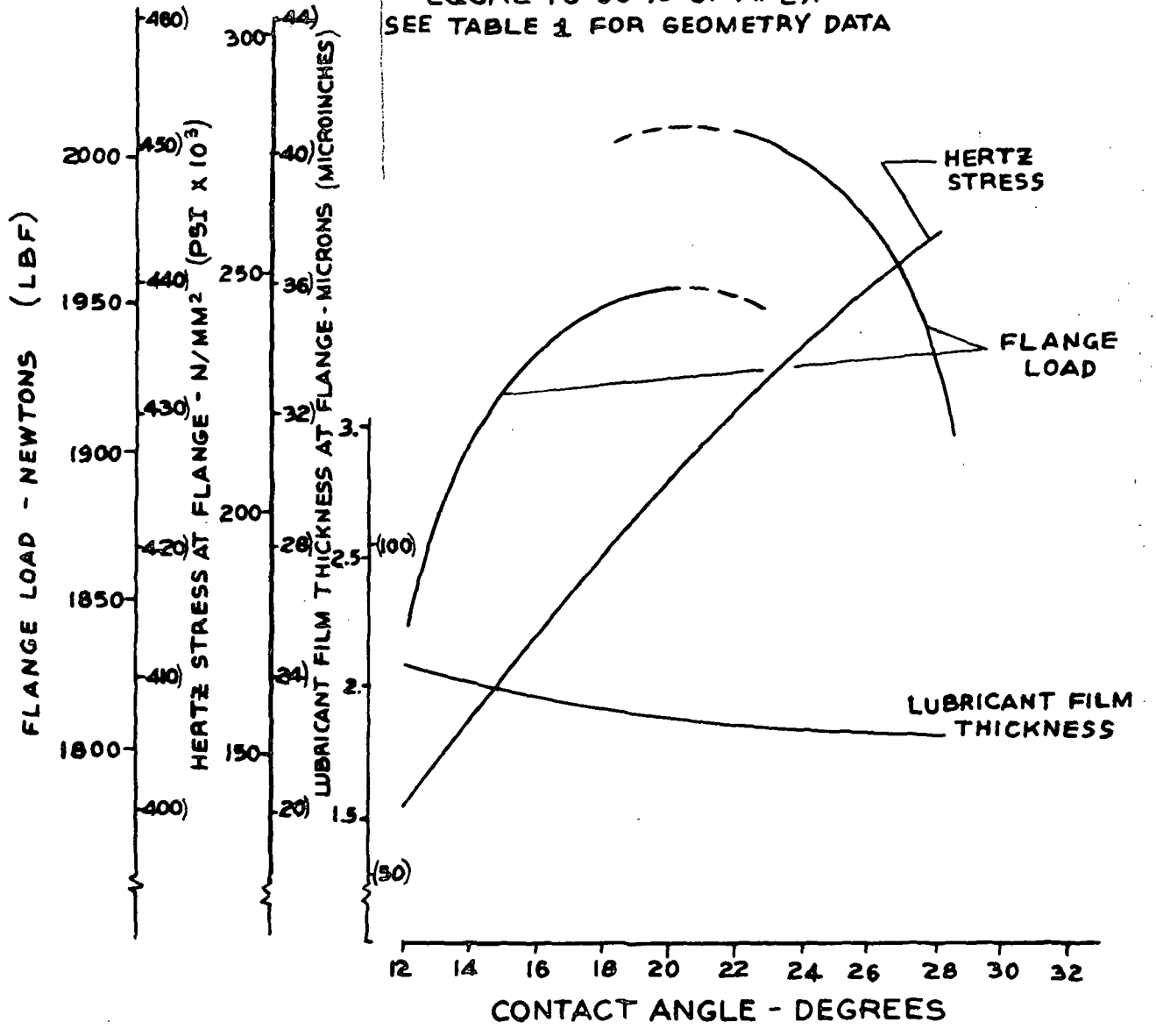

FIG. 17 FRICTIONAL HEAT GENERATION RATES
VS
CONTACT ANGLE
SEE TABLE 1 FOR GEOMETRY DATA

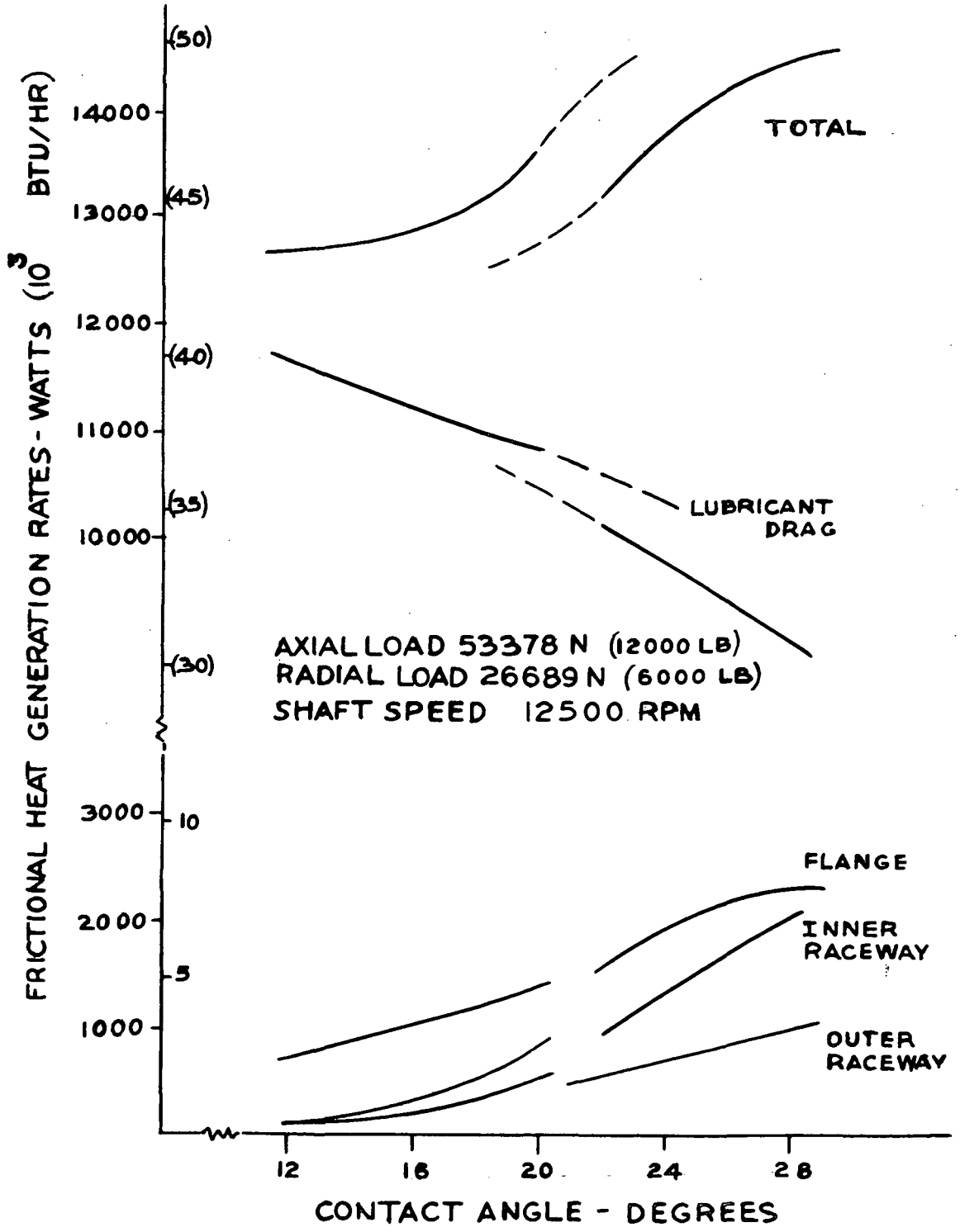

FIG. 18 FLANGE HERTZ STRESS, LUBRICANT FILM THICKNESS AND HEAT GENERATION RATE VS ROLLER END SPHERE RADIUS

CONTACT ANGLE = 24°
AXIAL LOAD = 53378 N (12000 LB)
RADIAL LOAD = 26689 N (6000 LB)
SHAFT SPEED 12 500 RPM
APEX LENGTH = 239.16 MM (9.416 IN.)

SEE ENCLOSURE 2 FOR DESIGN DETAILS

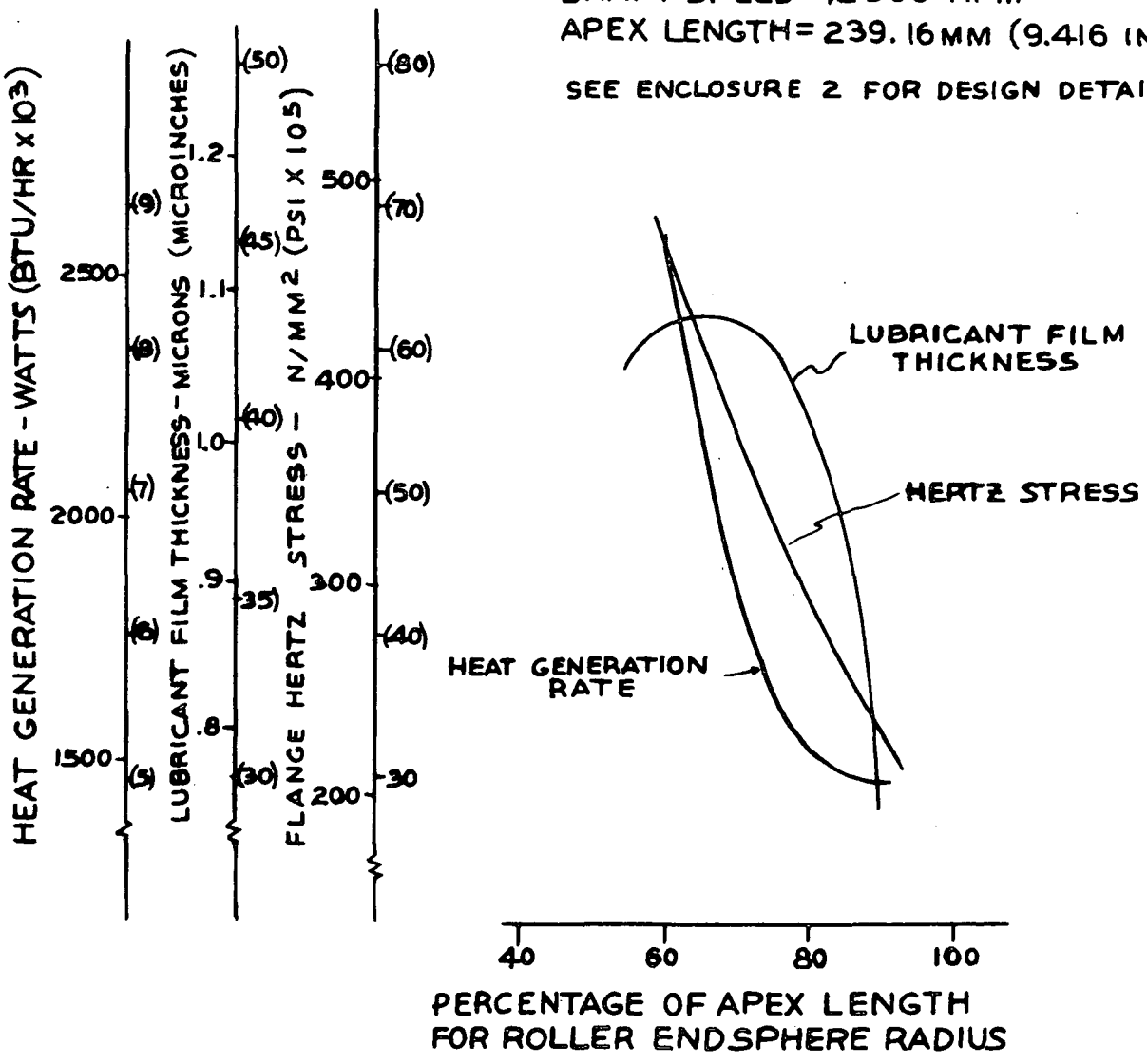

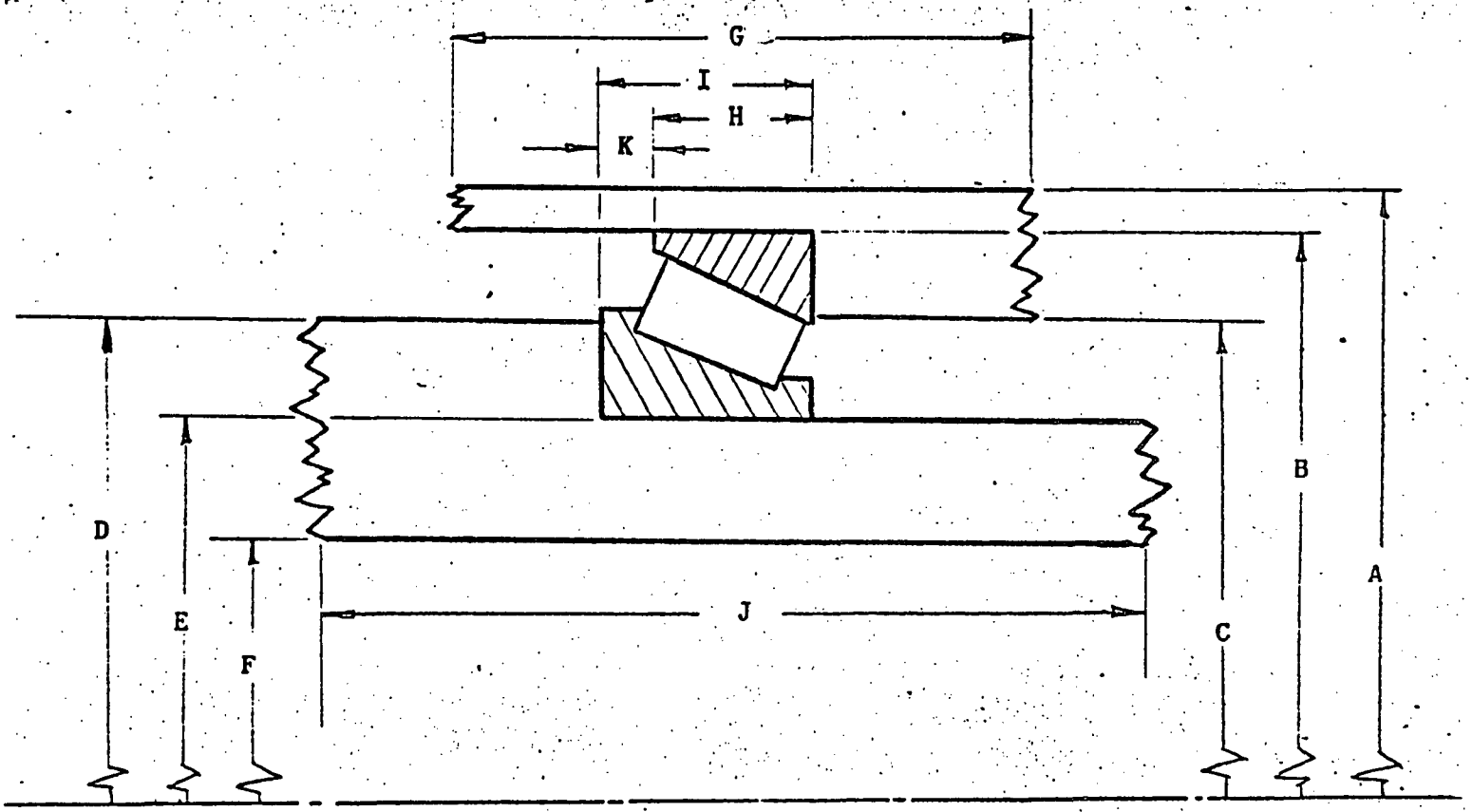

DIAMETERS, INCHES				WIDTHS OR EFFECTIVE LENGTHS, INCHES			
		MM	INCH			MM	INCH
A	HOUSING O.D.	273.50	10.750	G	HOUSING	203.20	8.000
B	BEARING O.D.	206.38	8.125	H	OUTER RING	38.10	1.500
C	HOUSING SHOULDER DIAMETER	190.50	7.500	I	INNER RING	47.63	1.875
D	SHAFT SHOULDER DIAMETER	146.05	5.750	J	SHAFT	165.10	6.500
E	BEARING BORE DIAMETER	120.65	4.750	K	OUTER RING-INNER RING (CUP-CONE) OFFSET	9.53	0.375
F	SHAFT I.D.	88.90	3.500				

AL73P010

FIG. 19 BEARING-SHAFT AND HOUSING ASSEMBLY DIMENSIONS

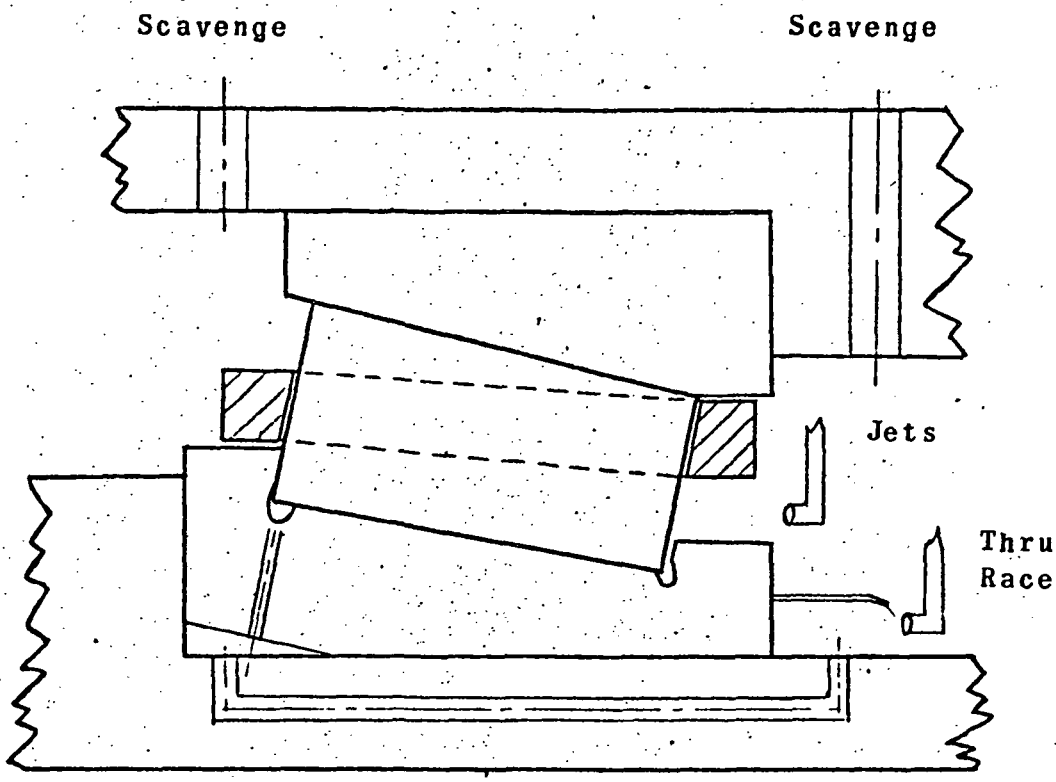

FIG. 20 BEARING BOUNDARY CONDITIONS AND LUBRICATION SCHEME

Boundary Conditions

Air
Temperature 293°K (75°F)
Velocity - Quiescent

Housing
Material Steel
End Temperatures
Side 1 372°K (210°F)
Side 2 364°K (195°F)

Shaft
Material Steel
End Temperatures
Side 1 372°K (210°F)
Side 2 364°K (195°F)

Lubrication Data

Lubricant Type MIL-L-23699

Input Via Jets
Number of Jets 2
Jet Diameter 2.54mm (0.10 in.)
Flow Rate 227 KG/Hr (500 lb/Hr)
Jet Efficiency 0.662
Inlet Temperature 264°K (195°F)

Input Through Race
Number of Flow Holes 30
Flow Hole Dia. 1.02mm 0.4°in.
Flow Rate 227 Kg/Hr (500 lb/Hr)
Inlet Temperature 364°K (195°F)

Lubricant Exit Via
Scavenges at Both Sides
Of the Bearing

Fig. 21 Lubrication Schemes Examined In The Bearing Optimization Study

21.1 JET, At The Roller Small End To The Gap Between The Cage and Inner Ring

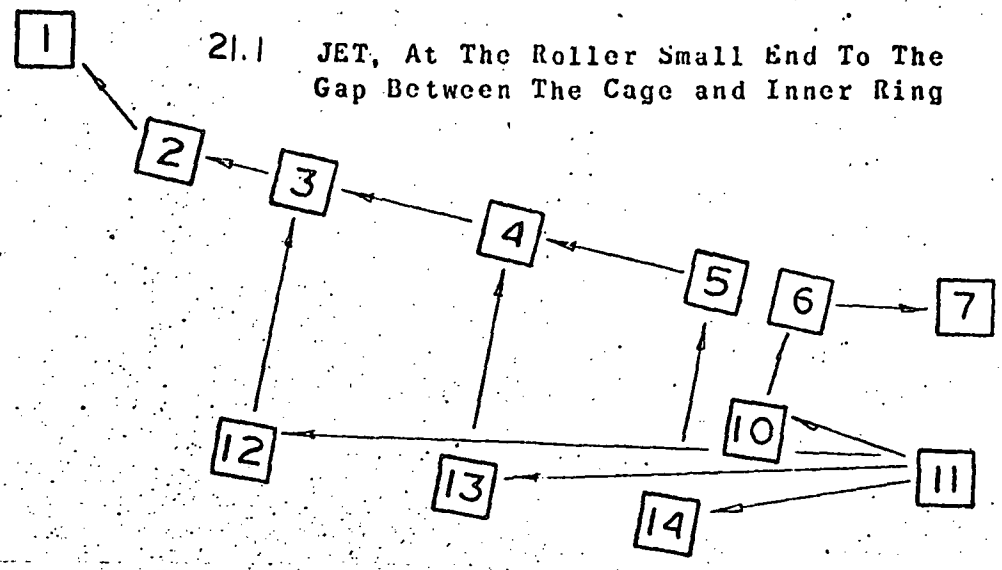

21.2 THROUGH RACE, To The Inner Ring Under Cut At The Roller Large End

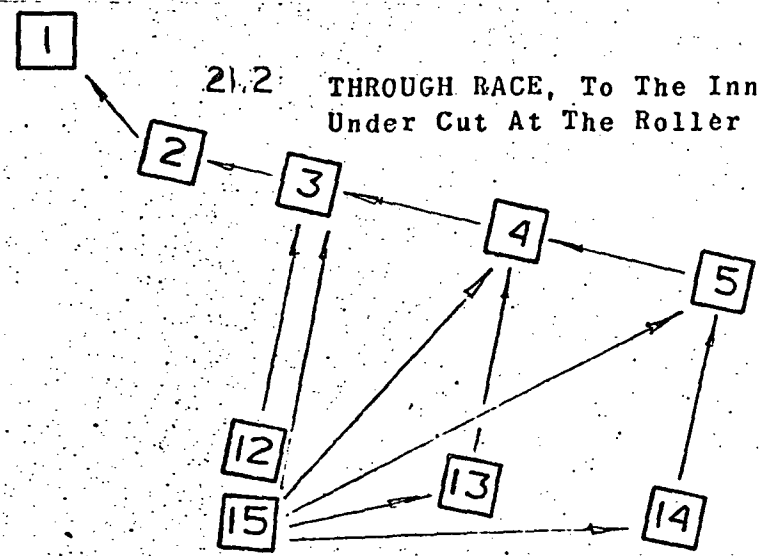

21.3 JET And THROUGH RACE

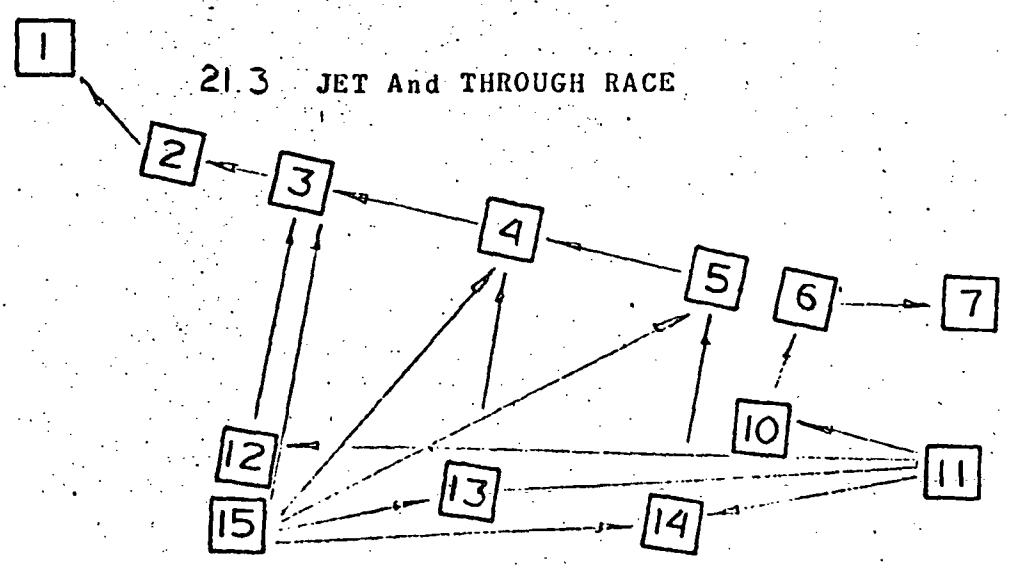

FIG. 22 FLANGE LUBRICANT TEMPERATURE AND FRICTIONAL HEAT GENERATION RATE VS LUBRICANT FLOW RATE
AXIAL LOAD 53378 N (12000 LBF)
RADIAL LOAD 26689 N (6000 LBF)
SHAFT SPEED 12500 RPM

SEE ENCL. 2 FOR DESIGN DETAILS

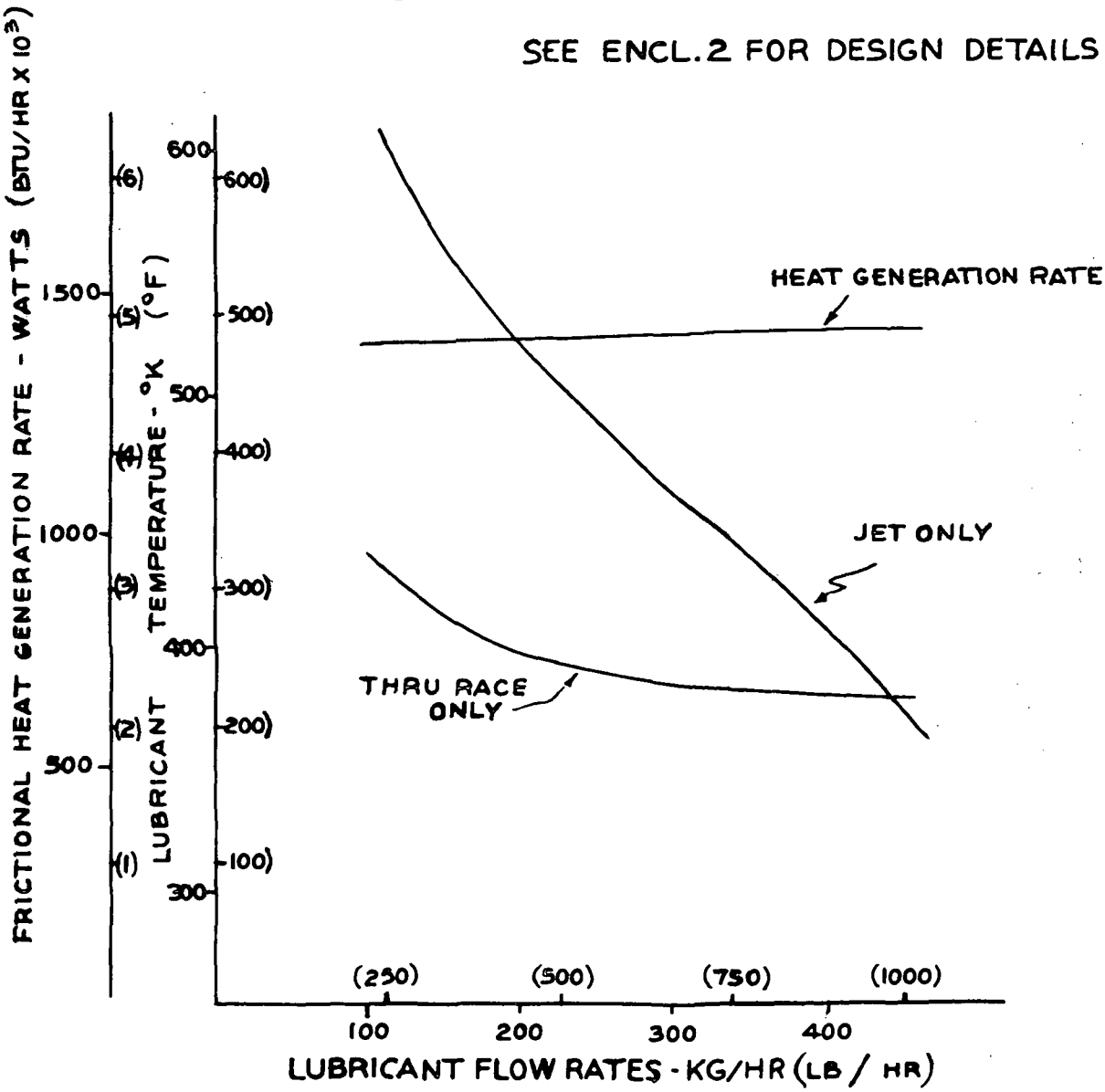

FIG. 23 INNER RACEWAY LUBRICANT TEMPERATURE AND FRICTIONAL HEAT GENERATION RATE VS LUBRICANT FLOW RATE

AXIAL LOAD 53378 N (12000 LBF)
RADIAL LOAD 26689 N (6000 LBF)
SHAFT SPEED 12500 RPM

SEE ENCLOSURE 2 FOR DESIGN DETAILS

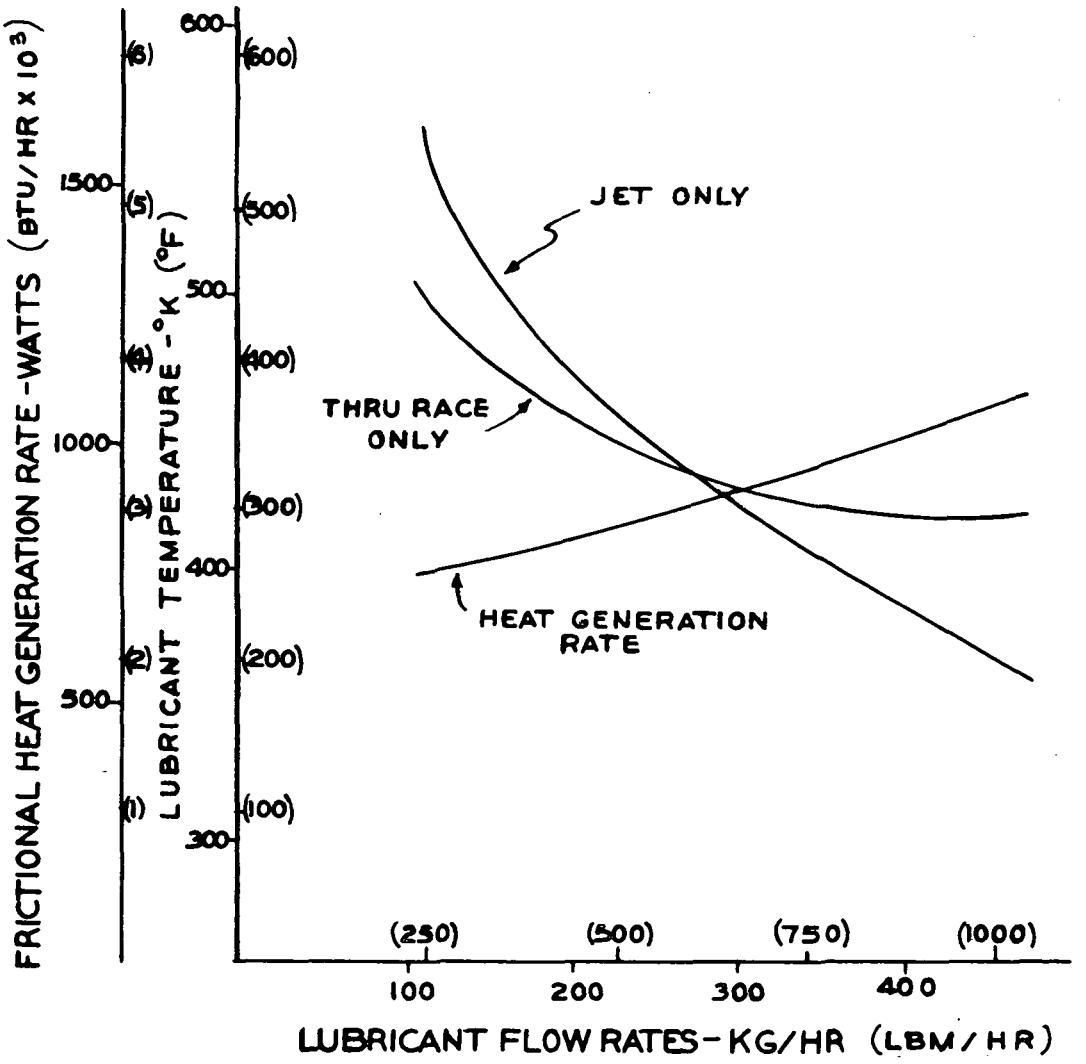

FIG. 24 OUTER RACEWAY LUBRICANT TEMPERATURE AND FRICTIONAL HEAT GENERATION RATE VS LUBRICANT FLOW RATE

AXIAL LOAD 53378 N (12000 LBF)
RADIAL LOAD 26689 N (6000 LBF)
SHAFT SPEED 12500 RPM

SEE ENCLOSURE 2 FOR DESIGN DETAILS

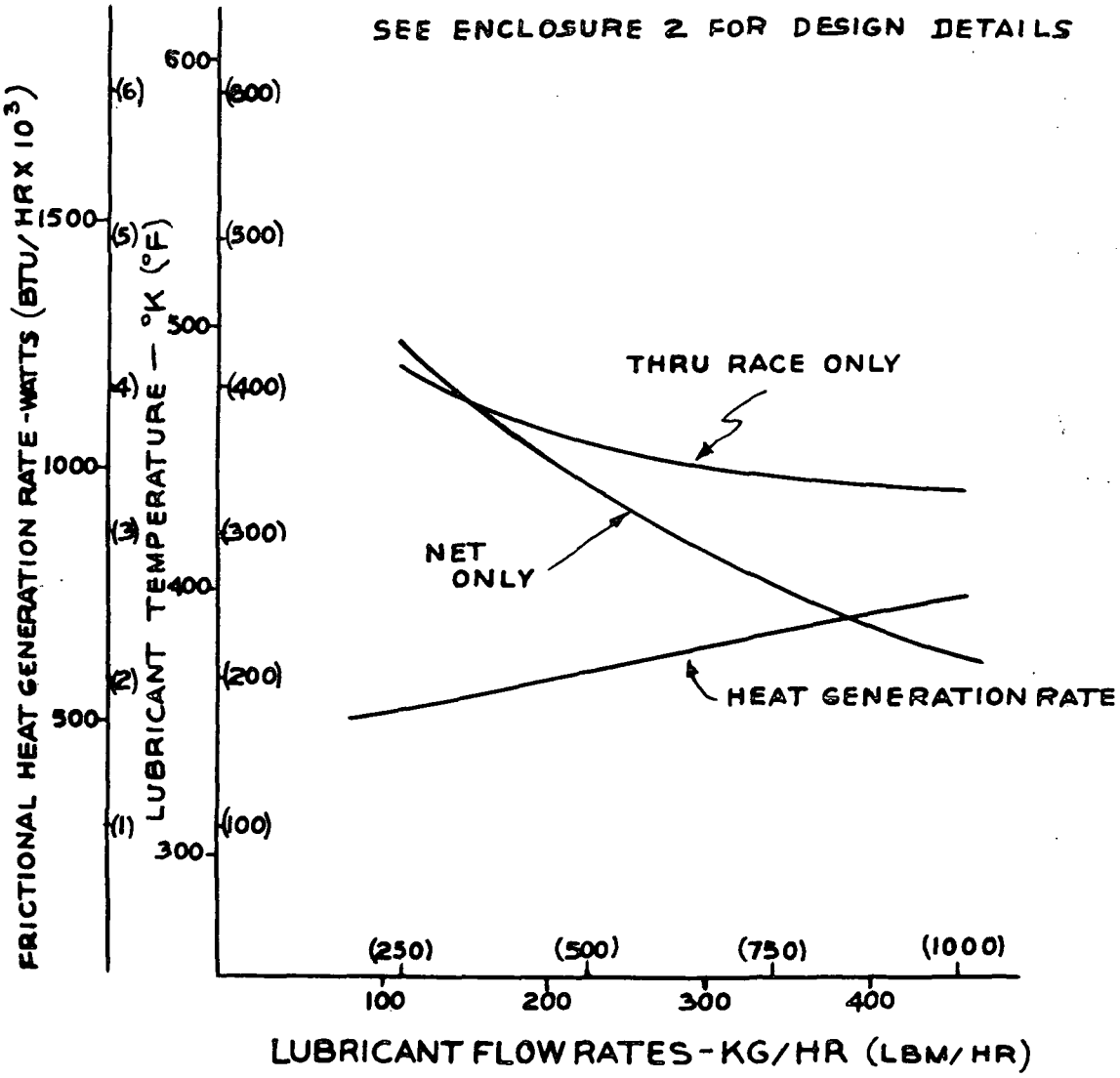

FIG. 25 LUBRICANT MEAN TEMPERATURE AND FRICTIONAL HEAT GENERATION RATE DUE TO LUBRICANT CHURNING VS LUBRICANT MASS FLOW RATE

AXIAL LOAD 53378 N (12 000 LB)
RADIAL LOAD 26689 N (6000 LB)
SHAFT SPEED 12500 RPM

SEE ENCLOSURE 2 FOR DESIGN DETAILS

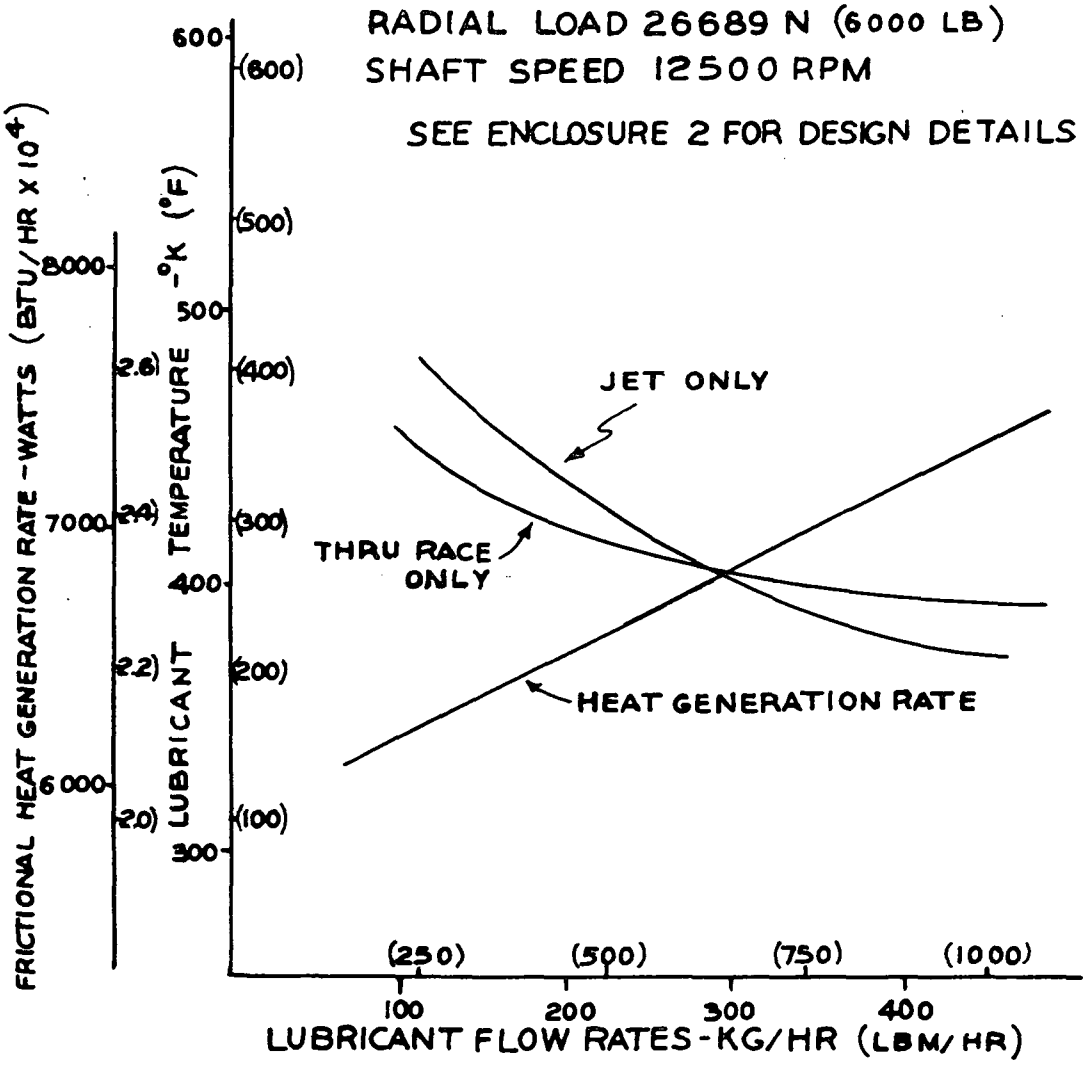

FIG. 26 FLANGE LUBRICANT TEMPERATURE AND FRICTIONAL HEAT GENERATION RATE VS LUBRICANT FLOW RATE

SEE ENCLOSURE 2 FOR DESIGN DETAILS

CONSTANT FLOW RATE = 226.79 KG/HR (500 LBM/HR)

AXIAL LOAD 53378 N (12000 LBF)

RADIAL LOAD 26689 N (6000 LBF)

SHAFT SPEED 12500 RPM

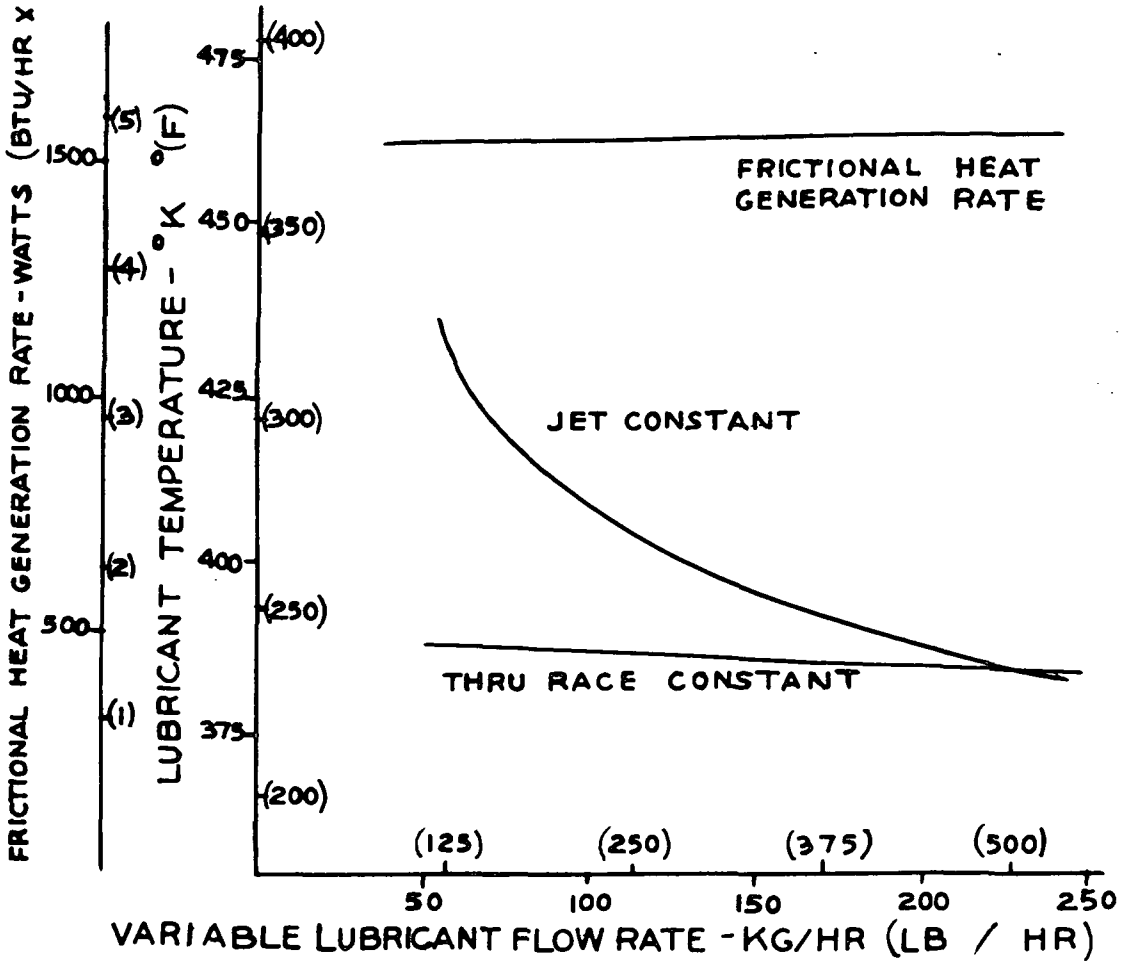

F-4186A R100

FIG. 27 INNER RACEWAY LUBRICANT TEMPERATURES AT CENTER AND SMALL END SIDE OF RACE AND FRICTIONAL HEAT GENERATION RATE VS LUBRICANT FLOW RATE

CONSTANT FLOW RATES=226.79 KG/HR (500 LBM/HR)

AXIAL LOAD 53378 N (12000 LBF)
RADIAL LOAD 26689 N (6000 LBF)
SHAFT SPEED 12500 RPM

SEE ENCL. 2 FOR DESIGN DETAILS

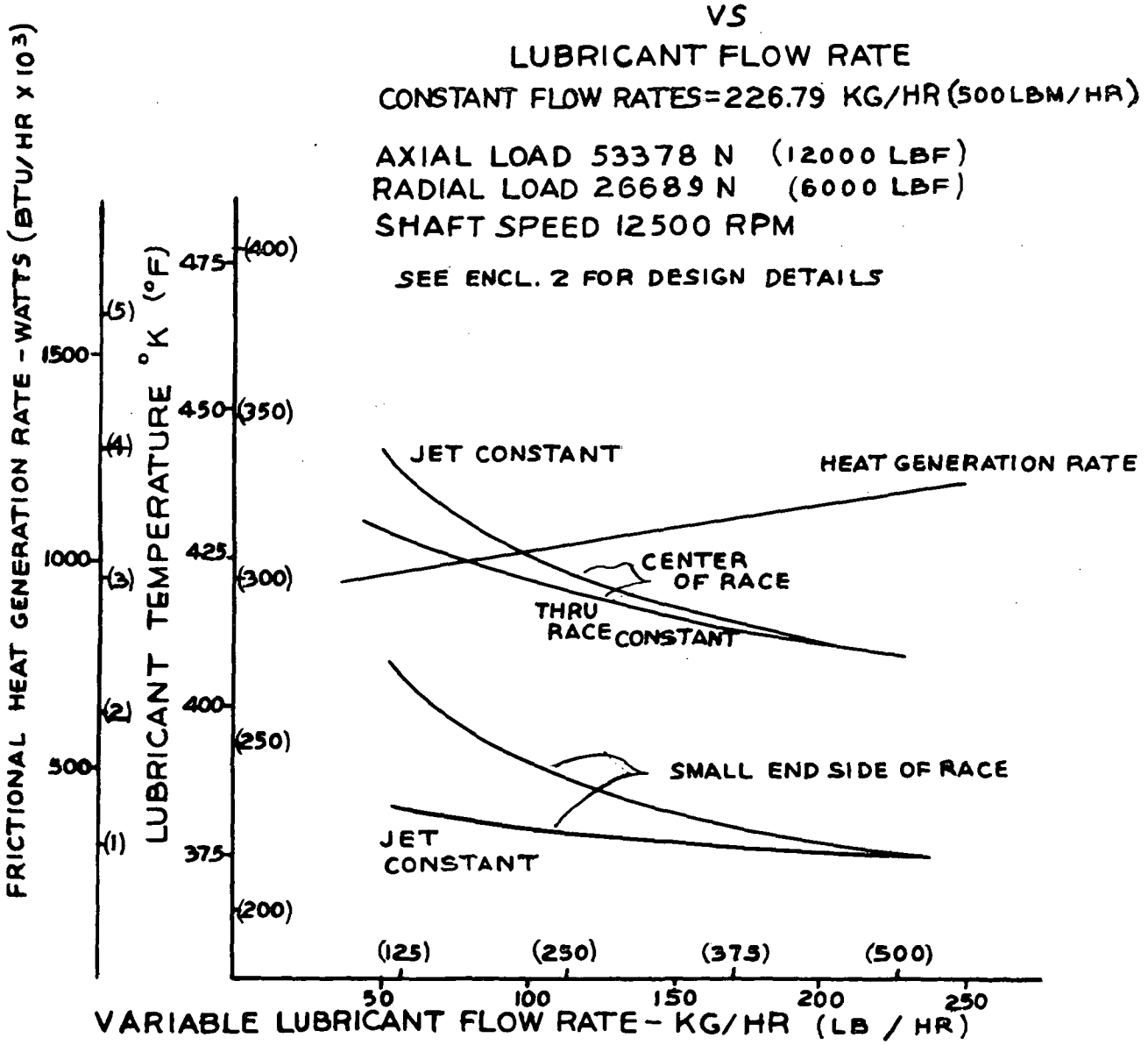

FIG. 28 OUTER RACEWAY LUBRICANT TEMPERATURE AT CENTER AND SMALL END SIDE OF RACE AND FRICTIONAL HEAT GENERATION RATE VS LUBRICANT FLOW RATE

CONSTANT FLOW RATE = 226.79 KG/HR (500 LBM/HR)

AXIAL LOAD 53378 N (12000 LBF)
RADIAL LOAD 26689 N (6000 LBF)
SHAFT SPEED 12500 RPM
SEE ENCL. 2 FOR DESIGN DETAILS

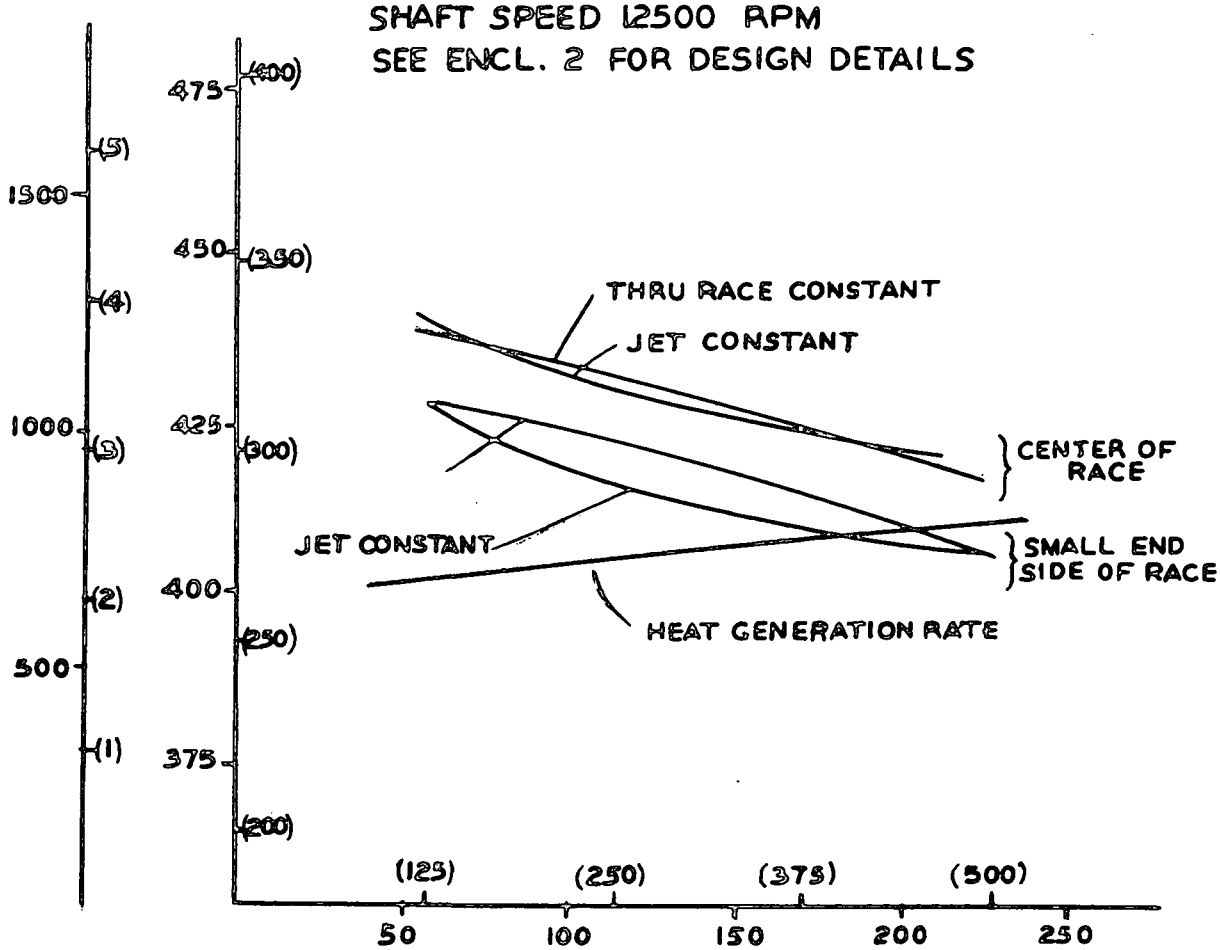

FIG. 28 LUBRICANT BULK TEMPERATURE AND FRICTIONAL HEAT GENERATION RATE VS LUBRICANT FLOW RATE

CONSTANT FLOW RATE = 226.79 KG/HR (500 LBM/HR)

AXIAL LOAD 53378 N (12000 LBF)
RADIAL LOAD 26689 N (6000 LBF)
SHAFT SPEED 12500 RPM

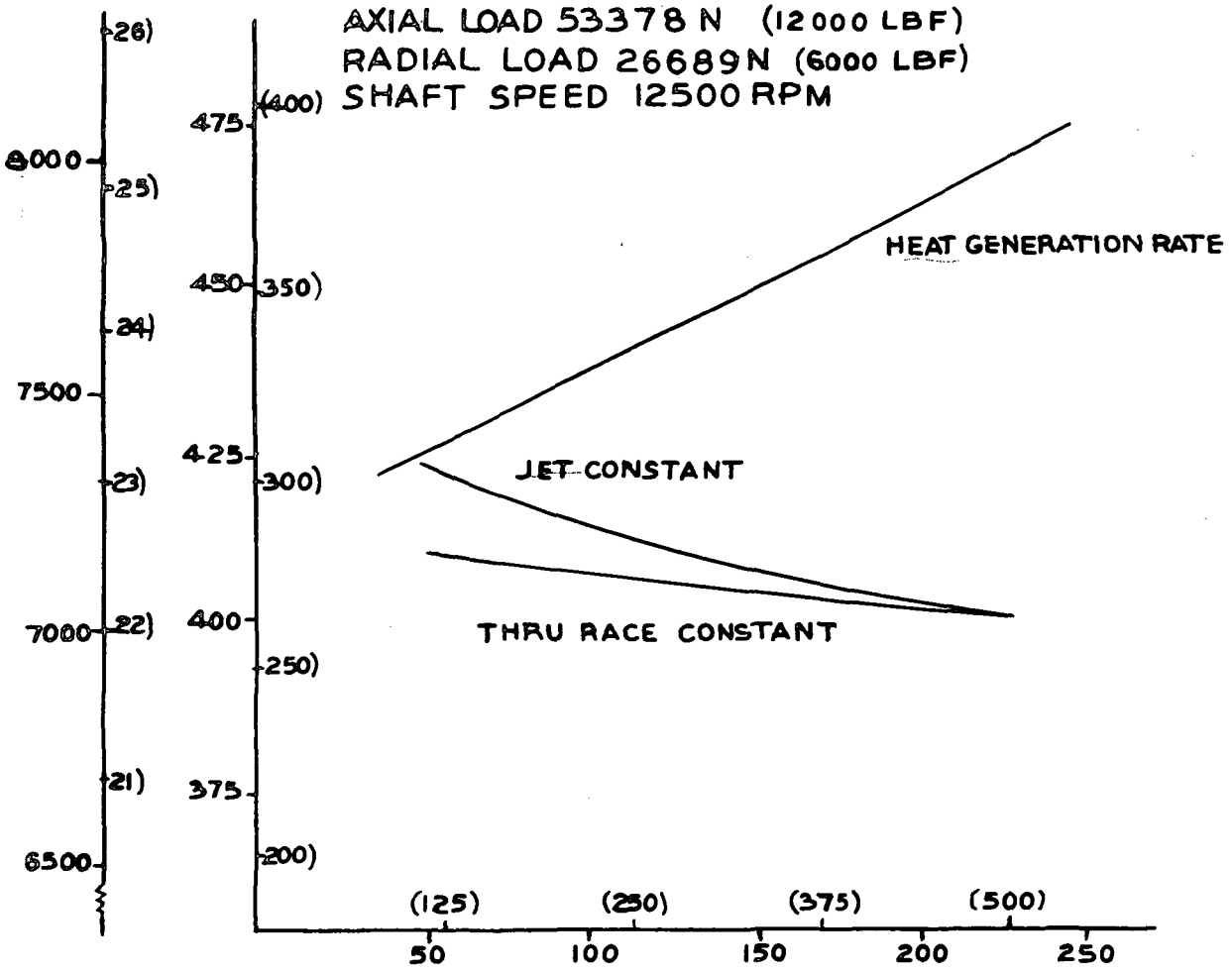

FIG.30 INNER RACE LUBRICANT TEMPERATURE, LUBRICANT MEAN TEMPERATURE AND CAGE SLIP PERCENT VS RADIAL LOAD

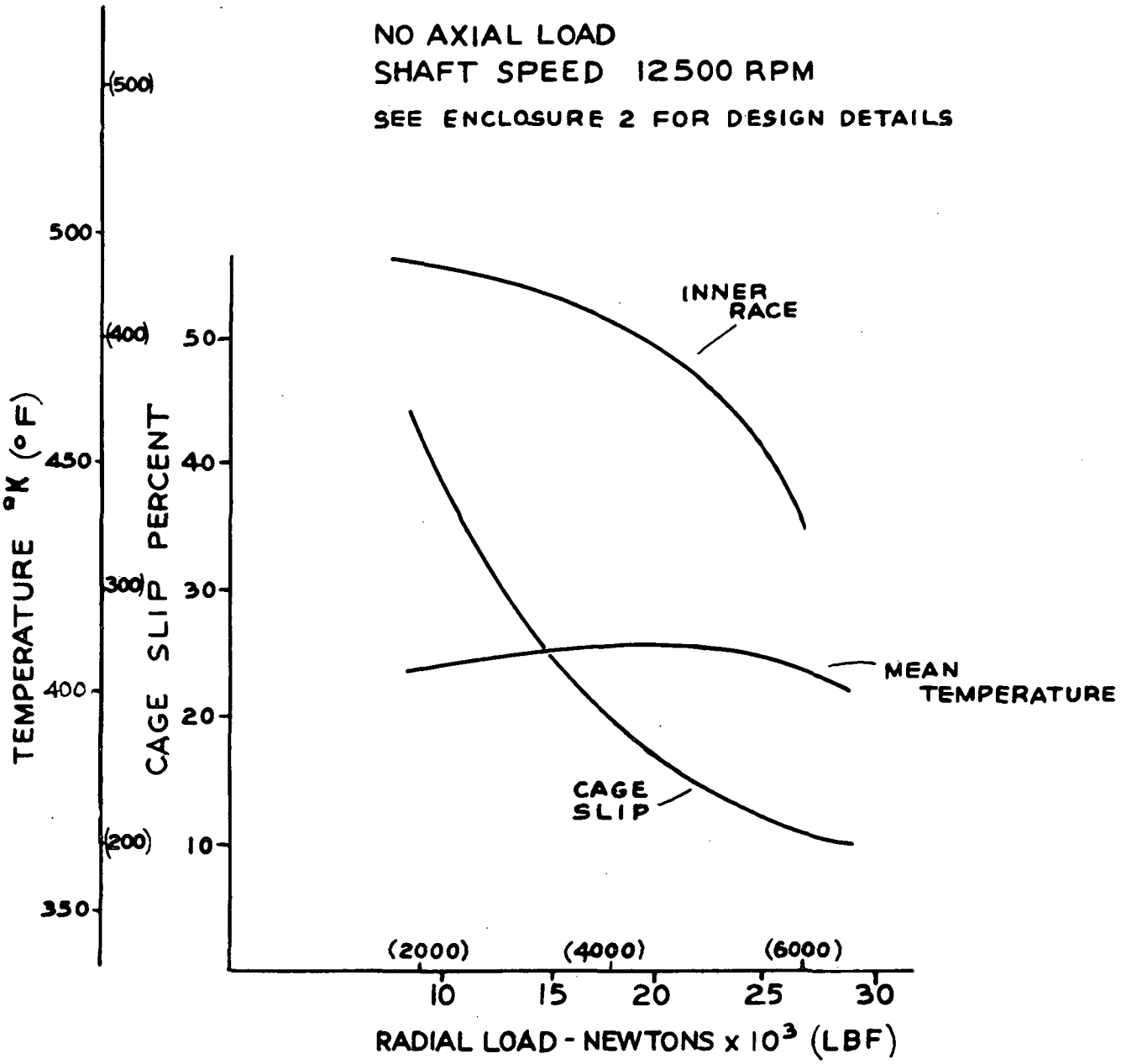

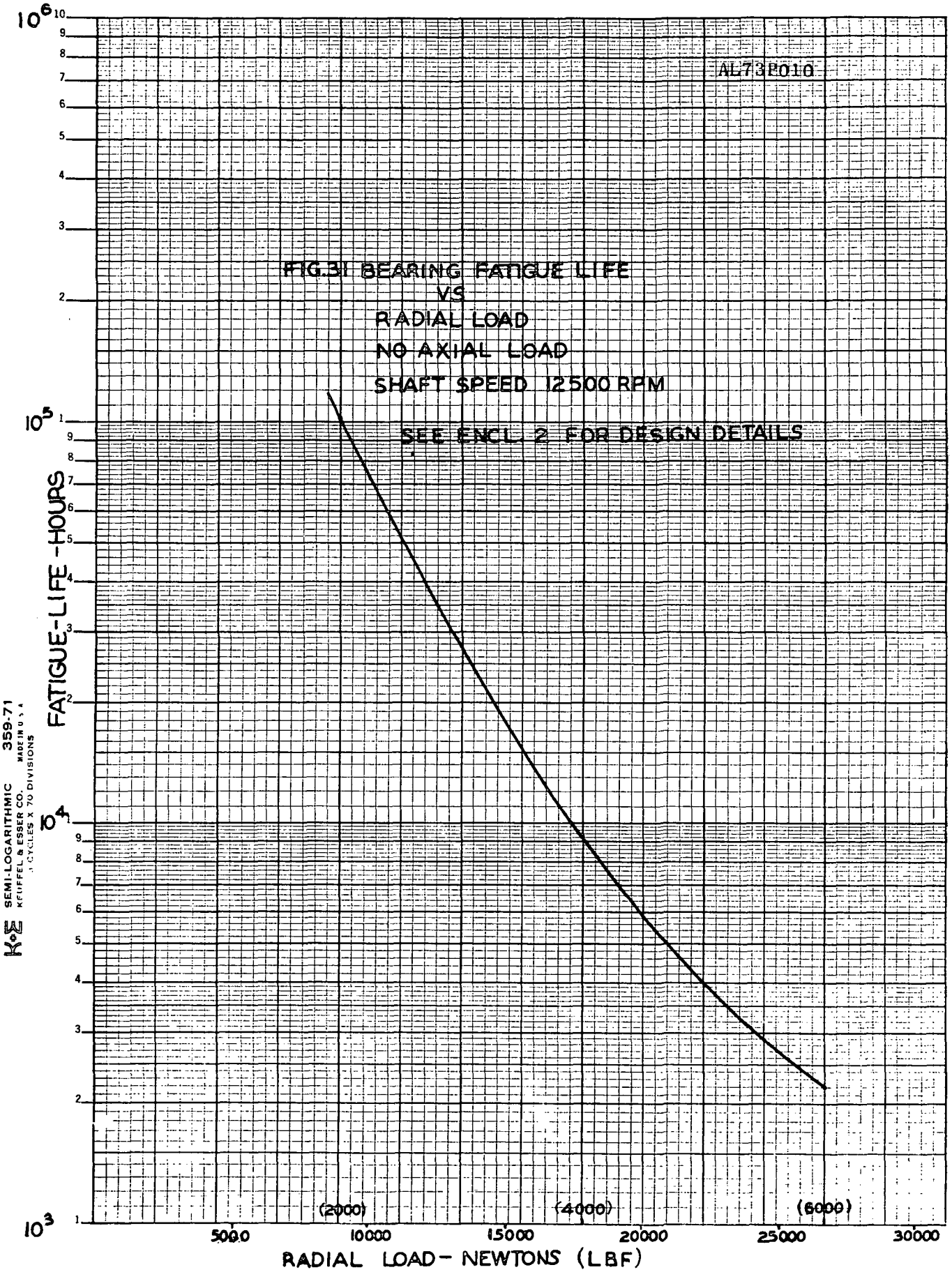
AL73P010
FIG.31 BEARING FATIGUE LIFE
VS
RADIAL LOAD
NO AXIAL LOAD
SHAFT SPEED 12500 RPM
SEE ENCL. 2 FOR DESIGN DETAILS
FATIGUE-LIFE-HOURS
RADIAL LOAD - NEWTONS (LBF)
(2000)
(4000)
(6000)
SEMI-LOGARITHMIC 359-71
KEUFFEL & ESSER CO.

ENCLOSURE 1

Contract NAS3-15700, Amendment No. 1

ATTACHMENT I.

(Revised 11-72)

TABLE I - BEARING SPECIFICATIONS AND OPERATING CONDITIONS

Bore - 4.750 in.
Width - 1.875 in.
O.D. - 8.125 in.
Roller length - (to be optimized)
Roller large end diameter - (to be optimized)
Roller end radius - (to be optimized)
Contact angle (cup) - (to be optimized)
Mean Pitch diameter - (to be optimized)
Raceway surface finishes - 6 μ in. rms
Roller surface finish - 4 μ in. rms
Large end flange surface finish - 6 μ in. rms
Number of rollers - 14 (approximately)
Inner ring, outer ring and roller steel - CVM SAE 4320
Shaft speed - 12,500 rpm
Radial load - 2000-6000 lbs.
Thrust load - 2000-12,000 lbs.
Lubricant temperature - 195°F

RESEARCH LABORATORY SKF INDUSTRIES, INC.

464680

BEARING DATA		SKF
VENDOR'S PART Nº		464680
VENDOR'S DWG Nº		464680
BRG TOLERANCE		CLASS 2
Nº OF ROLLERS (SEE ROLLER DETAIL)		20
MAX OPERATING TEMPERATURE		350°
CAGE WIDTH		1.780"
CONE INCLUDED ANGLE		36° 40' 32'
CUP INCLUDED ANGLE		47° 55' 12"
POCKET CLEARANCE	AXIAL	.009"-.019"
	CIRCUMFERENTIALLY	.005"-.015"
ROLLER DIA VARIATION (@ MEAN DIA.)		±.000050"
ROLLER EFFECTIVE LENGTH (MIN)		.950"
BASIC RATINGS @ 500 RPM	BRR	14,000
	BTR	16,000
	K	0.875
DEPTH OF CASE	RINGS	.063" MIN.
	ROLLERS	.043" MIN.

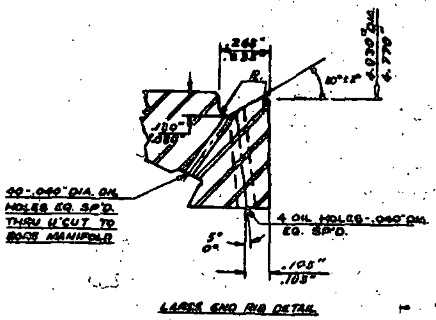

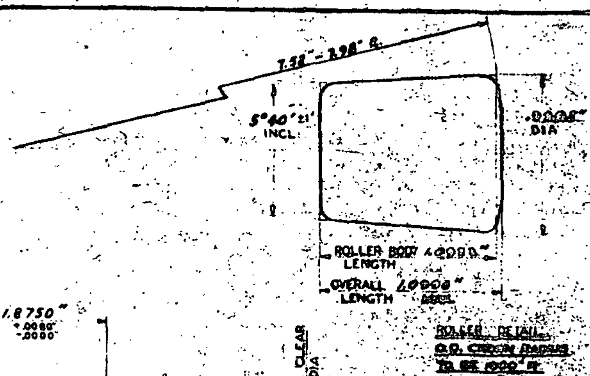

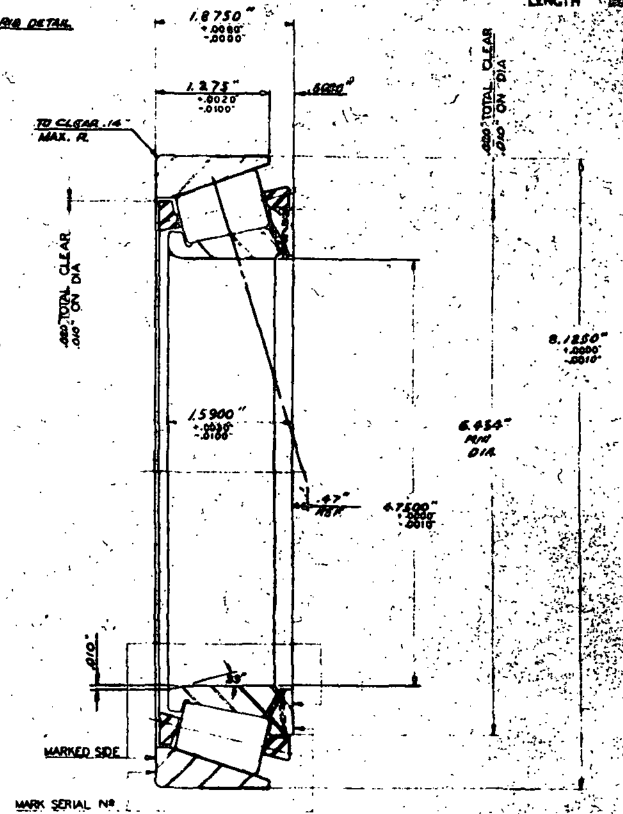

1. CONE TO BE MADE FROM CVM 3310 CARBURIZING STEEL (471657) CASE HARDNESS Rc 58 - 63, CORE HARDNESS Rc 38 - 45.
2. CUP TO BE MADE FROM CVM 3310 CARBURIZING STEEL (471657) CASE HARDNESS Rc 58 - 63, CORE HARDNESS Rc 38 - 45.
3. ROLLERS TO BE MADE FROM CVM 3310 CARBURIZING STEEL (471657) CASE HARDNESS Rc 58 - 63, CORE HARDNESS Rc 38 - 45.
4. CAGE TO BE MADE FROM AMS 6414 ONE PIECE MACHINED & BROACHED, CONE & CUP RIDING AS SHOWN NON - SEPARABLE
5. CAGE TO BE SILVER PLATED ALL OVER PER AMS 2410. THICKNESS PER SURFACE TO BE .001 - .002. DIM'S SHOWN ARE AFTER PLATING.
6.
7. CAGE TO BE 100% FLOURESCENT PENETRANT INSPECTED (470908)
8. 100% ETCH INSPECTION (471637)
9. 100% MAGNAFLUX INSPECTION (471682)
10. 100% VISUAL INSPECTION (470653)
11. 100% NOISE TEST (INNER RING ASSEMBLY)
12. 100% HARDNESS TEST (EITHER FACE OF CUP AND CONE - ROLLER SURFACE HARDNESS TO BE CHECKED TO A .04 AQL)
13.
14. SURFACE ROUGHNESS:

CONE ROLLER TRACK	6 AA	RACE RIDING LAND	25 AA
CUP ROLLER TRACK	6 AA	CAGE RIDING LAND	32 AA
ROLLER BODY	4 AA	CONE RIB FACE	6 AA
ROLLER SPHERICAL END	6 AA		

15. MAT'L IDENTIFICATION / CONTROL (471088)
16. CUP TO BE SERIALIZED & INTERCHANGEABLE WITH CONE ASSEMBLY
17. ROLLER SPHERICAL END CONTACT WITH CONE LARGE RIB FACE FLAT MUST BE TO THE MIDWAY POINT OF THE DISTANCE FROM THE ROLLER RECESS DIA TO THE RIB FACE UNDERCUT.

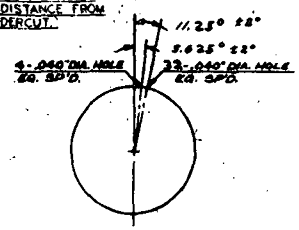

HOLE RELATIONSHIPS

114

OPTIMIZED BEARING DESIGN

ENCLOSURE 2

SKF INDUSTRIES, INC. PHILADELPHIA, PA.

BEARING, TAPERED ROLLER Nº 464680

DRAWN AMV

464680

CUST

AL73P010

APPENDIX A

ROLLER DIMENSIONS FOR A SPECIFIED BEARING SECTION AND VARIABLE CONTACT ANGLE

NOMENCLATURE

Symbol		Description
A	=	Minimum radial inner ring section height; m (in.)
APEX	=	Bearing APEX length; m (in.)
B	=	Minimum radial outer ring section height; m (in.)
C	=	Minimum inner ring flange width m (in.)
D	=	Roller large end diameter; m (in.)
Dm	=	Roller mean diameter; m (in.)
Ds	=	Roller small end diameter
E	=	Minimum distance between the roller large end/outer raceway contact point and the outer ring side face
em	=	Bearing mean pitch diameter; m (in.)
HT	=	Bearing radial section height; m (in.)
I.D.	=	Inner ring inside diameter m (in.)
L	=	Roller total length; m (in.)
O.D.	=	Outer ring outside diameter m (in.)
T	=	Bearing section limits; m (in.)
W	=	Bearing total width m (in.)
Z	=	Total number of rollers
α_i	=	Inner raceway contact angle depression radians
α_o	=	Outer raceway contact angle degrees or radians
α	=	Bearing mean angle degrees or radians
ν	=	One half of the roller included angle; degrees or radians

Computer program AE71Y001 requires full definition of bearing internal geometry as input. In order to use the program to evaluate bearing performance at a given contact angle it is required to establish a unique set of roller dimensions which will provide maximum load carrying capacity and which will fit within the bearing radial section. The following analysis was used to determine roller geometry for outer raceway contact angles of 12, 18, 20, 22, 24, 28°.

The knowns in this analysis were the bearing boundary dimensions; O.D. = 8.125 in., I.D. = 4.750 in., total width, w = 1.875 in., and the outer raceway contact angle (α_o). In addition, referring to Fig. 1A, dimensions A and B were both set equal to 0.2 inches, C was set equal to 15 percent of the total bearing width resulting in C = 0.282 inches and E was set to 0.025 inches. The above dimensions are consistent with good design practice.

By assuming values for half the roller included angle (γ), (see Fig. 2A) and the roller length to large end diameter ratio (L/D); the roller large and small end diameters plus the roller apex length can be found.

$$\varphi = \alpha_o - \gamma \tag{1A}$$

Since A equals B:

$$D = \frac{\frac{1}{2}(O.D. + I.D.) / \cos\varphi}{\frac{\tan\varphi}{\tan\gamma} - \frac{L}{D}(\tan\varphi - \tan\gamma)} \tag{2A}$$

$$L = \frac{L}{D} D \tag{2A}$$

$$D_s = D - 2L\tan\gamma \tag{3A}$$

$$\text{APEX} = \frac{D}{2\sin\gamma} \tag{4A}$$

By defining different pairs of L/D and ν, a large but finite set of different roller geometries was generated for each contact angle.

From the sets of roller dimensions generated, it remained to pick the particular set of dimensions which would fit within the bearing section and which would yield the maximum dynamic capacity for the given contact angle.

$$HT = \frac{O.D. - I.D.}{2} \qquad (5A)$$

The following inequalities are used to insure that the roller geometry is such that it remains within the available bearing section.

T_1 tests on radial height

$$\left(\frac{D+D_s}{2}\right)\cos\zeta + L\sin\zeta \leq HT - A - B \qquad (T_1)$$

T_2 tests on axial length considering inner ring flanges

$$\frac{L}{\cos\nu}\cos(\zeta - \nu) \leq W - 2C \qquad (T_2)$$

T_3 tests on axial length considering the outer ring width

$$\left(\frac{D+D_s}{2}\right)\sin\zeta + L\cos\zeta \leq W - C - E \qquad (T_3)$$

If all three conditions are met, then the roller size is compatible with the bearing section.

From the original set of roller dimensions generated, many have failed to pass one or more of the above inequalities and are eliminated from consideration. However, many sets of roller dimensions remain. From the remaining rollers, that roller which provided maximum dynamic load carrying capacity was selected as the optimum roller design for the given contact angle. A simplified equation was used to calculate the capacity of each remaining roller.

$$\text{CAPACITY} = D^{29/27} L^{7/9} \qquad (6A)$$

Having determined the roller size, the maximum number of rollers which can be put into the bearing is determined by considering the minimum distance allowed between rollers. In common practice, this distance is equal to 20 percent of the mean roller diameter. This allows for adequate cage web thickness. Therefore, the number of rollers z may be obtained as:

$$Z = \frac{\pi}{\sin^{-1}\left(\frac{D+0.2D_m}{e_m}\right)}$$

DM is the roller mean diameter, e_m is the bearing mean pitch diameter, Z must be rounded down to the next lowest integer.

Fig. 3A is a plot of the roller dimensions versus outer raceway contact angle which resulted from this analysis.

It is interesting to note that for the roller dimensions selected at each of the contact angles only two of the three dimensions T1, T2 and T3 are nearly totally utilized. For contact angles 20° and lower dimensions T1 and T2 were nearly fully utilized. For contact angles 22° and above dimensions T1 and T3 were those fully utilized.

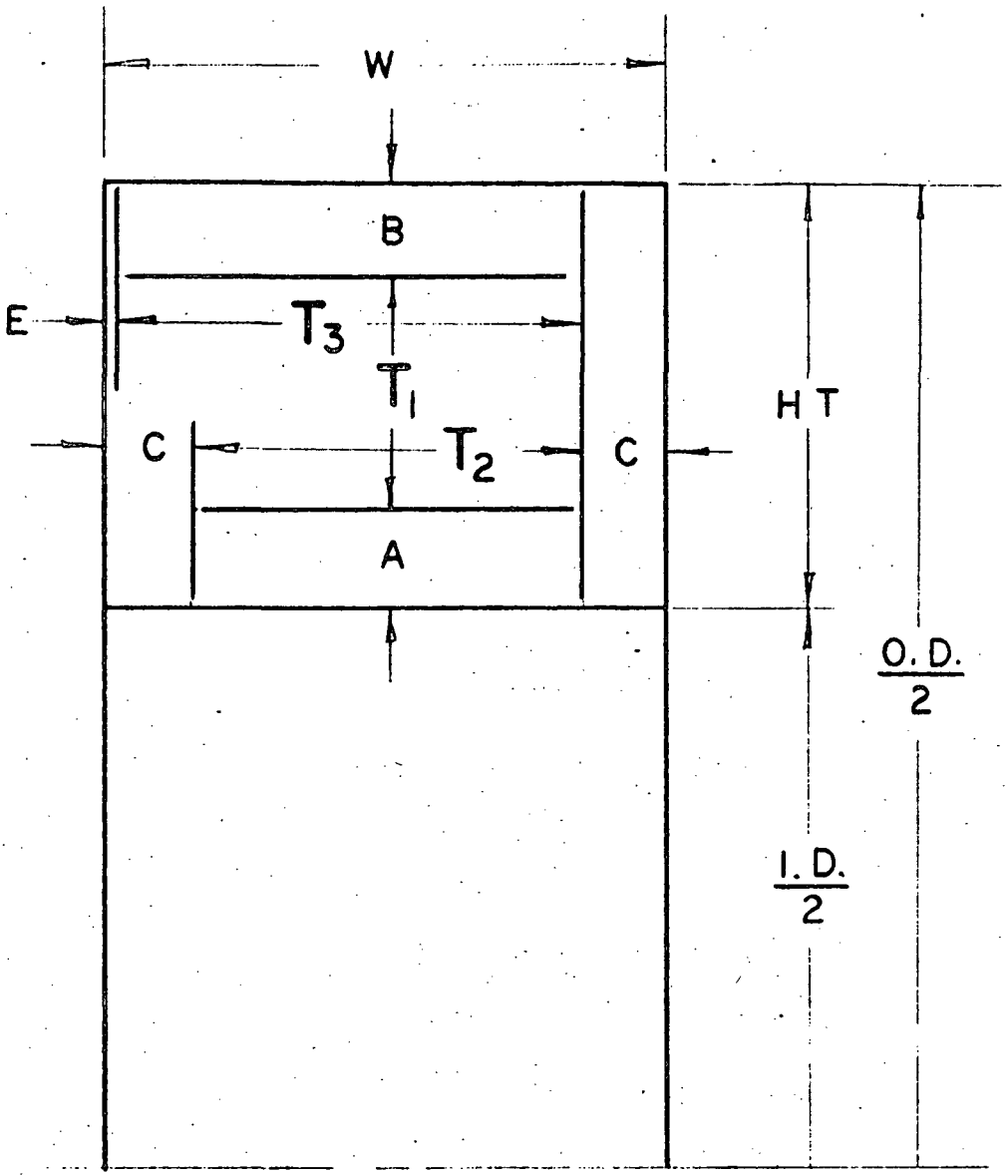

FIG. 1A BEARING SECTION
LIMITING DIMENSIONS
AND
ACCEPTANCE LIMITS T

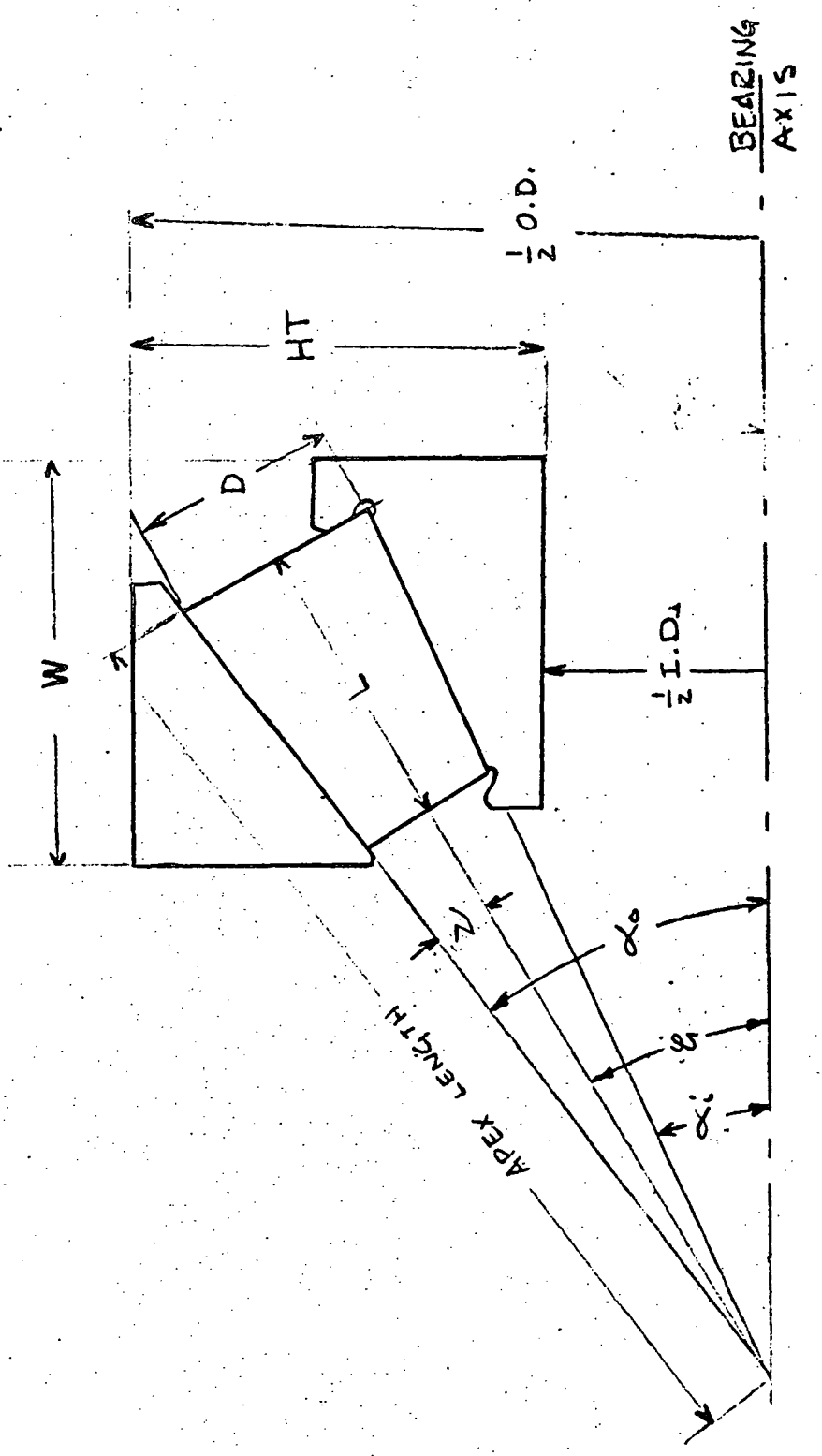

FIG. 2A TAPERED ROLLER BEARING GEOMETRY

FIG.3A ROLLER LENGTH, ROLLER INCLUDED ANGLE AND ROLLER LARGE END DIAMETER VS CONTACT ANGLE

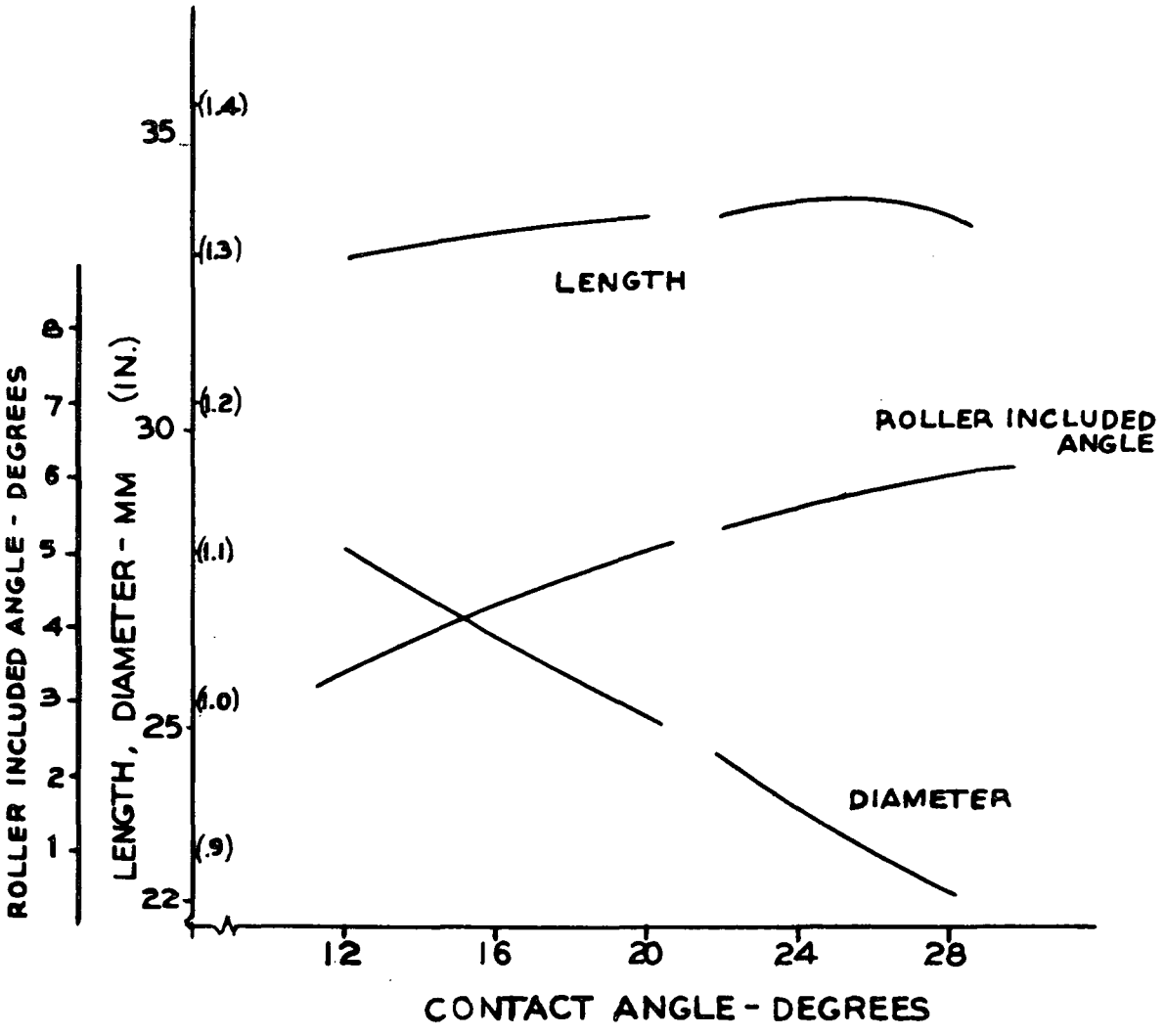

NASA Contract NAS3-15700
Final Report Distribution List

Address	Number of Copies
NASA-Lewis Research Center 21000 Brookpark Road Cleveland, OH 44135	
Attention: R. J. Parker (M.S. 6-1)	25
A. Ginsburg (M.S. 5-3)	1
W. J. Anderson (M.S. 23-2)	1
B. Lubarsky (M.S. 3-3)	1
N. T. Musial (M.S. 500-311)	1
H. Barnett (M.S. 500-206)	2
C. H. Voit (M.S. 5-3)	1
Report Control Office (M.S. 5-5)	1
Library (M.S. 60-3)	2
Office of Reliability & Quality Assurance (M.S. 500-111)	1
Technology Utilization Office (M.S. 3-19)	1
Office of Operations Analysis & Planning (M.S. 3-15)	1
NASA Scientific and Technical Information Facility Attention: Acquisitions Branch P. O. Box 33 College Park, MD 20740	10
NASA Ames Research Center Attention: Library Moffett Field, CA 94035	1
NASA Flight Research Center Attention: Library P. O. Box 273 Edwards, CA 93523	1
NASA Goddard Space Flight Center Attention: Library Greenbelt, MD 20771	1
Jet Propulsion Laboratory Attention: Library 4800 Oak Grove Drive Pasadena, CA 91103	1
NASA Langley Research Center Attention: Library Hampton, VA 23365	1

Address	Number of Copies
NASA Manned Spacecraft Center Attention: Library Houston, TX 77058	1
NASA George C. Marshall Space Flight Center Attention: Library Marshall Space Flight Center, AL 35812	1
NASA Headquarters Attention: RLC/N. F. Rekos Washington, DC 20546	1
Battelle Columbus Laboratories Attention: J. W. Kannel 505 King Avenue Columbus, OH 43201	1
Boeing Company Vertol Division, Boeing Center Attention: A. J. Lemanski P. O. Box 16858 Philadelphia, PA 19142	1
General Electric Company Aircraft Engine Technical Division Bearings, Fuels and Lubricants Attention: E. N. Bamberger Evendale, OH 45215	1
General Electric Company Attention: C. C. Moore Gas Turbine Division Schenectady, NY 12306	1
Industrial Tectonics, Inc. Attention: H. Signer H. Hanau 18301 Santa Fe Avenue Compton, CA 90024	1 1
Mechanical Technology Incorporated Attention: Library 968 Albany-Shaker Road Latham, NY 12110	1
TRW Marlin Rockwell Division Attention: A. S. Irwin 402 Chandler Street Jamestown, NY 14701	1

Address	Number of Copies
United Aircraft Corporation Pratt and Whitney Aircraft Division Attention: P. Holmes P. Brown Library 400 Main Street East Hartford, CT 06108	 1 1 1
Commanding Officer (SAV DL-EU-PP) Eustis Directorate U.S. Army Air Mobility R&D Laboratory Attention: L. Bartone R. Givens Fort Eustis, VA 23604	 1 1
AVCO Lycoming Division Attention: R. P. Cuny, Manager Mechanical Components Stratford, CT 06497	1
AFAPL-SFL Attention: E. Lake Wright-Patterson Air Force Base, OH 45433	1
Northwestern University Attention: Dr. H. S. Cheng Department of Mechanical Engineering and Astronautical Science Evanston, IL 60201	1
U.S. Army Air Mobility R&D Laboratory Lewis Directorate Attention: Lt. Col. G. J. Weden (M.S. 500-317) NASA-Lewis Research Center 21000 Brookpark Road Cleveland, OH 44135	1
Commanding General U.S. Army Aviation Systems Command Attention: Dr. James Chevalier (M.S. AMC PM-HLS) P. O. Box 209 St. Louis, MO 63166	1